TESIS DE LA UNIVERSIDAD DE ZARAGOZA

2015

20

Oihana Moreno Arotzena

Microfluidic-based 3d fibroblast migration studies in biomimetic microenvironments

Departamento

Instituto de Investigación en Ingeniería [I3A]

Director/es

García Aznar, José Manuel

ISSN 2254-7606

Prensas de la Universidad Universidad Zaragoza

Universidad Zaragoza
1542

Tesis Doctoral

MICROFLUIDIC-BASED 3D FIBROBLAST MIGRATION STUDIES IN BIOMIMETIC MICROENVIRONMENTS

Autor

Oihana Moreno Arotzena

Director/es

García Aznar, José Manuel

UNIVERSIDAD DE ZARAGOZA

Instituto de Investigación en Ingeniería [I3A]

2014

Microfluidic-based 3D fibroblast migration studies in biomimetic microenvironments

Dissertation presented by

Oihana Moreno-Arotzena

for the degree of Doctor of Philosophy in Biomedical Engineering

Faculty advisor

José Manuel García Aznar

Multiscale in Mechanical and Biological Engineering (M2BE)
Aragon Institute of Engineering Research (I3A)
University of Zaragoza, 2014

Instituto Universitario de Investigación
en Ingeniería de Aragón
Universidad Zaragoza

“Gu sortu ginen enbor beretik sortuko dira besteak…”

(Xabier Lete)

A los que están y a los que descansan en paz:

Amona eta attona, zuei.

Abuela y abuelo, a vosotros.

List of abbreviations

2D: Two-dimensional

3D: Three-dimensional

BME: Basement membrane extract

CDM: Cell-derived matrix

ECM: Extracellular matrix

ELISA: Enzyme-Linked ImmunoSorbent Assay

FA: Focal adhesion

FBS: Serum

FN:Fibronectin

FGM-2: Fibroblast Growth Medium-2

FXIII: Factor XIII

GF: Growth factor

HGF: Hepatocyte growth factor

IF: Interstitial flow

LPA: Lysophosphatidic acid

NHDF: Normal human dermal fibroblast

NMII: Non-muscle myosin II

PDGF-BB: Platelet-derived growth factor-BB

PDL: Poly-D-lysine hydrobromide

PDMS: Polydimethylsiloxane

RT: Room temperature

SEM: Scanning electron microscopy

SF: Stress fiber

TGF-β_1: Transforming growth factor-β_1

VEGF: Vascular endothelial growth factor

α-SMA: α-Smooth muscle actin

Abstract

Cell migration in 3D is a fundamental process in many physiological and pathological phenomena. Indeed, migration through interstitial tissue is a multi-step process that turns out from the cell-ECM interaction. It is a dynamic and complex mechanism that depends on the physic-chemical balance between the cell and its surrounding. Early stage of deep dermal wound healing process is a relevant migratory example, in which the fibroblast is the epicenter: the recruitment of the fibroblasts -by chemotaxis of PDGF-BB- to the clotted wound occurs. Likewise, this work focuses on studying the major underlying mechanisms of 3D fibroblast migration and the main microenvironmental cues involved within. To do so, we have confined two physiologically relevant hydrogels, made of collagen and fibrin, within microfluidic platforms.

Firstly, an integral comparative study of biophysical and biomechanical properties of both gels is presented. In these results, we have overcome the wide diversity of the existing data and special stress has been done in order to compare the microstructural arrangement, resistance to flow and elasticity. On the other hand, controlled chemical gradients have been generated and characterized within the microfluidic devices. Since biomolecules interact as purely diffusive factors or bound to the matrix proteins, in this work, distribution of PDGF-BB and TGF-β_1 across collagen and fibrin gels has been quantified. Finally, by taking advantage of the biophysico-chemical definition, we have characterized the migratory responses of human fibroblasts within the microsystems in the presence of a chemoattractant (PDGF-BB). Our results demonstrate that the local microarchitecture of the hydrogels determines the migratory properties of human fibroblasts in response to controlled chemotactic and haptotactic gradients, in a myosin II-dependent manner.

Resumen

La migración celular en 3D es fundamental en muchos fenómenos fisiológicos y patológicos. La migración, la cual resulta de la interacción célula-matriz, es un mecanismo dinámico y complejo que depende del equilibrio entre la célula y su entorno físico-químico. Concretamente, la etapa temprana del proceso de cicatrización de heridas profundas es un proceso migratorio ejemplar, en el cual el fibroblasto es el epicentro: se produce el reclutamiento de los fibroblastos -por quimiotaxis de PDGF-BB- del tejido circundante al coágulo. Este trabajo se centra en el estudio de los principales mecanismos subyacentes de la migración de fibroblastos en 3D y las principales señales microambientales involucradas en ella. Para ello, se han empleado modelos *in vitro* haciendo uso de plataformas microfluídicas para confinar dos hidrogeles fisiológicamente relevantes, compuestos por colágeno y fibrina.

En primer lugar, se presenta un estudio comparativo integral de las propiedades biofísicas y biomecánicas de los hidrogeles. En estos resultados, se ha hecho especial hincapié en comparar la conformación microestructural, la resistencia al flujo de fluido y la elasticidad. Por otro lado, se han generado y caracterizado gradientes químicos dentro de los dispositivos. Puesto que las biomoléculas interactúan como factores puramente difusivos o adheridos a las proteínas de la matriz, en este trabajo se ha cuantificado la distribución de PDGF-BB y TGF-β_1, en colágeno y fibrina. Finalmente, mediante esta definición físico-química, se ha caracterizado la respuesta migratoria de fibroblastos humanos dentro de los microdispositivos en presencia de un factor químico (PDGF-BB). Los resultados aquí mostrados demuestran que la microarquitectura local de los hidrogeles determina las propiedades migratorias de fibroblastos humanos en respuesta a gradientes quimiotácticos y haptotácticos, de manera dependiente de la miosina II.

Acknowledgments/Agradecimientos

Quisiera agradecer a todas las personas que han participado en este próspero recorrido: tanto desde lo personal, como lo profesional, por haberme ayudado a aprender destrezas genuinas. Especial lugar merece mi director de tesis y apoyo incondicional: Manu, mi más sincero agradecimiento por la oportunidad que me otorgaste para trabajar y aprender contigo en este emprendedor proyecto. Al final, tenías razón acerca del ascenso pirenaico, ¡vaya expedición! También, agradecer a la Universidad de Zaragoza y al European Research Council, el cual ha financiado el trabajo de investigación a través del proyecto ERC-2012-StG 306751.

A su vez, Mª Ángeles y Mª José, muchísimas gracias por el apoyo que me disteis, sobre todo, en la fase inicial de gestión del montaje y arranque del laboratorio. También fue sumamente gratificante la iniciación a la formación en la enseñanza de la mano de Mª José, lo cual ayudó a confirmar mi vocación. Extiendo mis agradecimientos a todo el grupo M2BE, el cual ha ido *in crescendo* en los últimos tiempos y le deseo el mayor de los éxitos. En especial, quisiera mencionar a Carlos, Cristina, Gracia, Mar, Nieves y Thomas, ya que ha sido muy grato trabajar con vosotros, muchas gracias.

En estrecha colaboración, Miguel, siempre dispuesto a ayudarme y a asesorarme. Te agradezco profundamente tu sincera generosidad, que ha sido un constante a lo largo de todo este tiempo. Tampoco me olvido de Alba y demás compañeros; mil gracias por todo el empeño y mucha suerte en vuestra producción científica.

All the performed laboratory management and experimental work have been possible thanks to the valuable opportunity that Prof. Roger Kamm conceded to me by inviting me as visiting student in his lab. The kindness of all the labmates, Bill, Jessie, Jordi, Ran, Sebastian, Sei Hien, Tamara, Vivek and Yannis, in

hosting and teaching me was exceptional. I am so glad and extremely grateful to all of you.

My stay in Boston was as good as it was, also because I was extraordinarily lucky with all of you guys: Claudia, Germán, Juan, Julia, Lotta, Sergio, Sot and *My American Family*, Isa and Sant. I have few words to describe it..: I really enjoyed the ride, thank you very much.

Qué hubiera sido de la etapa de Zaragoza sin tanta complicidad otorgada por tantos y tantas: Alberto, Ana, Carlos, Carmelo, Clara, Iosune, Johann, Miriam, Pilar, Sergio, electrónicos y telecos. Alicia, Araceli y Laura, mil gracias por hacerme entender de manera tan cercana cosas tan importantes. Chema y María, tan valiosa vuestra amistad; las rosas blancas son para esto... Noe, ahí desde el día *zero*... la invitación sigue en pie. Alaitz eta Oscar… porque el violín suena sin importar el número de cuerdas; no importa cuántos kilómetros de cuerda necesitemos, seguirá sonando.

Laguntasunaren berotasuna iritxi zaidalako… eskerrik asko denoi. "Haizea etorri, gure adatsak nahasi eta badoa" (Joseba Sarrionandia): Amaia C., Amaia O., Alberto, Alvaro, Ion, Jone, Patri, Zuzu. Carol, Iñaki, referencias vitales. Pagoak ukitzeko moduen gainetik: Anne, Alo, Argi, Gara, Goiatz eta Maitena. Eli, Nahika, izaite berezi horrengatik. Hain gutxian eta hainbeste urtetarako sortua: Denis, Eli, Izaro, Jaio, Lierni G., Lierni Z., Maddi, Maite eta… oroiminez, Maita.

Apaltasun osoz, pazientzia eta eskuzabaltasunagatik, eskerrik asko bihotzez familiari. Bereziki, azken urteetan distantzia guztiak murrizteko egindako ahaleginagatik, zuei: Aita, Ama, Ugaitz eta Janire. Eta nola ez, mattia, bidelagun behinena, eskaini didazun laguntza infinituagatik, milesker Eña.

Table of contents

List of figures

List of tables

Chapter 1
Introduction

In this introductory chapter the global scenario of the Thesis is presented. A general overview, along with the state of the art, describes the framework and motivation of the Thesis. Additionally, its objectives are listed and, finally, the structure of the Thesis in chapters is summarized.

1.1 Background

Cell migration is an elemental mechanism in physiological and pathological processes such as morphogenesis, cancer metastasis or tissue regeneration. It depends on a physicochemical balance between the cell and its surrounding. The non-cellular part of the tissue that gives structural support to the cells is known as the extracellular matrix (ECM) and it is comprised by a three-dimensional

fibrillar network along with biochemical signaling. Indeed, a complex and dynamic context-dependent cellular response drives migration, and the contractile actin cytoskeleton is known to play a key role involved in such mutual exchange [1].

1.1.1 Actin cytoskeleton and cell migration

Despite some old beliefs, cells are not only comprised of an elastic membrane that encloses a viscous cytoplasm along with a nucleus in the center, but they are also built by numerous components with distinct mechanical purposes. All cells contain a system of filaments that extend from the nucleus to the surface membrane known as the cytoskeleton. Its functions are diverse and essential in basic cellular events: it confers cell shape and compliance, participates in the intracellular transport and enables cells to move [2].

As shown in Fig. 1.1, the cytoskeleton comprises three main families of proteins and each one builds its own kind of filaments: microtubules, intermediate filaments and actin filaments [2]. Actually, each filament has different mechanical and biological missions. On the one hand, microtubules -the most robust filament network- have a major role regulating the intracellular transport, helped by kinesin and dynein molecular motors. As to the main duty of the intermediate filaments, it is protective by rendering architectural mechanical resistance to the cell. Finally, the actin filaments are responsible for contributing in the intracellular transport as well as for controlling cell motility by means of mechanotransduction.

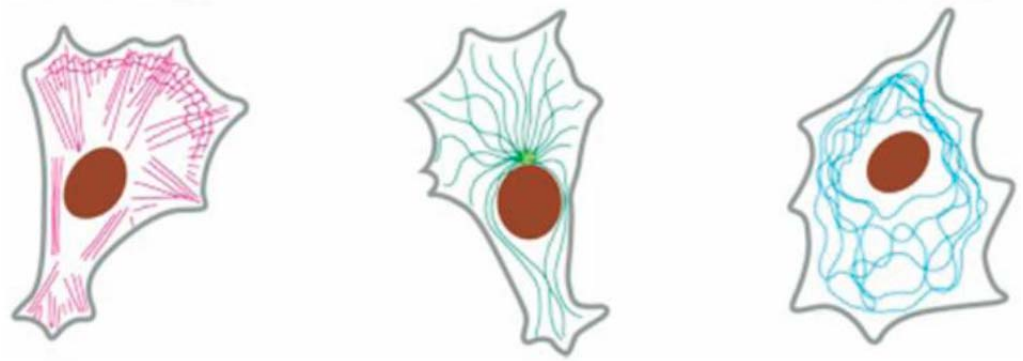

Fig. 1.1. Major components of the cytoskeleton. Schematic distribution of actin filaments, microtubules and intermediate filaments within the cell body. Adapted image from Alberts et al. [2].

Mechanotransduction is defined as the process by which cells sense mechanical inputs and transduce them into a cascade of biochemical signals leading to biological responses, e.g., cell movement [3]. The way cells feel and respond to environmental cues is mediated by a set of cellular receptors called integrins, which physically couple the cellular membrane to specific extracellular matrix protein-binding domains. The activation of the integrins is followed by a set of intracellular events that control the conformation of the actin-cytoskeleton during cell movement.

The main actin-based actors are shown in Fig. 1.2. When integrin transmembrane receptors are activated, they are recruited to form tethering sites called focal adhesions (FAs). Hence, through these supramolecular complexes located in the cell periphery, the actin-cytoskeleton is anchored to the ECM [4]. Next, actin stuck into long and aligned bundles, stress fibers (SFs), which are characterized by their contractile capability provided by the non-muscle myosin II (NMII) units that incorporates. NMII motor proteins slide over the actin filament generating contraction of the SFs [5]. Likewise, cells are able to exert

traction forces in the FAs as a response to the cell-ECM force balance, leading to cell movement.

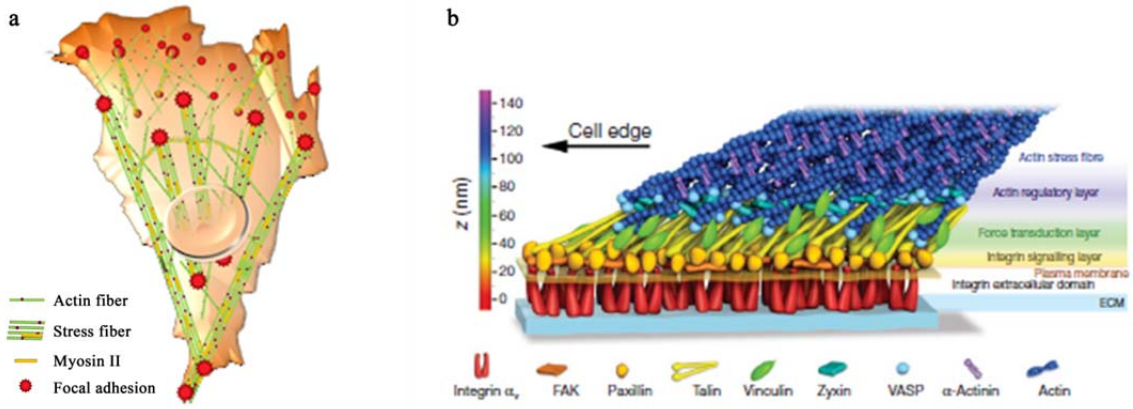

Fig. 1.2. The actin-based structures in the cell body. The main components responsible for cell movement are represented in the schematic picture (a). Schematic model of focal adhesion molecular architecture is shown in picture (b), which is from Kanchanawong et al. [6].

Indeed, migration for two-dimensional crawling cells is characterized by the subsequent execution of three main actions that occur by polymerization and depolymerization of actin [7], as shown in Fig. 1.3. Firstly, the protrusion of the leading edge by formation of lamellipodia and filopodia -structures highly rich in actin- takes place. Then, following the formation and force generation of new FAs, retraction of the trailing edge through NMII-contracting stress fibers occurs.

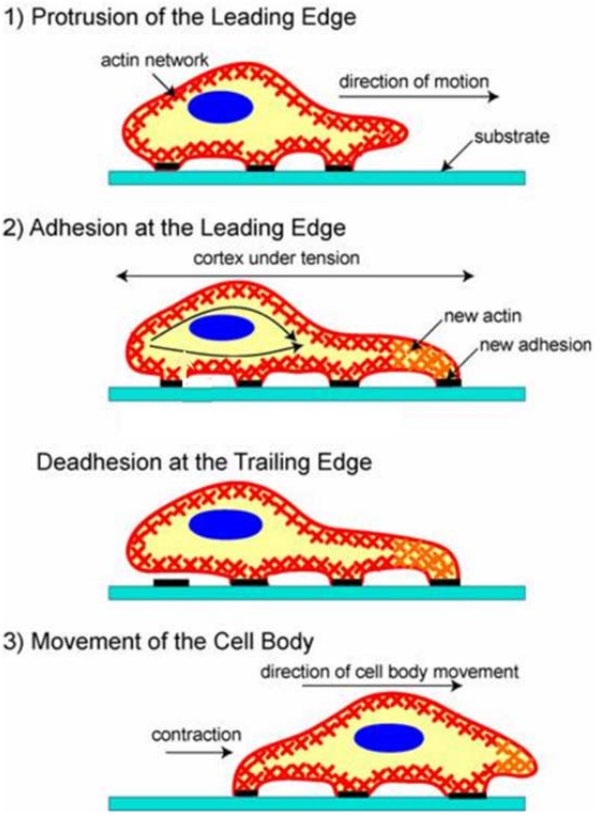

Fig. 1.3. Cell crawling in 2D. It comprises protrusion of the leading edge, adhesion formation and force generation, and retraction of the trailing edge. Image modified from Ananthakrishnan et al. [8].

Although two-dimensional (2D) migration assays have been extensively studied and have brought valuable knowledge on the molecular regulation of the basic processes of cell migration, physiological cell migration is generally better addressed by three-dimensional (3D) conditions. Moreover, a vast amount of work has cleared up that cellular mechanics [9, 10], as well as migratory mechanisms [11, 12], diverge profoundly when dimensionality is switched from 2D to 3D. Indeed, cells are displayed in a very distinct arrangement: they turn to be within confined networks -which resemble biomimeticly the ECM- instead of over unconfined planar substrates. Therefore, currently, complex 3D migration

bases are being studied by elucidating the environmental cues that impact on the process.

1.1.2 Extracellular matrix

The ECM is a complex network composed of numerous types of assembled proteins that hold cells together within specialized tissues [13]. The ECM renders architectural scaffolding and orchestrates the biochemical and biomechanical cues (see Fig. 1.4). Hence, it means a heterogeneous multi-cue microenvironment in the cellular surrounding [14], by which cell behavior is modulated.

Cell migration through interstitial tissue is a multi-step process that turns out from the cell-ECM interaction [15]. The way in which cells sense and respond to the environmental cues is complex and dynamic. Cells sense the mechanical properties and convert them into biological responses through the cytoskeleton by exerting traction forces, modifying the cell tension state and initiating signaling cascades [16–20]. Simultaneously, biochemical signals are able to influence sensing capabilities [21]. Integrated, both inputs together, have drastic effects on the cell-phenotype and, thus, on basic cellular events. Therefore, since the ECM is key to modulating mechanotransduction, and hence cell migration, it has an integral ubiquitous role in physiological and pathological processes [16, 17, 22–28]. Actually, its pathological compliance can lead to severe diseases such as metastasis or impaired wound healing [25, 29].

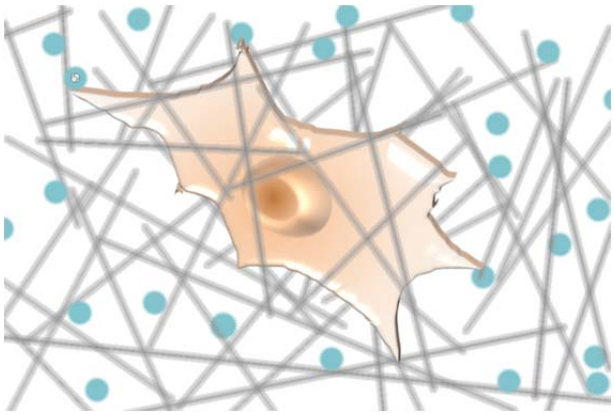

Fig. 1.4. Cellular microenvironment. The cell is surrounded by the fibrillar network (grey lines) and biomolecules (green circles). Image based on that published by Griffith and Swartz [23].

Currently, diverse natural ECM-protein monomers are used at the benches since they self-assemble easily upon physiological conditions and are biomimetic hydrogel approaches for applying to 3D *in vitro* studies [30, 31]. Their biophysicochemical properties act as competing mechanisms [32–34], making entangled and delicate while decoupling the specific effect of each property on the cellular response.

3D cell migration depends on the physicochemical balance between cell deformability and physical tissue constraints [35]. The matrix composition compromises the ligand density, cross-linking level and architecture [28]. Actually, ligand density correlates with anchorage-sites for integrins. Cross-linking concentration arbitrates the degradability of the network by proteolytic enzymes and the fibrillar 3D arrangement -porosity, pore size and fiber diameter- [36] and raise dramatically the stiffness of the gel [30, 37]. Meanwhile, the microstructure determines the permeability of the matrix, which directs the transport of biomolecules and local hydraulic asymmetries in the cell surrounding [23]. In fact, the ligand density [38, 39], stiffness [32, 40],

microstructure [12, 34, 41–44], local permeability gradients [45, 46] and external loading [18, 47] have been demonstrated to have a direct impact on cell migration.

The biochemical environment results from the synergy of autocrine and paracrine signaling [23]. Imposed or unintentionally, growth factors (GFs), chemokines and other biomolecules are carried throughout the pore-mesh originating chemical gradients. While transporting, the matrix may act as factor-reservoir by offering available binding sites to the biomolecules. Therefore, they may get bound or remain as soluble factors. Moreover, transport nature is influenced by the interstitial-flow, which meanwhile acts as an external-load [18]. Hence, during molecular transport, convective and diffuse processes occur; the ratio between both phenomena is defined by the Peclet number, which is proportional to the molecular size. Therefore, the caused chemical gradients at the microscopic level and in the local pericellular vicinity yield heterogeneous in a context-dependent manner [23].

All this together, points to the bearing role of the ECM in the cell migration development. In fact, it regulates mechanotransduction by controlling the biophysical arrangement of the matrix as well as the availability of the chemical factors. As mentioned before, cell migration is a major mechanism in pathophysiology. In this regard, wound healing is one exemplary regenerative process, in which the display of both the fibrillar layout and the biomolecules is crucial delimiting the boundary between the acute and impaired evolution.

1.1.3 Wound healing physiology and mechanotransduction

The main protector of our body against external aggressions is the skin. A cross section of its structure is shown in Fig. 1.5. It is formed by three main

layers. The epidermis consists mostly of stratified epithelium tissue. The dermis provides support and nutrients to the epidermis. Although the dermis is rich in fibroblasts, mast cells, blood vessels, nerves, etc., its main constituent is the connective tissue, which avoids damage from everyday stretching and other mechanical insults. Beneath the epidermis is the hypodermis, composed mainly by adipose tissue to protect the internal structures.

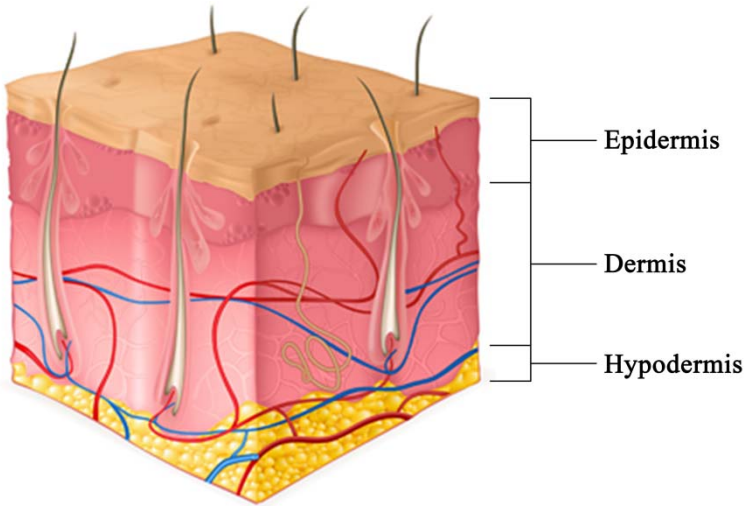

Fig. 1.5. Skin cross section. It is formed by epidermis (epithelium tissue), dermis (fibroblasts, connective tissue and blood vessels) and hypodermis (adipose tissue) [48].

Skin is exposed regularly to injuries. Superficial wounds are repaired by the closure of the epithelial sheet. Conversely, full-thickness dermal wounds, not only require the repair of the epithelial sheet, but also the injured connective tissue requires its biosynthesis and remodeling. In this regard, acute wound repair is orchestrated in a standardized manner (see Fig. 1.6), in which the extracellular matrix and growth factors play a crucial role.

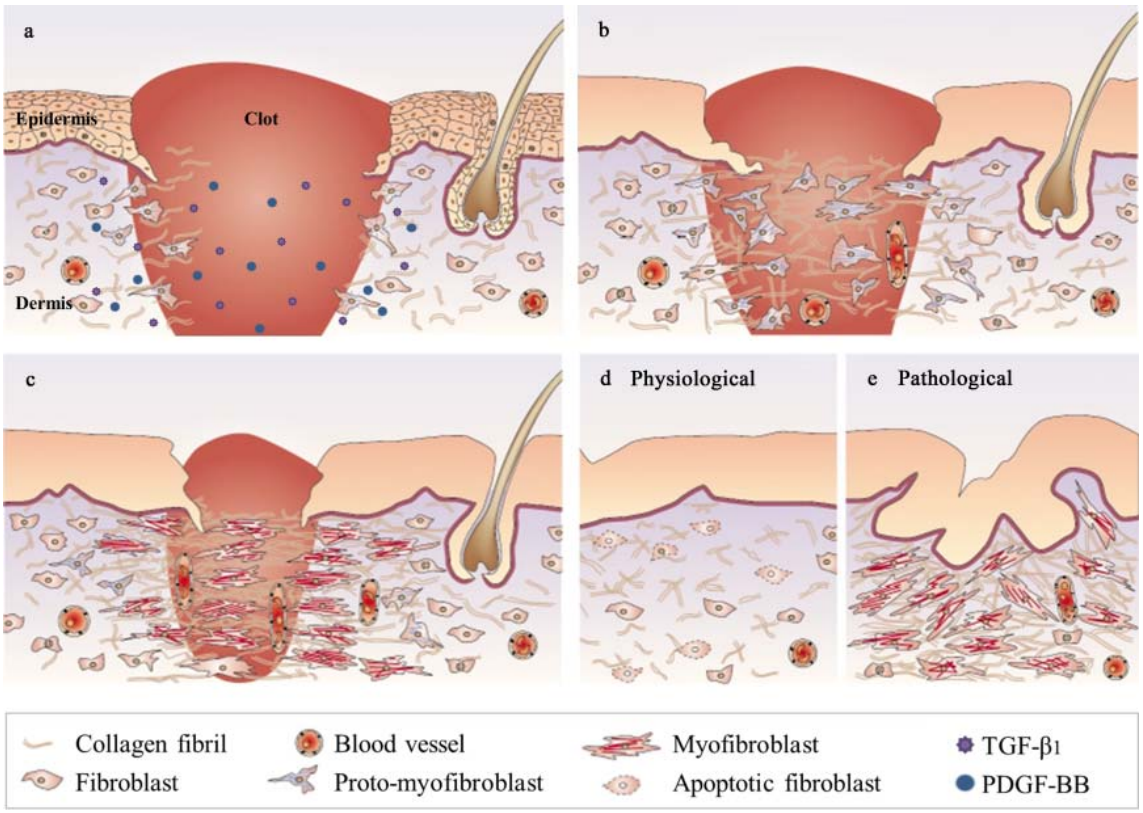

Fig. 1.6. Wound healing physiology and mechanotransduction. When a full-thickness dermal wound is filled by a fibrin clot, local growth factors stimulate fibroblasts from the adjacent intact dermis to invade this provisional matrix (a). These migrating fibroblasts, along with vessels, fill the wound, which results in the formation of granulation tissue (b). Migrating fibroblasts exert traction forces on the collagen matrix, which results in its reorganization along lines of stress. The development of mechanical stress stimulates fibroblasts to develop stress fibers and to produce collagen, so they acquire the proto-myofibroblast phenotype (b). Then, proto-myofibroblasts become differentiated myofibroblasts by synthesizing α-smooth muscle actin and generating increased contractile force. This complex process of remodeling results in shortening of the collagen matrix with the corresponding wound closure (c). When a normal healing wound closes, myofibroblasts disappear by apoptosis and a scar is formed (d). However, in many pathological situations, such as hypertrophic scar formation, myofibroblasts persist and continue to remodel the ECM, which results in connective-tissue contracture (e). Modified image and caption from Tomasek et al. [29].

In order to stop the bleeding -homeostasis-, platelets stick along with collagen, initiate the clotting cascade [49] and release numerous factors, such as transforming growth factor-β_1 (TGF-β_1) and platelet-derived growth factor-BB (PDGF-BB). The PDGF-BB chemoattractant recruits the macrophages and fibroblasts into the fibrin clot, which carry out the cleansing of the area -inflammation-. Meanwhile, macrophages release vascular endothelial growth factor (VEGF), so new blood vessels are formed in order to nourish the wound site. To migrate, fibroblasts are activated from the quiescent state, into the migratory phenotype -known as proto-myofibroblasts-. So fibroblasts repopulate the damaged tissue, proliferate and synthesize collagen, leading to the granulation tissue. Then, by TGF-β_1 (along with the increased rigidity in the ECM) fibroblasts differentiate into myofibroblasts -their contractile phenotype- and remodel and contract the wound edges. At this point, the re-ephitelization also occurs [50].

In physiological wounds, as the wound is repaired, the myofibroblasts disappear by apoptosis. However, their persisting activity leads to pathological tissue deformation such as in hypertrophic scars, fibrosis and during stromal reaction to tumors [51], which have major implications while sustaining regular function or tissues. In fact, non-healing wounds can turn on a major disability or even death [49, 52]; e.g., about 3 to 6 million people in the United States of America are affected by these disorders [53]. In consequence, gaining knowledge with regards to wound healing-concerning mechanisms has become necessary.

Thus, in the last years, a lot of effort has been directed towards a thorough study of wound healing processes by developing diverse means to perform *in silico* [54], *in vitro* [55] and *in vivo* [56] models. Particularly, fibroblast-centered studies have increased [57–59], since they are one of the critical actors in healing full-thickness dermal wounds.

1.1.4 Fibroblast mechanics and 3D *in vitro* studies

Collagen biosynthesis and remodeling are key to not only pathophysiological repair processes, but also are implicated in controlling the interstitial fluid pressure, aging and tumorigenesis. Fibroblast is the major cell type seeking such functions and, therefore, fibroblast-matrix interaction research is a pivotal factor for the design in tissue engineering [22, 51, 60–62]. This relationship is an adaptive response exhibited by dual-mode of cell signaling: GF context and biomechanical environment [62].

In fact, these studies have been distributed into a four-quadrants diagram displayed by Rhee et al. [62]. As shown in Fig. 1.7, fibroblast behavior has been studied using 2D models -referred as high tension- as well as 3D hydrogel-systems -cited as low tension-. Moreover, pro-migratory or pro-contractile environments have been generated within those substrates using PDGF-BB and lysophosphatidic acid (LPA) or serum, respectively.

Actually, very distinct structural and behavioral responses have been identified depending of the dimensionality of the assay. Fibrillar-confinement models have shown to be more tissue-like environments. In 3D, fibroblasts interact with collagen through dendritic extensions to detect changes in tissue mechanics and, hence, exhibit distinct patterns of migration and remodeling in a context-dependent manner [60, 63, 64]. In planar substrates, they can modulate their cytoskeletal function in response to surface mechanics by acto-myosin activity, but they have little capacity to modulate the overall molecular organization and mechanical properties of the ECM-coated surfaces [62]. In 2D, since fibroblasts are not able to form the dendritic structures, they generate lamellipodia and robust SFs and FAs [65]. However, in *in vivo*-like conditions SFs and FAs are

observed only in activated conditions such as in differentiated myofibroblasts [66, 67].

Furthermore, akin the cell phenotype, pro-migratory and pro-contractile environments raise important differences in physiology. Actually, it is an adaptive response between the fibroblast state and the biophysical environment. During repair, fibroblast migration is an early event; whereas expression of α-smooth muscle actin (α-SMA), differentiation and, hence, wound contraction occur later. In fact, in physiological wound healing, as fibroblasts repopulate and renew the matrix, TGF-β_1 and the increased ECM stress -yielding from their own remodeling activity- hallmark wound closure by myofibroblast differentiation and their mechanoregulatory functions [68].

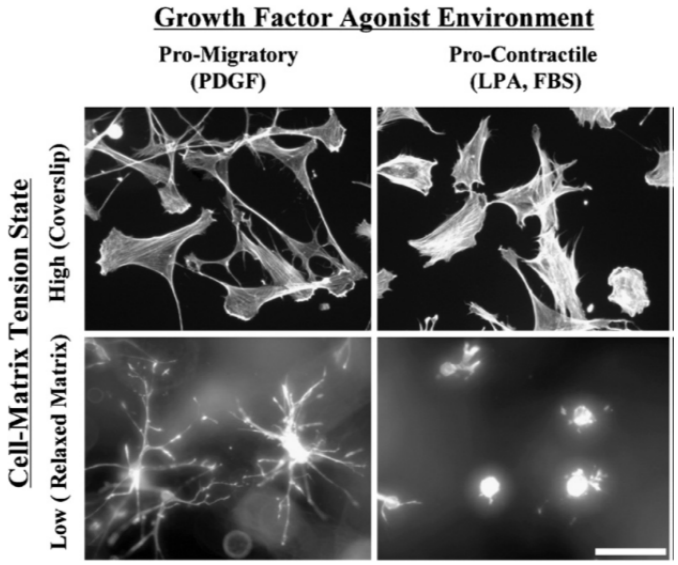

Fig. 1.7. Four quadrants of fibroblast mechanics research. Fluorescence images of cells stained for actin cytoskeleton are shown in the corresponding quadrant. Image from Rhee and Grinnell [62].

In this regard, fibroblasts-concerning wound healing phenomena have been widely studied employing 3D models. On the one hand, Grinnell et al. [69]

compared scaffold contractility and remodeling behavior of 3D floating and restrained collagen lattices (refer to Fig. 1.8). Floating matrices remodeling was stimulated by serum, LPA or PDGF-BB, whereas restrained matrices required serum or LPA to contract. Briefly, they concluded that whether cells are or not under tension changes the mechanism by which they remodel collagen networks. In this regard, what Liu et al. [57] recently published has added new insights into the contraction mechanism of the hydrogels, demonstrating that 3D collagen contraction differs depending on cell tension and GF stimuli in a myosin II-dependent manner.

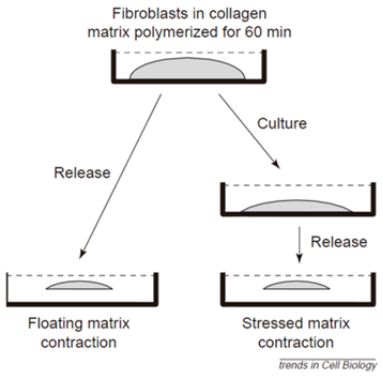

Fig. 1.8. Models for collagen contraction studies. Floating as well as stressed matrices are employed for that purpose. Image from Grinnell [68].

Moreover, human fibroblast has been comparatively studied in 3D vs. 2D within four distinct substrates with respect to its morphology, cell adhesion, actin cytoskeleton and migration by Hakkinen et al. [70]. Cell-derived matrix (CDM), basement membrane extract (BME), collagen I and fibrin were chosen for that purpose. While fibroblast failed to spread in BME, they did spread well in CDM, collagen I and fibrin, presenting more elongated and less spread than in 2D. In addition to this, they saw distributed focal adhesions over the cell body and fewer, thinner and more peripherally-located stress fibers in comparison to the

typical 2D layout. Besides, surprisingly, 3D cell migration was determined to be mesenchymal-mode and cell speed was measured to occur more rapidly in 3D than in 2D. In this quantification, due to the molecular composition, cells migrated -from fastest to slowest- as follows: CDM, collagen I, fibrin and BME, successively.

Fibroblast transmigration has also been assessed employing several gel-systems. Grinnell et al. [71] proposed nested collagen matrices to study fibroblast transmigration and GF specificity (see Fig. 1.9). Contracted cell-containing collagen matrices -also called dermal equivalents- were embedded within another cell-free collagen gel; hence, migration occurred outwards. In these experiments, they found that cells would migrate upon PDGF-BB stimulation, whereas LPA and serum promoted matrix remodeling and contraction. Besides, migrating fibroblasts were bipolar with leading dendritic extensions. Additionally, Miron-Mendoza et al. [64] applied the nested collagen matrices in order to study fibril flow and tissue translocation. In these results, collagen fibril flow was produced in the outer matrix toward the interface with the dermal equivalent by the traction forces exerted by the cells. Actually, up to 1 mm gap -between the two gels- closure was visualized achieved by such process.

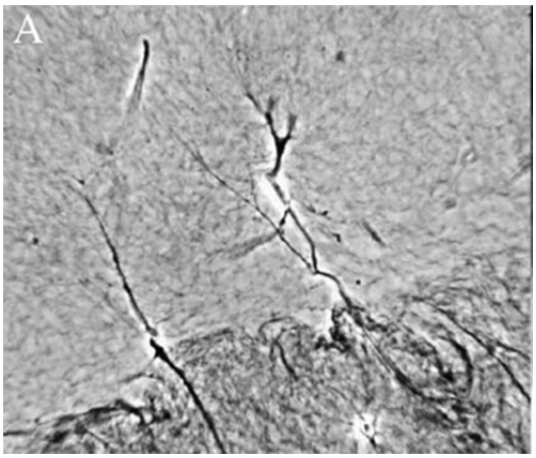

Fig. 1.9. Migrating dendritic fibroblasts. H&E-stained migrating fibroblasts in nested collagen matrices. Image from Grinnell et al. [71].

In addition, transmigration through collagen-fibrin interfaces has also been pursued. Greiling et al. [72] embedded fibroblast-containing contracted collagen hydrogels into fibrin. Since the number of migrating cells decreased upon removal of fibronectin (FN) from either gels, they demonstrated that FN is required within both gels for fibroblast transmigration from the collagenous stromal into the fibrin clots. Likewise, as shown in Fig. 1.10, Shreiber et al. [47] performed a chemotaxis experiment by inducing rat dermal fibroblast migration with PDGF-BB. In their set-up, a GF-containing fibrin gel was placed next to the cell-containing collagen gel. Besides, the gels were mechanically stressed or not. In short, they suggested that a complex response of the fibroblasts may exist since traction forces of the cells appeared to be dependent on gel type and stress-state. In this regard, Rouillard and Holmes [73] have underlined the applied uniaxial mechanical restraint to increase the efficiency of the transmigrating fibroblasts. To do so, they designed a fibrin-filled slit within fibroblast-populated collagen gel, as a wound representation.

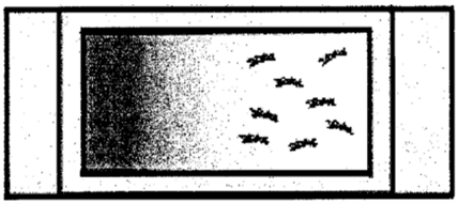

Fig. 1.10. Collagen to fibrin transmigration by PDGF-BB. Scheme of the experimental set-up employed by Shreiber et al. [47].

Multiple modes govern 3D migration and a great range of protrusive structures have been proposed [26, 74]. This variability has been pointed out to be context-dependent, by adapting dynamically the migration mode to local architecture, proteolytic and mechanical properties [44, 75–77]. Actually, distinct signaling pathways and molecular mechanisms are required for its regulation [78]. As said beforehand, cell migration of slow-moving mesenchymal cells -such as fibroblasts- is directed by multi-spatial cues or taxis phenomena [78].

Although mesenchymal movement has been considered mainly lamellipodial and has not yet been associated with blebbing, 3D environments allow motility under minimal adhesion forces [74, 79]. Actually, employing collagen lattices, Jiang and Grinnell [61] suggested that the entanglement of the fibroblast dendritic extensions to the matrix represents a novel integrin-independent mechanism of cell anchorage that uniquely depends on the three-dimensional character of the matrix, which is shown in Fig. 1.11. Additionally, Petrie et al. [75] showed that fibroblasts in 3D were able to change between lamellipodial and lobopodial (with more cylindrical protrusions) migration in function on the elasticity of the substrate. The non-linear elastic collagen hydrogels drove the cells to express a lamellipodial-based motility, whereas those within linear-elastic dermal explants and cell-derived matrix (CDM) substrates behaved with a

lobopodial-based migration. This finding pointed out that fibroblasts use at least two distinct modes of 3D cell migration.

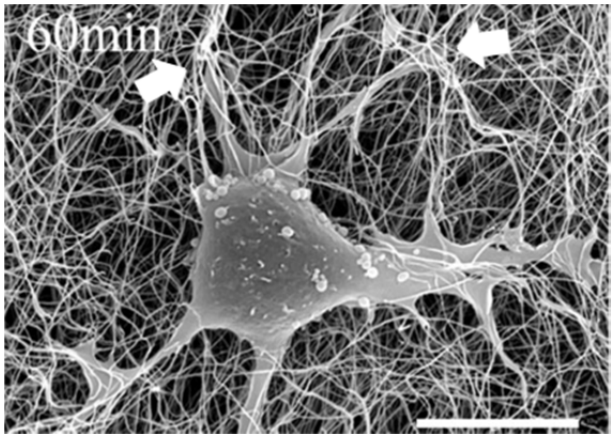

Fig. 1.11. Entanglement of collagen fibrils with fibroblast dendritic extensions. The white arrows marked in the SEM image denote entanglement points. Scale bar corresponds to 10 μm. Image from Jiang and Grinnell [61].

In this regard, as to the interpretation that biophysical microenvironment has a direct impact on fibroblast response, Miron-Mendoza et al. [80] considered the specific role of matrix stiffness and pore-size. Indeed, they designed collagen lattices with varied pore-sizes by raging the collagen concentration between 1-4 $mg \cdot ml^{-1}$. Moreover, they employed cross-linked and uncross-linked matrices to perform the experiments. Hence, by characterizing the stiffness and pore-size of the gels, and assessing the migratory trend of the fibroblasts in nested collagen matrices, they demonstrated that migration was stiffness-independent, but influenced by the pore-size. In these results, they measured a maximal cell migration at 2 $mg \cdot ml^{-1}$ for constrained matrices.

Relevant progress has been done approaching the 3D fibroblast mechanics. However, since it is a very complex phenomenon in which multiple environmental cues are involved, there are still a lot of biological questions

opened. Indeed, mimicking the *in vivo* cellular-niche, by means of assays that allow greater control and versatility during the studies, could help addressing those unclear issues stemming from the microenvironmental complexity.

1.1.5 Microfluidics as a novel technology for wound healing

The incorporation of microfluidics to *in vitro* assays directed to study basic cellular processes has overtaken several difficulties that large-scale *in vitro* experiments have implied, such as the limited control of the many potentially important physiological factors. Microfluidics presents unique opportunities for the rational design of novel physiologically-relevant *in vitro* models, leading to a transformation of the mechanotransduction studies. Actually, microfluidic systems allow greater control and versatility while designing and performing experiments by combining multiple stimuli and, hence, creating more *in vivo*-like environments. Additionally, real time monitorization is also facilitated, so qualitative and quantitative studies in 3D environments can be performed.

Due to all these advantages, microfluidic platforms have risen and been applied for studying 3D migration events [81, 82], addressing multiple biological questions involved in cell migration. Numerous works have been directed to approach pathophysiological 3D processes comprehending key perspectives on angiogenesis [83, 84], metastasis [85, 86] and neuroscience [87, 88], among others. As an example, fibrosarcoma cells invading the endothelium sheet are shown in Fig. 1.12.

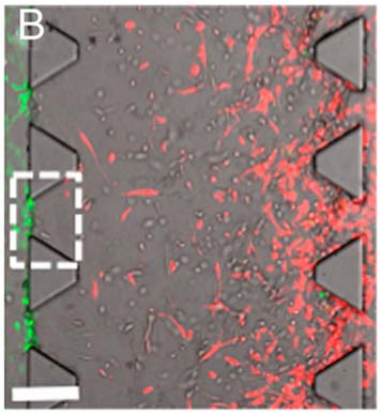

Fig. 1.12. Fibrosarcoma invasion into the endothelium. Fibrosarcoma cells (HT1080, red) invade through the ECM (gray) toward the endothelium (MVEC, green). Scale bar: 300 μm. Image published by Zervantonakis et al. [86].

Wound healing approaches have also been studied by means of these microdevices, focusing on 2D epithelial closure, since epithelial sheet migratory dynamics in physiology also corresponds to a 2D-manner. As shown in Fig. 1.13, Murrell et al. [89] employed multiple laminar flows to selectively cleave cells enzymatically, allowing to generate a damage-free denudation. They concluded that free space alone is sufficient to induce movement of the epithelial sheet; hence, decoupling the contribution of free space and cell damage, typical of conventional wound healing scratch assays. Likewise, in another microfluidic-based enzymatically generated wound model, Felder et al. [90] tested the effect of hepatocyte growth factor (HGF) in wounded epithelium.

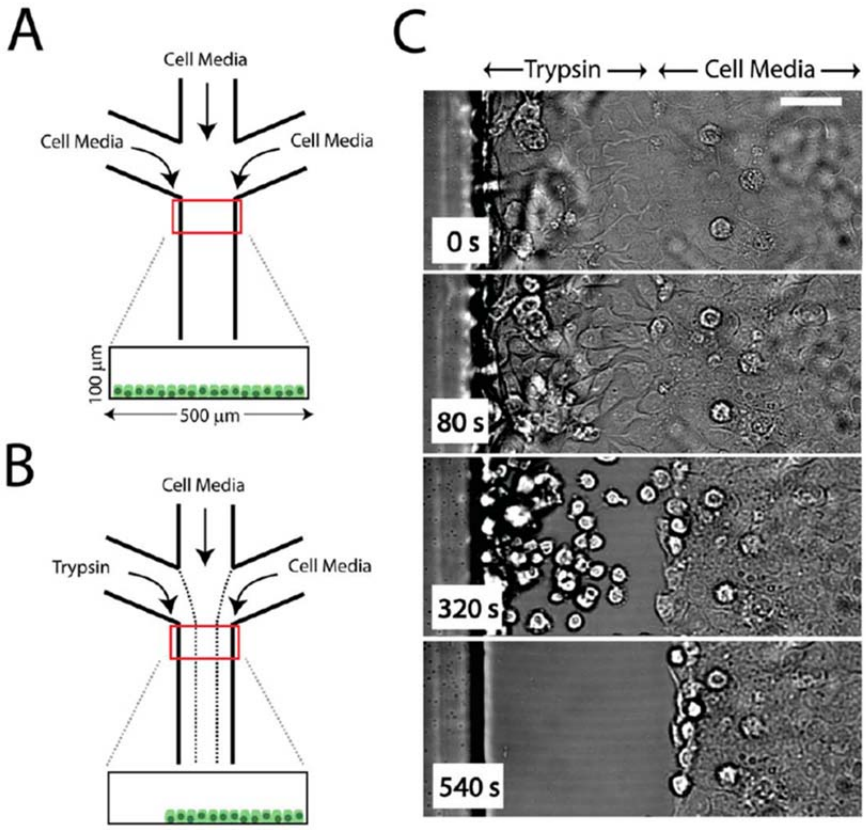

Fig. 1.13. Enzymatic denudation of epithelial sheet. (A) Schematic of the experimental set-up. Three inlets supply cell media to an epithelial sheet cultured in the 500mm wide, 100mm high channels. This is done under no flow. (B) After cells have reached confluence, 15 ml·min^{-1} flow is applied, leading to three separated laminar streams. One stream contains 0.05% trypsin, while the other two contain cell media. This cleaves cells from the channel as shown in (C). On average, cleavage takes 5 min. Images are acquired in brightfield. The figure and caption are from Murrell et al. [89].

As far as we know, 3D fibroblast migration has not been studied by using microfluidic devices. However, microfluidic platforms are a useful tool for adding new insight into the underlying mechanisms by controlling the microenvironmental complexity and, hence, the taxis phenomena that determine 3D fibroblast migration.

1.2 Objectives

The Thesis focuses on studying the major underlying mechanisms of 3D fibroblast migration and the principal microenvironmental cues involved during the early stage of wound healing, when recruitment of the fibroblasts -by chemotaxis of PDGF-BB- to the clotted wound occurs. To do so, two physiologically-relevant matrices, collagen I and fibrin, have been chosen and confined within microfluidic platforms in order to quantify fibroblast migration in 3D. In addition, by means of comparative analysis, we characterize integrally both matrices from a biophysical and biochemical point of view.

Hence, the research contains a wide range of material techniques for the development of hydrogel characterization, as well as microfluidic approaches for the 3D cell culture and migration assays. Seeking to achieve the beforehand mentioned main goal, the research has been divided into partial objectives in order to be fulfilled during the Thesis.

1. *To carry out the fine-tuning of the general and microfluidic techniques.* Among them, the main transversal procedures are cited below:

    - *Design and fabrication of microfluidic platforms for 3D cellular studies.* A device made by combining soft lithography and replica molding techniques. Akin the geometry, the central micropillars allow confining the hydrogels within them to perform versatile experiments.

    - *Hydrogel preparation and cell seeding.* Physiological recipes for collagen I and fibrin hydrogel preparations are designed. Their composition, as well as the yielding properties influence the cellular response during the assays.

- *Cell tracking and staining.* Microfluidic platforms allow for direct visualization of cells within it. In fact, live as well as fixed imaging is set-up taking advantage of it.

2. To fulfill an integral and comparative biophysical and biomechanical characterization of collagen and fibrin gel-scaffolds. In order to define these sorts of microenvironmental cues that would impact on fibroblast migration, the microstructure is analyzed by Scanning Electron Microscopy and Confocal Reflectance, the resistance to flow is measured by permeability experiments and rheology is employed for the biomechanical response evaluation.

3. To stablish and quantify the chemical conditioning in collagen and fibrin networks. It is required for the induced physiologically-relevant biochemical signaling, in which cells will be embedded during the 3D *in vitro* assays. In this regard, chemical gradients are generated and Enzyme-Linked ImmunoSorbent Assays (ELISAs) as well as computational modelling are carried out for determining their spatial distribution through the microdevices.

4. To elucidate the 3D migratory mechanisms of fibroblasts. Adopting the hydrogel-containing microsystems, diverse *in vitro* migration assays are performed employing collagen and fibrin gels. A chemical gradient of a chemoattractant (PDGF-BB) is generated through the hydrogels. In this way, and taking advantage of the biophysical and biochemical characterization accomplished beforehand, new insights are added to the fibroblast migration knowledge by analyzing the role of non-muscle myosin II.

Finally, we find it important to highlight that, within the Thesis period, not only did the author of the present work achieve the listed objectives, but also co-managed the creation and set-up of the new Mechanobiology Laboratory of the University of Zaragoza. Although, traditionally, the M2BE Group expertise has been simulation-based, currently our group incorporates an experimental research line as well. In this context, this Thesis has been the leading outcome of this novel laboratory.

1.3 Outline

In order to introduce the above mentioned aims in an organized manner, the content of the Thesis is divided into seven chapters and an appendix. Therefore, although each part is treated as a whole, all of them are required to be considered within the overall picture. The content of each chapter is summarized in this section.

- *Chapter 1.* Being the current introductory chapter, the global framework of this Thesis is provided. The background describes the state of the art and motivation of the Thesis, to proceed outlining its objectives and chapter structure.
- *Chapter 2.* The main transversal methods used during this work are described in this chapter. The microfluidic device fabrication as well as hydrogel preparation and cell seeding, among others, are detailed.
- *Chapter 3.* An integral and comparative characterization of the biophysical and biomechanical properties of the hydrogels is presented. In this chapter, the specific motivation of such

characterization, the required materials and methods, the obtained results and a final discussion are included.

- *Chapter 4.* The transport phenomena arising from the establishment of chemical gradients -including diffusion and binding- through the hydrogel-containing microfluidic platforms is studied. In these results, the chemotactic as well as haptotactic cues that are induced, within collagen and fibrin networks, in such heterogeneous chemical environments are elucidated. Hence, and introductory background of the topic, the employed materials and methods, the outcomes and a concluding discussion are detailed within this chapter.

- *Chapter 5.* The migration experiments performed using the microfluidic platforms are presented. Varied chemical conditions have been employed in order to quantify and compare the fibroblast migratory response in collagen and fibrin lattices. In order to detail the implemented *in vitro* experiments, in this chapter, an introductory overview, descriptive section for the applied materials and methods and the final discussion are incorporated.

- *Chapter 6.* A summary of the concluding remarks of the Thesis and brief suggestions with respect to the future research lines are combined. The yielded publications are also cited within the chapter.

- *Chapter 7.* The main conclusions, as well as the beforehand proposed future work, written in Spanish are included.

- *Appendix A.* It comprises detailed protocols cited throughout the document.

Chapter 2
Development of microfluidic systems for 3D cellular studies

Microfluidics is a means able to control the microenvironmental complexity. Actually, it offers versatility for a rational design of the experiments and real-time visualization allowing quantification. As said beforehand, in this work we have applied these platforms in order to study fibroblast migration in 3D. Previously, and framed within this Thesis, the laboratory was set-up by equipment purchase and installation. During its management, several procedures were also fine-tuned during this period in order to stablish the microfluidic techniques within the newly-built laboratory. Hence, in this chapter the major transversal procedures are detailed, i.e., the fabrication of the devices and the hydrogel preparation.

2.1 The microfluidic platform

The microdevice yields from the combination of soft lithography and replica molding techniques; this synergy provides versatility. The SU8 mold obtained by photolithography is reused to replica mold against the polydimethylsiloxane (PDMS) multiple times. Besides, the photolithography allows for flexibility while designing the desired geometry -along with time and cost minimization-, so modifications of the motives are easily overtaken.

2.1.1 Microdevice design and fabrication

The design of the microfluidic platform, shown in Fig. 2.1, comprises in the central region of the geometry a gel-cage, in which the hydrogel is pipetted using the auxiliary channels. The micropillars that enclose the area are responsible, by hydrophobic surface tension, to retain the gel solution while being injected and to keep it confined once the network is polymerized, without further spreading to the subsequent compartments. Additionally, at both sides of the gel, two main channels are in direct contact to it, through which condition media is inserted. Likewise, cells could also be included along with the media or embedded within the hydrogel solution, depending on the experimental design.

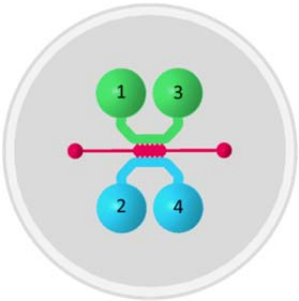

Fig. 2.1. The microfluidic device. A central hydrogel-cavity (pink) is comprised between the two main media-channels, addition and opposite ones (green and blue). The inlet ports are numbered.

With regard to the fabrication process of the device, the schematic steps are shown in Fig. 2.2. Briefly, the microfluidic device is formed by bonding a geometry-containing polymeric PDMS-layer to a glass coverslip. To do so, a positive-relief SU8 stamp is patterned with the desired geometry by soft lithography, which detailed protocol is included in Appendix A Protocol A.1. The stamp serves as mold to pour and cure the polymer onto it (see Fig. 2.3), so the PDMS-side contains etched the desired geometry within. The "open geometry" is closed and brought to a channel-layout by irreversibly bonding it against a coverslip by using plasma treatment. The detailed protocol of the replica molding and bonding methods are detailed below.

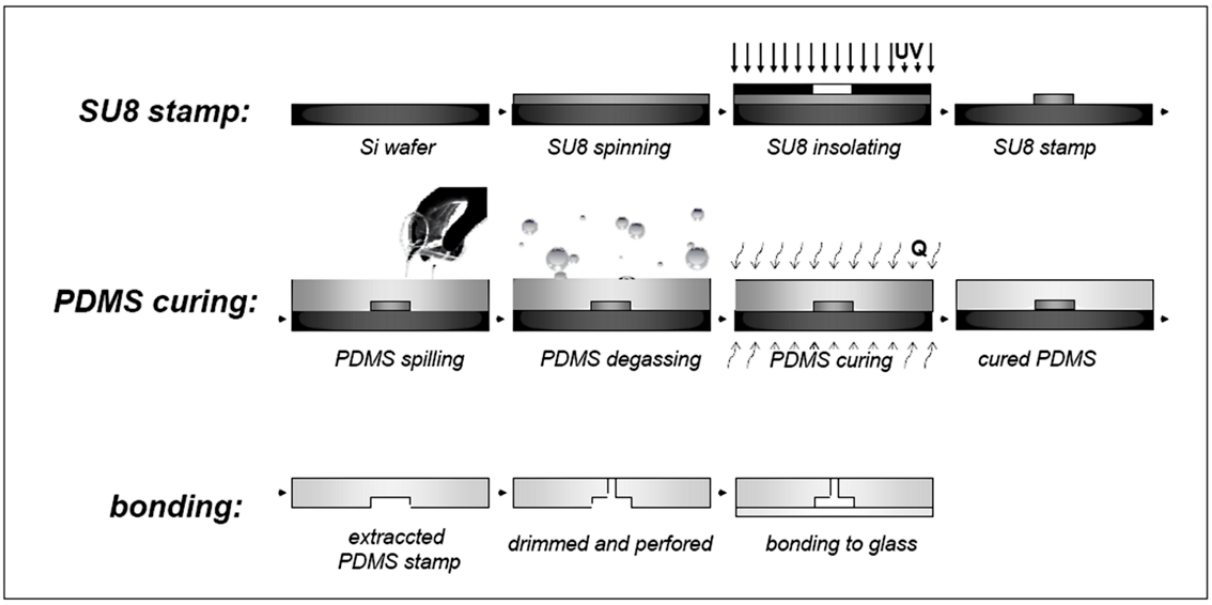

Fig. 2.2. Scheme of the fabrication process of the device. Soft photolithography and replica molding are required for the procedure [91].

Reagents and materials:

- SU8-mold wafer with the desired geometry and depth.
- 35 mm glass-bottom petri dishes from Ibidi (81158).

- Polydimethylsiloxane (PDMS) from Dow Corning GmbH (Sylgard 184): store at RT.
- Perfluorinated trichlorosilane from UCT Specialties (T2492-KG): store at RT.
- Poly-D-lysine hydrobromide (PDL) from Sigma (P7886): store at -20ºC.
- Cell culture grade water from LONZA (17-724): store at RT.

Reagent preparation:

- PDL:
    - Mix 100 mg of PDL with 100 ml of cell culture grade water with a stirring bar for 30 mins.
    - Then filter and aliquot it.
    - Aliquots should be stored at -20ºC and defrost at 37ºC before their use.

Procedure:

- The SU8-mold should be silanized* by placing the wafer inside a desiccator for 2 hours with 10 ul of perfluorinated trichlorosilane; in this manner, the irreversible bonding of PDMS to wafer is avoided.
- Then, PDMS should be mixed by 10:1 base to curing agent ratio.
- After degassing the liquid polymer, it is poured onto the silicon wafer (see Fig. 2.3).
- It should be degassed again and placed into the oven at 80ºC overnight.
- In order to extract the replica molded-layer of PDMS, it is required to allow the wafer to cool down and relax.
- The first PDMS replica after the silanization should be removed and discarded since its residues are cytotoxic.
- The subsequent layers are made analogously.

- Once the PDMS layer is extracted, it is trimmed with an 18 mm diameter punch and perforated the gel and the main channel inlet-ports with 1.5 and 4 mm biopsy punches, respectively.
- Afterwards, the polymeric layers are cleaned by a residue-free tape and autoclaved with a humid cycle.
- Next, the PDMS layers are placed into a closed box and autoclaved again with a dry cycle.
- They are put into the oven at 80ºC overnight in order to dry them.
- Once they have reached the room temperature, the PDMS layers along with 35 mm-glass bottom petri dishes are plasma treated and bonded irreversibly.
- Right after, 40 ul of PDL solution is added into each device in sterile conditions and kept in the incubator for at least 4 hours. This step will enhance the hydrogel-PDMS surface attachment.
- Then, they should be thoroughly washed with cell culture grade water and maintained in the oven at 80 ºC for 36 hours approximately.
- Finally, the devices are ready for their use once they are allowed to cool down. It is recommended to use them within the following 10 days.

Note: The washing process should ensure to profoundly clean all the walls of the devices. If not, cytotoxic effects arise from the remaining PDL.

*Silanization should be performed after 40 uses of the mold, approximately.

Fig. 2.3. PDMS pouring. The liquid polymer is spilled onto the SU8 mold in order to let it cast patterned, after degassing it.

2.1.2 Hydrogel preparation and cell seeding

Collagen I and fibrin gels were chosen as natural gel-scaffolds in order to perform comparative analyses while studying diverse aspects, e.g., biophysico-chemical properties and 3D fibroblast migration. In order to achieve *in vivo*-like microenvironments, physiological polymerization conditions were adopted in order to ensure the closest biomimetic self-assembly of the matrices and optimal cellular conditioning. In these specifications, the fine-tuned procedures for the hydrogels have derived as follows.

Collagen gels and cell seeding. Hydrogel made of collagen I was chosen to model the connective tissue. The protein content was set at 2 $mg \cdot ml^{-1}$ and the pH at 7.4, while polymerization temperature was held at 37 ºC. In this procedure, we followed the methodology proposed by Shin et al. [92], as specified in the following protocol.

Reagents:

- Collagen type I from Becton Dickinson (BDAA354236): store at 4ºC.
- DPBS 10x +Ca +Mg from Gibco (14080-048): store at 4ºC.
- Phenol red sodium salt from Sigma (114537): store at RT.
- NaOH from Sigma (655104): store at RT.
- Cell culture grade water from LONZA (17-724): store at RT.
- Medium of interest depending on the cells in use.

Reagent preparation:

- Collagen type I:
    - It is critical to store the collagen always at 4ºC, in order to keep the quality of the product. Due to this, minimize the time in which the collagen will be out of the fridge. During the manipulation time it should be kept on ice.
- PBS10x with phenol:
    - The concentration of the phenol red chosen is the one used for DMEM 10x from Sigma (D2429): 0.159 g/l.
    - Warm the DPBS 10x in a water bath for several hours and shake it in order to avoid any precipitation.
    - Pour 0.0636 g into 400 ml of DPBS 10x and mix it thoroughly.
    - Filter and aliquot it.
    - The dissolution could be kept at RT for 6 months tightly closed.
- 0.5 N NaOH dissolution:
    - Little by little, put 5g of NaOH into 250 ml of cell culture grade water. It is important to do it gradually since the reaction is exothermic.
    - Mix it with a stirring bar until the dissolution appears to be clear.
    - Filter and aliquot it.

- The dissolution could be kept at RT for 6 months tightly closed.

Procedure:

- A humidity box is required. For example, it is appropriate to use a pipette tip box (without tips, including the rack) with deionized water; then autoclave it and keep it overnight in the incubator; so the humid box reaches 37ºC in sterile conditions.
- Vortex slightly all the reagents before each use and keep them over ice for the whole procedure. They should be put on ice 5 minutes before the beginning of their manipulation.
- Include a 500 ul eppendorf tube on ice in advance of the procedure.
- A final volume of 200ul of collagen gel is prepared at pH 7.4.
- Within the total volume these proportions should be kept:
  - 10% of DPBS 10x w phenol
  - 30% of media*
  - collagen type I at 2 mg/ml
  - the amount of NaOH to bring the mixture up to pH 7.4
  - the rest of the volume should be cell culture grade water
- Iterations should be done until the desired pH** is reached for the gel.
- As an example, a possible reagent quantity is shown below. Notice that the order of the components while adding into the tube should be maintained.
- First, these portions are added:
  - 20 ul of DPBS 10x w phenol
  - 8.2 ul of NaOH dissolution
  - 12 ul of cell culture grade water

- Then, the collagen –which is in the fridge- is placed over ice and the corresponding amount is added. As soon as it is mixed gently, the tube should be brought back to ice:
    - 99.8 ul of collagen type I at 4.01 mg/ml
- Right after, the chilled media* is added to the mixture carefully and the tube is placed again over ice:
    - 60 ul of media* (the media volume can be varied conveniently; so the water amount should be adjusted accordingly)
- Bring the humidity box into the hood quickly.
- At this point, as the samples are ready by injecting the gel solution into the devices (see Fig. 2.4), they should be placed into the humidity box.
- Once, all the samples are ready, the humidity box should be kept in the incubator for 20 mins***. The time is set-up for a maximum gel volume of 20 ul; for bigger gels the time should be increased. For example, gels of 300 ul (employed for other purposes) are maintained for 1 hour approximately.
- Finally, the samples are hydrated with media at 37ºC and placed in sterile dishes to keep them in the incubator. The gel should be kept for 12-24 hours**** in the incubator to allow the stabilization of the gel.

Note1: It has been probed that all kind of DMEM generate a sort of precipitates which can be identified as black spots throughout the gel while looking with the microscope. Thus, and due to the suitability of the cells in use (NHDF), FGM-2 has been used to grow the cells and make the gels.

Note2: If serum is required for supplementing the media, the serum is centrifuged at 3000 rpm for 20 mins in order to avoid some precipitates to be seen while carrying out the experiments. However, it is usual to still have a few small spots when serum or other reagents are added.

Note3: Depending on the cell type and experimental design, they may be adjusted some features of the gel such as the pH or/and collagen concentration or/and cell concentration. It is important to remark that by changing those biochemical conditions, the microstructural and biomechanical properties of the gel will also be affected.

*In the case that cells are wanted to be embedded within the gel, the pellet that turns out from the regular passage is reconstituted (refer to Appendix A Protocol A.2); to do so, media is added up to the desired concentration. Thus, while adding 60 ul of this resuspension to the gel mixture, a concentration of approximately 0.45-0.5·10^6 cells/ml within the final gel should result. The suspension should be kept on ice for few minutes before its addition to the gel volume in order to avoid prepolymerization.

**For this purpose, a pocket pH-meter is used (from HACH, H138). However, any other appropriate pH-meter could be used. Moreover, as a reference, the color code shown below could also be used:

***For those gels injected within 300 um-deep microfluidic devices, in order to ensure the three-dimensionality of the cellular arrangement all over the z-axis, they should be flipped several times as follows: 3.5 mins, 8.5 mins, 13.5 mins, 18.5 mins. Each time point is determined with respect to 0 mins point, which is the moment in which the device is placed regularly within the humid box. At time point 20 mins the gel should be hydrated.

**** If the cells are going to be placed on top of the gel, they could be spread before the full stabilization of the gel so it could stabilizes the whole set-up together.

Fig. 2.4. Hydrogel injection. Once the gel solution is readily mixed and placed on ice, the necessary amount is pipetted into the microfluidic device.

Fibrin gels and cell seeding. Since fibrin is the major component of the clot, hydrogels made of such protein have been used in order to mimic it. In this representation, as indicated in Chapter 3, physiological concentration values of each constituent have been applied. Hence, out of the final volume, fibrinogen was included at 3.3 $mg \cdot ml^{-1}$, along with 1 $U \cdot ml^{-1}$ of FXIII, 1 $U \cdot ml^{-1}$ of thrombin and 5 mM of $CaCl_2$. In addition, during the preparation of the gels, a pH of 7.4 and a temperature of 37ºC were maintained as detailed in the protocol below.

Reagents:

- Human Fibrinogen (plasminogen, fibronectin, factor XIII depleted) from American Diagnostica (Product Nº ADG448/1 or ADG448): store at 4ºC.
- Human Alpha-Thrombin from American Diagnostica (Product Nº 470HT): store at -20ºC.
- Human factor XIII from American Diagnostica (Product Nº 413): store at -20ºC.
- Calcium chloride from Sigma (ref. C1016): store at RT.
- Cell culture grade water from Lonza (ref. 17-724F): store at RT.
- Medium of interest depending on the cells in use.

Reagent preparation:

- Fibrinogen reconstitution:
  - Add 2 ml of water to the vial
  - Keep it in a water bath at 37ºC for 30 mins -each 10 mins mix it by hand carefully-. It should be transparent and homogeneous by the end.
  - Centrifuge the viscous solution at 4ºC and 3000rpm for 10 mins
  - Aliquot it as convenient and freeze it at -80ºC. Notice that each aliquot should be thawed not more than once
- Thrombin:
  - It should be kept always at -20ºC; while manipulating should be kept over ice. It will not freeze because of the solvent of the dilution (50% (v/v) glycerol/water).
  - For a vial at 21459.23 U/ml: since a lower concentration is required for the solution, it should be diluted within the same solvent to 60 U/ml (by mixing 1 ul from the vial with 356.6 ul of solvent, for example). It is important to prepare fresh dilution for each set of gels.

- Factor XIII:
  - It should be kept always at -20ºC; and manipulating should be kept on ice. It will not freeze because of the solvent of the dilution (50% (v/v) glycerol/water and 0.5 mM EDTA added).
  - For a vial at 2000 ug/ml: since a lower concentration is required for the solution, it should be diluted within the same solvent to 660 ug/ml (by mixing 2 ul from the vial with 4.06 ul of solvent, for example). It is important to use fresh dilutions for correct polymerization.
- Calcium chloride:
  - It is dissolved in cell culture grade water at 0.009 g/ml.
  - In order to complete the dissolution, vortex and filter it.

Procedure:

- A humidity box will be required. For example, it is appropriate to use a pipette tip box (without tips, including the rack) with deionized water; then autoclave it and keep it overnight in the incubator; so the humid box reaches 37ºC in sterile conditions.
- Keep all the reagents until the end of the procedure on ice.
- Put in the water bath the fibrinogen aliquot to defrost it.
- Meanwhile, FXIII, thromin, $CaCl_2$ and media should be put on ice.
- Two transparent eppendorf (500ml) tubes (*a* and *b*) are needed per gel. Place all the eppendorf tubes that will be necessary over ice. As an example, this protocol will be detailed for the preparation of 8 gels; so 8 tubes from each type (*a* and *b*) are required.
- In addition, another two Eppendorf (500ml) tubes (*t1* and *t2*) are also required to prepare the gel solutions *1* and *2*.

- Once the fibrinogen has been gently thawed (it should be transparent) place it over ice too.
- Add 4.5 ul FXIII to tube *t1*.
- Add 4 ul of thrombin to tube *t2*.
- Then, include to tube *t2* 15.2 ul of $CaCl_2$ and mix it carefully.
- Add 44.55 ul of fibrinogen to tube *t1*, mixing it carefully to avoid bubbles.
- Next, supplement the tube *t2* with 133.6 ul of media*.
- Once solution *1* (tube *t1*) and solution *2* (tube *t2*) are ready, pipette them as below:
    - 5.45 ul of solution *1* into each *a* tube
    - 9.55 ul of solution *2* into each *b* tube
- Soon after, for each gel-sample the following steps should be followed:
    - Fix a 20 ul pipette at 15 ul** and take all the content from tube *b*.
    - All at once, and as close to the ice as possible, mix carefully this content with the one within the corresponding tube *a* and inject de gel where desired as soon as possible.
    - In order to allow the gel to polymerize, keep it for 10 minutes*** inside the humid box placed in the hood at RT.
    - At this point, take the gel out of the humidity box and place it within a convenient container. Hydrate the gel with media at 37ºC and keep it within the incubator for 12-24 hours**** to allow for the stabilization of the gel.

Note1: notice that the indicated volumes are subjected to the initial concentrations of the reagents. If they are modified, the volumes should be adapted too. Finally, the individual concentration of the components has been

selected to be a physiologically-relevant representation, so the following final concentrations should be comprised within the gel as below:

- 3.3 mg/ml of fibrinogen
- 22 ug/ml of FXIII
- 1 U/ml of thrombin
- 5 mM of $CaCl_2$
- 55.67 % (v/v) of media

Note2: For the fine-tuning of this protocol, fibroblasts (NHDF) has been used (refer to protocol A.2 in Appendix A). To do so, FGM2 Bullet-Kit as cell culture media has been used. If another type of media is required, it has to be noted that the content of serum could affect the polymerization process of the gels due to the amount of plasma constituents.

Note3: If serum is required for supplementing the media, the serum is centrifuged at 3000 rpm for 20 mins in order to avoid some precipitates to be seen while carrying out the experiments. However, it is usual to still have a few small spots when serum or other reagents are added.

Note4: Depending on the cell type and experimental design, they may be adjusted some features of the gel such as reagent concentration or/and cell concentration. It is important to remark that by changing those biochemical conditions, the microstructural and biomechanical properties of the gel will also be affected.

*****In case the cells are wanted to be embedded within the gel, the harvested pellet that turns out from the regular passage is reconstituted; to do so, media is added up to the desired concentration. Thus, by adding 133.6 ul of this

resuspension to the solution *t2*, a concentration of 0.45-0.5·10^6 cells/ml within the each final gel should result.

**This value will determine the final volume of the final gel. If a bigger gel is needed, the pipette could be fixed to another volume and the content of the *b* tube taken carefully to the mix it with the *a* tube up to the total volume of the fixed volume. Since the polymerization is so fast, the last step should be done as soon as possible.

*** For those gels injected within 300 um-deep microfluidic devices, in order to ensure the three-dimensionality of the cellular arrangement all over the z-axis, the devices should be flipped several times as follows: 5 secs, 15 secs, 35 secs, 1 min, 2 mins, 4 mins, 7 mins. Each time point is determined with respect to 0 secs point, which is the moment in which the device is placed regularly within the humid box. At time point 10 mins the gel should be hydrated (see Fig. 2.5).

**** If the cells are going to be placed on the top of the gel, they could be spread before the full stabilization of the gel so it could stabilizes the whole set-up together.

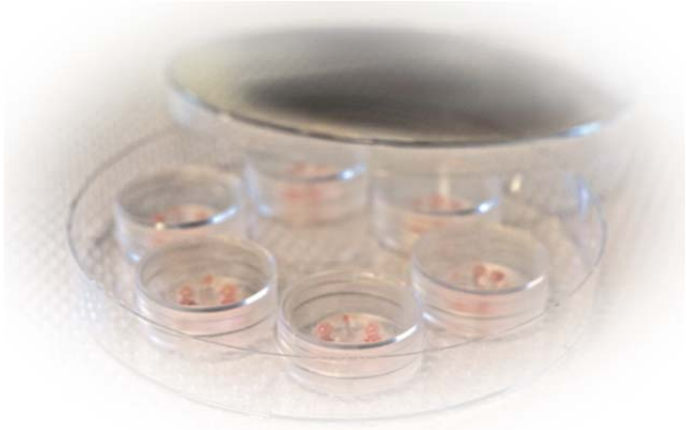

Fig. 2.5. Microfluidic devices ready to run the experiments. Once hydrated, they are kept within a petri dish in the incubator to allow for stabilization.

2.2 Microenvironmental design

The biological machines allow for the simultaneous control of multiple environmental properties. A biomimetic definition of the biophysical and biochemical properties has been crucial to the development of this work, since they are potentially important factors impacting on the mechanotransduction. Hence, fibroblasts were allowed to migrate through collagen and fibrin matrices with known microenvironmental cues, as shown in next sections.

2.2.1 Biophysical and biomechanical characterization of hydrogels

In order to elucidate the biophysical and biomechanical factors affecting in the migration experiments, an integral characterization of such properties of collagen and fibrin hydrogels was carried out. On the one hand, Scanning Electron Microscopy (SEM) and Confocal Reflection Imaging have been employed in order to determine the fibrillar arrangement. Additionally, pressure gradient generation has allowed for permeability measurements. Likewise, rheological experiments have revealed the

mechanical response of the networks. The required methodology for these tests is described in this section.

Scanning Electron Microscopy (SEM). In order to gain microstructural information of the networks, Scanning Electron Microscopy (SEM) has been used. This technique has large depth of field and uses electrons instead of light to form images. Hence, provides topographical high-resolution rich information of the samples. The protocol detailed below has been followed in order to visualize the hydrogels (also summarized in Chapter 3 Section 3.2).

Reagents:

- Glutaraldehyde from Sigma.
- Osmium tetroxide EM grade from Ted Pella, Inc.

Procedure:

- The hydrogels should be polymerized within tube-rings fabricated by PDMS and the rings should be pretreated with 5% BSA/PBS overnight.
- Once the hydrogels are allowed to stabilize for 24 hours within the incubator, they are ready for their processing.
- They are fixed with 2.5% glutaraldehyde overnight at 4ºC, followed by 1% osmium tetroxide EM grade for 1 hour at room temperature.
- Dehydration in 30%, 50%, 70%, 80%, and 95% ethanol solutions for 10 mins are performed.
- Gels were freeze-fractured in liquid nitrogen before a final dehydration step in 100% ethanol.

- Next, they are critical point-dried.
- The samples should be sputter-coated with gold-palladium for 4 minutes and visualized afterwards.

Pressure gradient generation: permeability quantification. The resistance to flow that collagen and fibrin hydrogels exert was measured. Darcy's Law determines the relation between the pressure difference and the permeability (as demonstrated in Chapter 3 Section 3.2). Therefore, the hydrogels within the microdevices were exposed to a pressure gradient and the permeability was quantified by applying the experimental set-up detailed within this subsection.

Procedure:

- The hydrogels are allowed to polymerize within the microfluidic devices.
- After stabilized for 24 hours in the incubator, the samples are ready for the experimental set-up.
- Medium-tubes are inserted into the channel reservoirs (refer to Fig. 2.6):
    - First, tube 1 and 4 should be inserted carefully.
    - Once they are tightly sealed, tubes 2 and 3 are inserted.
    - In order to properly seal the tube-reservoir joints, it is also helpful to add a little bit of silicone on it.
- Then, the tubes should be filled thoroughly pipetting in order to stablish the desired pressure difference among both sides of the gel. Note that 1 cm-H2O difference would be equivalent, rounded, to 100 Pa.

- The pressure drop is traced by measuring over time (e.g., each 15 minutes) the media column high difference.
- By fitting the experimental points to Darcy's law, the permeability value (K) is obtained, as detailed in Chapter 3 Section 3.2.

Fig. 2.6. Application of pressure gradient. It is employed for measuring the permeability of the scaffold hydrogels.

Rheological experiments. The objective of the rheological tests was to determine the mechanical response of the hydrogels. Hence, we quantified strain sweeps and observed how the shear moduli changed with varying strain. A general procedure is shown below and additional specific features of the assays are included in Chapter 3 Section 3.2.

Procedure:

- The samples are mixed on ice and pipetted on the rheometer plate by filling its gap, as shown in Fig. 2.7.
- To avoid any evaporation, the shear gap should be covered with oil.
- The curing reaction is allowed to perform and stabilize for 24 hours, prior to experimental procedures are begun.
- The experimental conditions should be maintained constant all over the measurements.

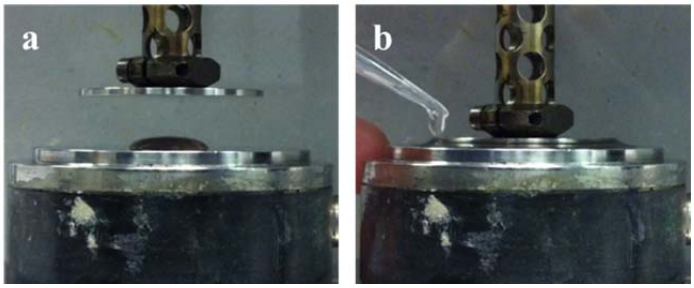

Fig. 2.7. Picture-sequence of the experimental set-up in the rheometer. The sample was pipetted on the rheometer plate (a) and after adjusting the gap, it was covered with the oil (b).

2.2.2 Chemical conditioning of hydrogels within microfluidic platforms

The genuine design of the microdevice allows for the modification and control of the chemical environment to which cells are exposed. Sometimes, it is necessary a simple media replacement for an actual cell culture or to generate an inhibition environment. Additionally, the generation of linear chemical gradients between both main channels is supported by such platforms. Indeed, distinct chemical factors have been applied to establish controlled heterogeneous distributions. In this manner, we have also quantified the nature of the spatio-temporal distribution of the compound

transport -diffusion or binding- by combination of Enzyme-Linked ImmunoSorbent Assay (ELISA, detailed in Chapter 4 Section 4.2) and computational predictive simulations.

Media replacement. Media (or other liquids) requires to be renewed or replaced for numerous procedures. The necessity for such elementary and crucial action ranges culture maintenance of the cells in 3D or media change for washing or additional intent. The following methodology indicates the recommended steps.

Reagents:

- Cell culture media (containing/not chemical factors) or any other required replacement aqueous fluid.

Procedure:

- Aspirate media from the reservoirs.
- Pipet the new media or any other desired aqueous fluid in one reservoir inlet of each side of the device: 1 and 2, for instance (refer to Fig. 2.2).
- Let the liquid to stabilize: it will first stabilize between both reservoirs of the same side of the device (between 1-3 and 2-4) and, then, it will equilibrate the pressure differences between the both main channels of the device (green and blue channels).
- While equilibrium is achieved, convective transport of the biomolecules occurs (as well as diffusive); afterwards, diffusion transport still occurs. So replacement of the nutrients and other factors is performed.

Note: in each channel a final volume of 100-140 ul is required.

Chemical gradients: dextran, PDGF-BB and TGF-β_1. In case of the media replacement, a homogeneous chemical environment within the networks is achieved. However, if an asymmetric chemical distribution is needed, the procedure should be distinct from the previous one. Hereby method describes examples of several chemical gradients generated in this work.

Reagents:

- Diluent: cell culture media FGM-2 (for GFs) or PBS (for dextran).
- Chemical factor:
  - Platelet-derived growth factor-BB (PDGF-BB) from Abcam.
  - Transforming growth factor-β_1 (TGF-β_1) from BD Biosciences.
  - 20 kDa-fluorescein isothiocyanate-dextran from Sigma-Aldrich.

Reagent preparation:

- At the desired concentration, dilute the chemical factor within the corresponding diluent.

Procedure:

- Aspirate media from the reservoirs.
- As fast as possible or simultaneously -with a multichannel pipette- the following should be done (refer to Fig. 2.2):
  - The required chemical factor is added to one reservoir of the addition channel of the device (green).
  - No-factor-containing media is added to one reservoir of the opposite channel of the device (blue).

- Wait for 30 minutes before starting any experiment in order to let for thermal equilibrium.

2.3 Cell imaging within microdevices

One of the upgrades that microfluidic-based assays have brought is the capability for direct visualization of cells within it, since a coverslip #1.5 acts as device bottom. In fact, live as well as fixed imaging was performed taking advantage of it. Particularly, time-lapse images were taken in order to track cells in phase contrast and by wide-field fluorescence, when stained with cell-tracker (refer to Appendix A Protocol A.4). In addition, for quick viability tests, the Live/Dead Kit was employed in order to stain the cells (see Appendix A Protocol A.5): it discriminates live from dead cells by simultaneously staining with green-fluorescent calcein-AM to indicate intracellular esterase activity and red-fluorescent ethidium homodimer-1 to indicate loss of plasma membrane integrity.

Immunofluorescence. Cells arranged within both fibrillar networks, collagen and fibrin, were fixed and inmunostained for vinculin and phalloidin in order to assess the focal adhesion formation and the cytoskeleton layout. The protocol is shown below.

Reagents:

- Mouse monoclonal [hVIN-1] to Vinculin antibody from Abcam (ab11194): aliquot and store it at -20ºC.
- Alexa Fluor® 488 Goat Anti-Mouse IgG (H+L) antibody from Molecular Probes (A11029): aliquot and store at -20ºC.

- Alexa Fluor® 594 Phalloidin from Molecular Probes (A12381): aliquot and store at -20ºC.
- 4% paraformaldehyde (PFA) from Affymetrix: store at 4ºC.
- Triton X-100 from Calbiochem: store at 4ºC.
- Goat serum from Sigma: aliquot and store at -20ºC.

Procedure:

- Fixation with 4% PFA
  - Aspirate the media.
  - Fix cells with 4% PFA for 18 min.
  - Wash cells 5 times with PBS for 5 min.
- Permeabilization
  - Permeabilize cells for 10 min with 0.1% Triton X-100 in PBS at room temperature.
  - Wash cells 3 times with PBS for 5 min.
- Blocking with BSA
  - Block with 5% BSA/PBS and 3% goat serum for 4 hours.
- Labeling
  - Add primary antibody anti-vinculin (1:100) in 0.5% BSA/PBS and incubate overnight at 4ºC.
  - Wash cells 5 times with PBS for 20 min with 0.5 BSA/PBS.
  - Add secondary antibody Alexa Fluor 488 (1:200) and phalloidin conjugated with TRITC (1:100) in 0.5% BSA/PBS for 3 hours at room temperature in the dark.
  - Wash cells 3 times with 0.5 BSA/PBS and 2 times with PBS.
- Image the samples as soon as possible (see Fig. 2.8). Meanwhile, store them at 4ºC in the dark hydrated with PBS.

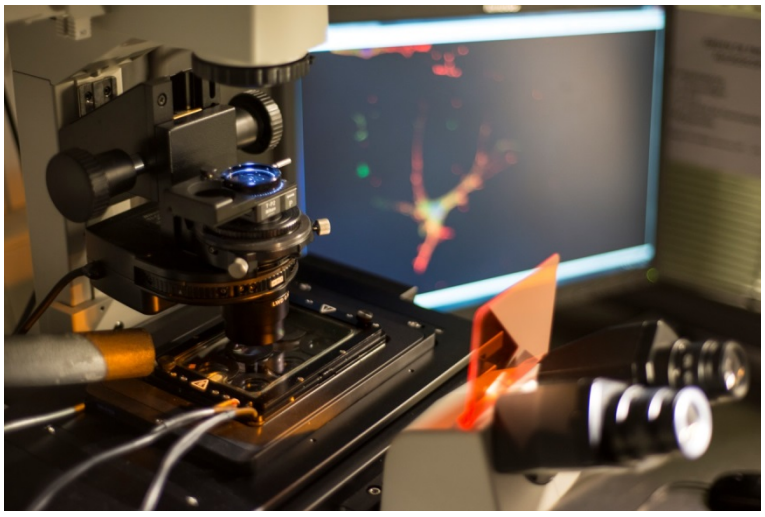

Fig. 2.8. Visualization of stained samples by confocal microscopy.

Chapter 3
A comparative biophysical characterization of collagen and fibrin hydrogels

Fibrin and collagen gels have been widely employed for *in vitro* assays as well as tissue engineering and regeneration purposes. Actually, a large amount of work has been done in order to characterize these physiologically-relevant scaffolds, mostly focusing on their microstructure and stiffness. However, the diverse preparation and testing techniques make it difficult to correlate data among all these works. Moreover, additional stress has to be done yet in order to determine permeability capabilities of the 3D networks, since it regulates diffusion of nutrients and other growth factors through the scaffolds. Therefore, in this chapter, an integral comparative study of biophysical and biomechanical properties of fibrin and collagen gels is presented. In

this manner, analogies and differences may imply major effects on the cellular behavior by inducing distinct microenvironmental cues.

3.1 Introduction

As indicated in the introductory chapter, the skin acts as the main protector against external aggressions [50]. However, it is exposed regularly to injuries. Although acute wounds are repaired systematically -hemostasis, inflammation, proliferation and remodeling-, pathological development can turn on major disabilities -fibrosis and chronic ulcers- or even death [49, 52]. Actually, non-healing wounds affect about 3 to 6 million people in the United States [53]. This makes an upper-impact initiative having a better insight into the wound healing process. Therefore, in the last years a lot of effort has been undertaken towards a thorough knowledge of such processes by means of *in vitro* assays.

Particularly, the construction of these physiologically-relevant *in vitro* models requires a profound analysis of the extracellular matrix (ECM). Actually, the ECM plays a key role modulating the mechanotransduction and cellular behavior in wound healing [93, 94]. However, sufficient stress has not been done yet for a profound analysis of the fundamental regulatory role of it.

The ECM is a complex three dimensional network that provides architectural scaffolding for cellular adhesion and migration, as well as initiates crucial biochemical and biophysicomechanical cues that are required for physiological functions such as tissue morphogenesis, differentiation and homeostasis [95–97]. In fact, multiple syndromes are caused due to pathologic compliance of the matrix, such as fibrosis or cancer development [25, 29], which show the inherent relevance of the ECM.

Indeed, while recreating the wound healing process, the most employed biomimetic scaffolds are collagen and fibrin hydrogels [60, 64, 66, 71–73]. Both proteins, collagen I and fibrinogen, have major impact during the healing process [49]. The main constituent of the clot and granulation tissue is the fibrin, while collagen I plays a dominant role within the surrounding healthy connective tissue [50]. Therefore, to understand the main physiological differences and analogies between both matrices is crucial for a better knowledge of their behavior and interaction, as well as for their use on *in vitro* assays.

Collagen I is the most abundant fibrous protein within the interstitial ECM, accounting for up to 30% of the total protein in the human body [25, 52]. Upon physiologic conditions -such as temperature, pH and ionic strength-, triple-stranded helix arrays of collagen molecules build up to form fibrils. Then, they bundle to form collagen fibers that later on self-assemble into the 3D interconnected fibrillar network [25, 98]. Actually, it is the outstanding structural element of the ECM, since collagen supplies tensile strength, regulates cell adhesion, supports taxis phenomena and migration, and directs tissue development [98].

In hemostasis, clotting cascade is activated. The formed thrombin cleavages the fibrinopeptides from the middle of the fibrinogen molecule to produce fibrin monomers [99]. Their assembly became into oligomers that lengthen to form protofibrils, which, twisted, aggregate into fibers by lateral weak interactions. The three-dimensional (3D) network is constructed as the fibers branch. Under physiological ionic conditions, factor XIII (FXIII) is activated by thrombin in presence of calcium ions. Then, the clot is stabilized by the formation of covalent bonds introduced by the activated FXIII, leading to a rigid and elastic structure [99–103]. Its mechanical properties will determine the clot's response: it has to be able to

plug to stop bleeding, whereas its structure must be strong enough to withstand the pressure of arterial blood flow [104].

Given the relevance of collagen and fibrin as natural components of the ECMs, multiple studies have analyzed the biomechanical properties of both hydrogels [104–111]. Actually, all these works have extensively studied Scanning Electron Microscopy (SEM) [112] and Confocal Reflection imaging micrographs [113–115] in order to elucidate microstructural features, such as fiber arrangement and diameter. Likewise, rheological [108, 109, 116–119], axial tensile tests [106, 107] and other techniques [120, 121], as well as assays at individual fiber level [108, 122–126], have been performed.

Most of these works have focused their studies on the global stiffness of these gels due to its crucial role on regulating many cellular processes in 2D [1, 127–130]. Nevertheless, there are several works investigating the impact on cell events of the interstitial flow [18, 33, 131–134] and the confinement level of the networks [34, 41, 43, 45]. Furthermore, the hydraulic resistance to fluid flow of the gel-scaffolds has also been started to be analyzed for improving nutrient diffusion in scaffolds for tissue engineering applications [135, 136] or to study the 3D cell migration on *in vitro* experiments [33, 57, 131, 137], although some regards remain not fully understood yet.

The wide range of scaffold composition and measurement methods make difficult to compare and extrapolate the biophysical and biomechanical characterizations [138]. Therefore, in this work we aim to carry out an integral quantitative comparison of the bio-mechano-physical properties of both hydrogels, under similar conditions, for different bioapplications of *in vitro* 3D studies.

3.2 Materials and methods

3.2.1 Preparation of fibrin and collagen gels

Fibrin gels. As detailed in Chapter 2 Section 2.1, regarding fibrin hydrogels, Human Fibrinogen -plasminogen, fibronectin, factor XIII depleted- (American Diagnostica GmbH) was diluted in its buffer (50 mM Tris, 100 mM NaCl and 5 mM EDTA) as indicated from the provider. After mixing it with Human FXIII (American Diagnostica GmbH), the mixture was allowed to polymerize in presence of Human Alpha-Thrombin (American Diagnostica GmbH) along with $CaCl_2$ (Sigma) and cell culture media FGM-2 BulletKit (Lonza). While mixing, all the reagents were kept on ice. Once the samples were prepared, they were maintained in a humidity chamber in order to allow the mixture to polymerize. Finally, the hydrogels were hydrated and stored in the incubator for 24 hours before initiating any experiment. The gels reached a pH of 7.4, being the concentrations of each constituent -out of the final volume- set at 3.3 $mg \cdot ml^{-1}$ for fibrinogen, 1 $U \cdot ml^{-1}$ for FXIII, 1 $U \cdot ml^{-1}$ for thrombin and 5 mM for $CaCl_2$, respectively.

Collagen gels. The procedure for collagen gels was adapted from a previous work of Shin et al. [92], as specified in Chapter 2 Section 2.1. Collagen type I (BD Biosciences) was buffered to a final concentration of 2 $mg \cdot ml^{-1}$ with 10x DPBS – calcium, magnesium- (Gibco), cell culture media FGM-2 BulletKit (Lonza) and cell culture grade water (Lonza). The dilution was brought to pH 7.4 adding NaOH. Manipulation of reagents and mixture was maintained on ice. As soon as the mixture was ready, they were allowed to polymerize inside humid chambers, in the incubator. Next, the gels were hydrated and stored in the incubator for 24 hours before experimentation.

3.2.2 Scanning electron microscopy (SEM)

This procedure was performed in collaboration with the Microscopy Service of the Universitat Autònoma de Barcelona and the methodology is detailed in Chapter 2 Section 2.2. Thus, hydrogels were fixed with 2.5% glutaraldehyde (Sigma-Aldrich), followed by 1% osmium tetroxide EM grade (Ted Pella, Inc.). Then, dehydration in 30%, 50%, 70%, 80%, and 95% ethanol solutions, respectively, was performed. Gels were freeze-fractured in liquid nitrogen, before a final dehydration step in 100% ethanol was done. Using the Baltec CPD030 critical point dryer, the samples were sputter-coated with gold-palladium for 4 minutes employing an Emitech K550. Afterwards, visualization was carried out using high resolution imaging with a Merlin Field Emission Scanning Electron Microscope (FESEM) from Zeiss working at 1kV beam voltage and magnifications of 80-120 kX.

3.2.3 Confocal reflection imaging

Performance of the acquisition by confocal reflection was obtained by using a Leica SP2 equipped with a 63x/1.4 N.A. oil immersion lens. The samples were excited with 488 nm using an Argon laser and detected within 479-498 nm.

3.2.4 Microstructural analysis

In order to elucidate and compare the microstructural features of both 3D networks, fibrin and collagen, confocal reflection and SEM images were acquired as detailed beforehand. Actually, for the parameterization of the study, the void ratio and fiber radius were evaluated by means of the free software ImageJ (http://rsb.info.nih.gov/ij). As for the fiber radius measurements, three independent sets of each hydrogel and several fiber measurements were employed. These data are shown as mean ± SEM.

Regarding the void ratio calculi, confocal reflection images were used. Firstly, the raw images were made binary. Later on, the fiber to pore ratio was calculated by means of areas comprised by white (pores) or black (fibers) pixels of the binary images. This measurement was carried out for three independent hydrogels out of each type of gel, so data are shown as mean ± SEM.

3.2.5 Permeability experiments

Regarding the experimental set-up employed to measure Darcy's permeability (K) of the hydrogels, they were allowed to polymerize within microfluidic devices, which were fabricated following a previous work of Shin et al. [92]. Then, medium reservoir tubes were inserted into the channel outlets (shown in Fig. 3.1 and detailed in Chapter 2 Section 2.2), following a previous work of Sudo et al. [139]. The media columns' high difference in both sides of the gel caused a pressure gradient, being the initial one of 500 and 13 mm H_2O for fibrin and collagen gels, respectively.

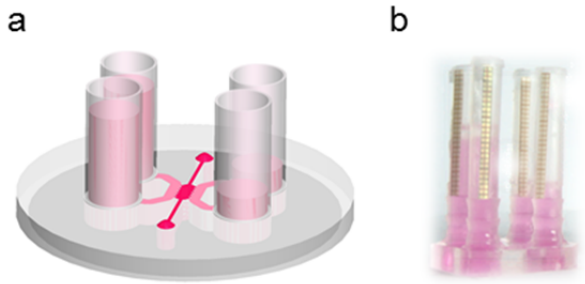

Fig. 3.1. Scheme of the experimental set-up for permeability measurements. Pressure gradient generated by media columns' high difference through the microfluidic device comprising a central gel cage (fuchsia) and two main media channels (pink).

From Darcy's law, it is established the relation between the pressure difference and the permeability as:

$$\Delta P(t) = \Delta P(0) \cdot e^{-ct} \quad (3.1)$$

where t is the time, $\Delta P(t)$ is the pressure difference for each time point, $\Delta P(0)$ is the initial pressure difference and the constant c is related to the permeability K as shown below [139]:

$$K(m^2) = \frac{c \cdot \mu \cdot L \cdot A_r}{\rho \cdot g \cdot A} \quad (3.2)$$

being μ and ρ the viscosity and the density of the fluid respectively, L the length of the gel through which the pressure drop is established, A_r the area of the media reservoirs, g the gravitational acceleration and A the cross sectional area to flow.

Therefore, by monitoring and measuring the pressure difference drop and fitting the equation (3.1) into the measured data points (pressure difference vs. time), the exponent coefficient c was obtained for each hydrogel. Subsequently, by solving the equation (3.2) for K, the Darcy's permeability values were determined, to characterize the interstitial resistance to flow.

3.2.6 Rheology

The rheological experiments were carried out in collaboration with the Materials and Components Section of the Instituto Tecnológico de Aragón (ITAINNOVA). The current methodology is summarized in Chapter 2 Section 2.2. For these measurements a Bohlin Gemini 200 HR Nano rheometer was used. The lower torque limit of the instrument was of 3 nNm in oscillation. We performed all tests using a cone-plate geometry with diameter 40 mm, a cone angle of 1º gap and a truncation height of 30

μm. The temperature was set and held at 37°C, controlled with a Peltier plate to ±0.1°C.

The samples were mixed on ice and pipetted on the rheometer plate by filling its gap, as demonstrated in Fig. 3.2. To avoid any evaporation, the shear gap was covered with a 0.1 Pas oil, the same one used for the calibration. Then, we started the measurements.

The curing reaction was traced measuring the evolution of the shear modulus over time at a constant temperature of 37°C, oscillation frequency of 1 $rad \cdot s^{-1}$ and applied strain amplitude of 0.005.

The dependence of the sample moduli on the oscillatory strain amplitude was measured at constant temperature of 37°C for excitation frequencies of 0.1 Hz and 0.01 Hz. The strain amplitude was varied in a logarithmically equidistant interval of ten measurement points per decade, from 0.001 to 1. For each point, six periods were accumulated.

Fig. 3.2. Sequenced pictures of the gel filling process on the rheometer. Once the sample was mixed, it was pipetted on the rheometer plate (a), adjusted the gap (b), covered with the oil (c) and got ready to run the experiment (d).

3.3 Results

Hereby work a complete biomechanical and architectural characterization of hydrogels was carried out. Actually, the set of experiments that we proposed allowed understanding diverse key aspects of the gel comprehending its microstructure, resistance to flow and mechanical response. Although the approach could be applied to study any kind of scaffold, a systematic comparison of two physiologically-relevant and widely used hydrogels, fibrin and collagen, was analyzed.

3.3.1 Microstructural study

The void ratio of the hydrogels was chosen to assess the porosity of both fibrin and collagen gels. For the quantification, confocal reflection images were employed, which are shown in Fig. 3.3. Fibrin networks presented a higher fiber density than collagen matrices, leading to a void ratio of approximately 70% and 80% respectively, as indicated in Table 3.1.

Table 3.1. Microstructural characteristics of the hydrogels.

	Collagen	Fibrin
Fiber radius (nm)	79.51±33.16	66.53±13.57
Pore size (μm)	2.84±0.94	1.69±0.33
Void ratio (%)	80.15±1.82	71.46±1.00

In order to evaluate the fiber radius, SEM images were also acquired. As shown in Fig. 3.4, during collagen hydrogel assembly, fibers tended to form bundles leading to thicker fibers, which explained the wide variability presented in the radii measurements, being nearly 80 nm for the collagen fiber radius (see Table 3.1). In

addition, fibrin fibers showed up mainly individually and their radii were measured to be around 70 nm, as collected in Table 3.1.

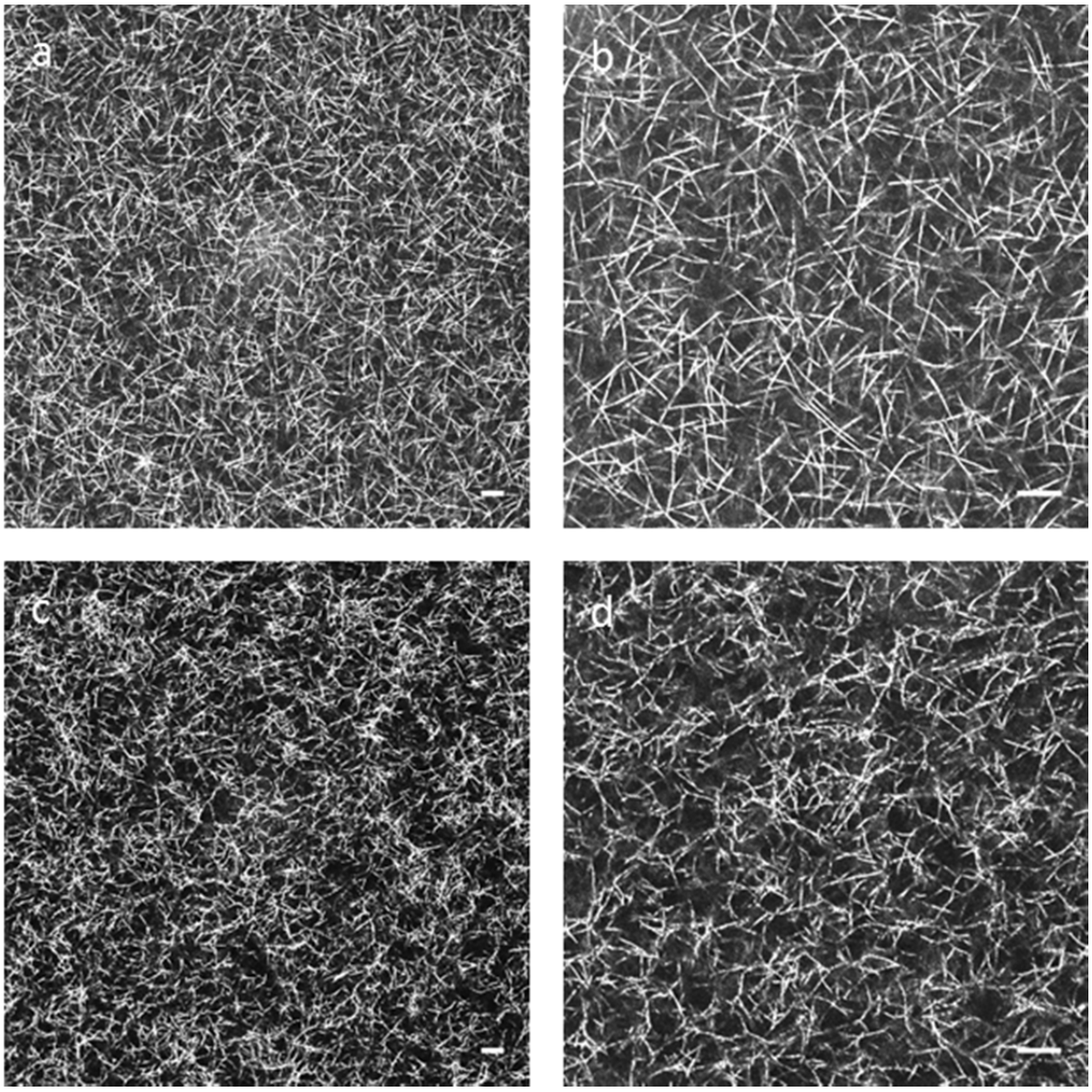

Fig. 3.3. 3D network of hydrogels. Confocal reflection images show the arrangement of the fibrillar networks for (a-b) fibrin and (c-d) collagen gels. Images (a) and (c) show a general view; while (b) and (d) are zoomed images of the right-bottom corner of the previous images, respectively. Scale bars correspond to 10 μm.

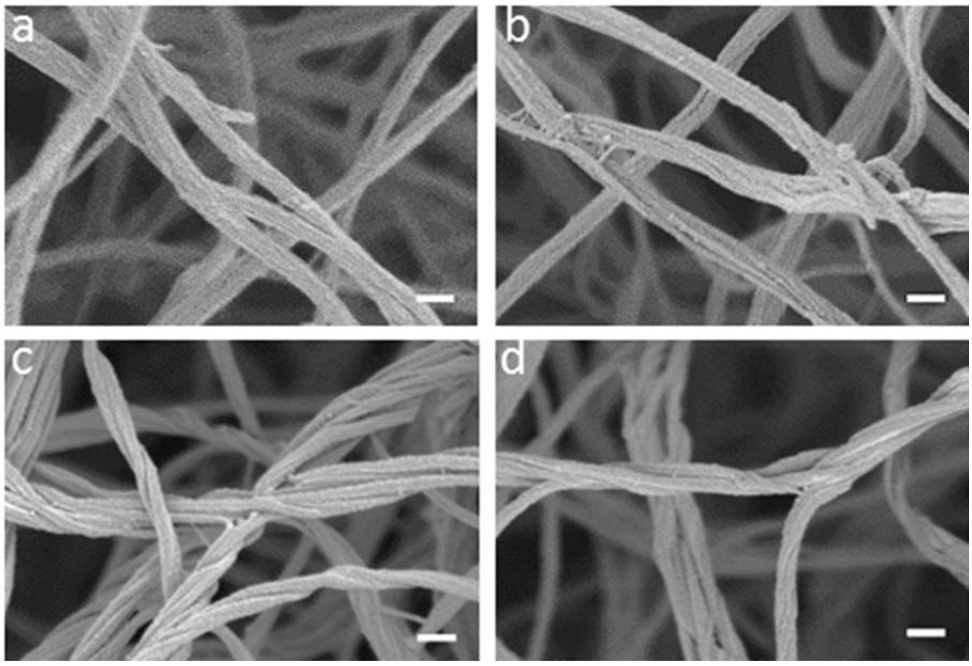

Fig. 3.4. Fiber layout within the hydrogels. SEM images of (a-b) fibrin and (c-d) collagen gels acquired at magnifications comprehended between 80-120 Kx show the morphological features of the fibers. Scale bars correspond to 200 nm.

3.3.2 Permeability quantification

Concerning the resistance to flow of the hydrogels, it was quantified the pressure difference drop over time (see Fig. 3.5). It was done by means of measuring the media columns' high difference each 10 or 15 minutes for fibrin or collagen, respectively. As shown in Fig. 3.5, the obtained data curves were then fitted within an exponential function formatted as in equation (3.1) achieving a R^2-value of 0.96 and 0.98, respectively, for fibrin and collagen. As gathered in Table 3.2, the exponent coefficient values (c) were of 0.13 h^{-1} or $4.00 \cdot 10^{-05}$ s^{-1} for fibrin, and of 0.24 h^{-1} or $7.00 \cdot 10^{-05}$ s^{-1} for collagen.

Table 3.2. Resistance to fluid flow.

	Collagen	Fibrin
Exponent coefficient, c (s^{-1})	$4.00 \cdot 10^{-05}$	$7.00 \cdot 10^{-05}$
Darcy's permeability, K (m^2)	$5.73 \cdot 10^{-13}$	$1.00 \cdot 10^{-12}$

Particularizing for each 3D network and solving the equation (3.2) for K, it was obtained the Darcy's permeability for fibrin and collagen to be of $5.73 \cdot 10^{-13}$ m^2 and $1.00 \cdot 10^{-12}$ m^2, accordingly (see Table 3.2). Hence, as represented in Fig. 3.6, these values denote the velocity with which the pressure difference drops towards the equilibrium in the case of each gel, departing with an equal pressure difference. This points out the resistance that a particular 3D network exerts to the fluid transport.

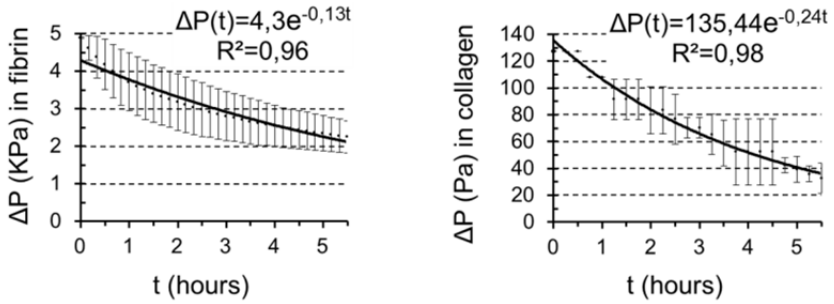

Fig. 3.5. Pressure difference drop over time in hydrogels. The experimental data points of the pressure difference vs. time are plotted and fitted into the exponential function for fibrin (left) and collagen (right) gels. The exponent coefficient turns out the value of the permeability (K).

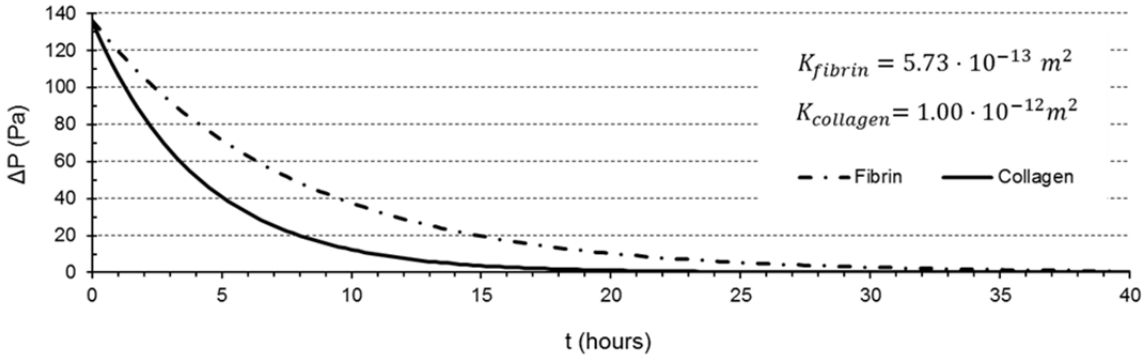

Fig. 3.6. Normalized exponential functions of the hydrogels. The quantification of the permeability (*K*) allows interpreting the resistance to flow of each hydrogel.

3.3.3 Mechanical response

As soon as the gel solution was pipetted and set within the rheometer plate, the polymerization was traced for 3 hours. Fig. 3.7 shows the evolution of the complex shear modulus (G*) over time, at a constant temperature of 37ºC. The sample was kept at rest *in situ* for 24 hours since curing reaction initiation, in order to finish the polymerization and stabilize the sample before any subsequent rheological experiment.

Afterwards, strain sweep assays were performed for excitation frequencies of 0.1 and 0.01 Hz. Fig. 3.8 outlines the measured elastic (G') and viscous (G'') shear modulus of fibrin and collagen gels, in function of the applied strain amplitude. Both materials were characterized by a substantial strain hardening, which is characteristic of these biopolymer hydrogels. It occurred within the strain range of 10-100% and 50-100%, for fibrin and collagen, respectively. For the measured excitation frequencies, the registered moduli were similar within the experimental error. The measured value of the shear modulus (G') of fibrin was of 300 Pa. This value was twenty times higher than the one quantified for collagen gels, which was of 15 Pa.

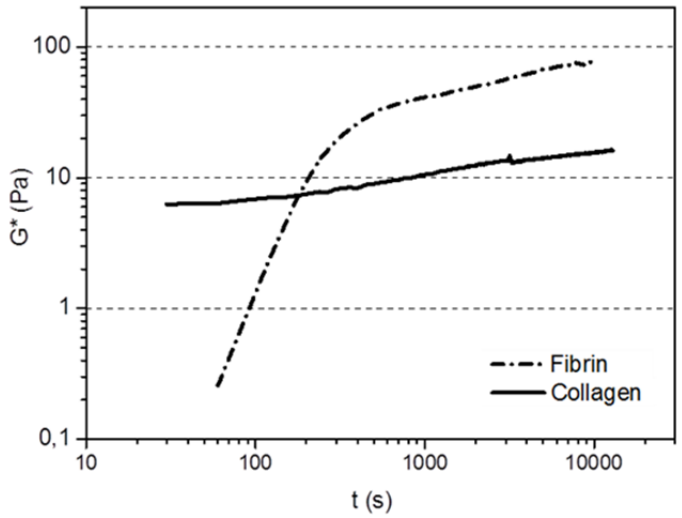

Fig. 3.7. Time evolution of the complex shear modulus (G*) of hydrogels. The temperature was set and held at 37ºC, excitation frequency was 1 rad/s and strain amplitude 0.005. Note that polymerization in case of the fibrin gel was not yet completed.

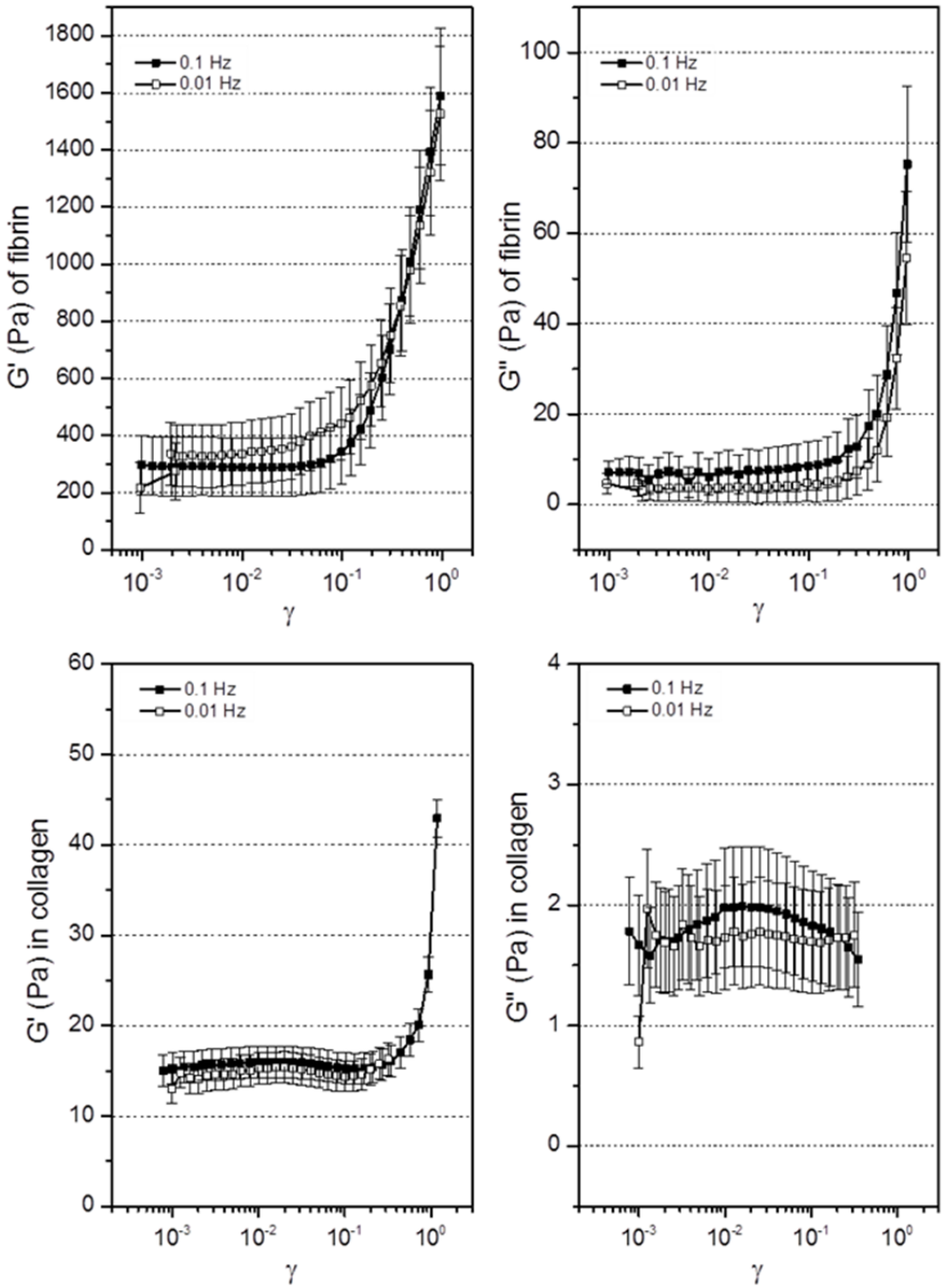

Fig. 3.8. Strain sweeps of hydrogels. Elastic (G') and viscous (G'') shear modulus are shown in function of the strain amplitude (γ), presented in parts per unit, at frequencies of 0.1 Hz and 0.01 Hz. The temperature during the experiment was kept at 37°C.

3.4 Discussion

Lately, many works have been directed towards the characterization of hydrogels. In fact, their bioapplication in tissue engineering or *in vitro* experiments raised remarkably [105–108], due to the biomimetic features of these materials while recreating natural ECMs. These extensive studies are essential to understand the mechanics and architectural characteristics underling the biopolymers. Nevertheless, the broad diversification of the mixture and measuring techniques makes difficult while cross widely correlating the data [138]. Hence, the purpose of the current study was to perform an integral biophysical and biomechanical study of two hydrogels highly relevant in biological processes and widely used for *in vitro* assays: fibrin and collagen. Moreover, the preparation and measuring methods were maintained all over the study, which allowed for a systematic comparison of all the properties.

As a starting point, physiologically-relevant concentrations and experimental conditions were chosen to perform the study for both gels. As to the collagen gels, it has been noted the physiological concentration to be 1-4.5% [140]. Actually, we followed the detailed protocol of Shin et al. [92], which has been fully detailed in Chapter 2 Section 2.1. Hence, 2 $mg \cdot ml^{-1}$ of collagen I protein, pH of 7.4 and a polymerization temperature of 37ºC were chosen, similarly to other published works [33, 44, 70, 86].

Regarding the fibrin gels, several publications have noted the physiological amounts to be ranged as indicated below: fibrinogen between 2-4 $mg \cdot ml^{-1}$ [102, 104, 141], FXIII at 22$ug \cdot ml^{-1}$ [101], thrombin between 1-3 $U \cdot ml^{-1}$ [113, 122, 141, 142], $CaCl_2$ from 1.4 mM on [141, 143, 144], and pH at 7.4 [143]. Thus, the concentrations of each constituent out of the final volume were set at 3.3 $mg \cdot ml^{-1}$ for fibrinogen, 1 $U \cdot ml^{-1}$ for FXIII, 1 $U \cdot ml^{-1}$ for thrombin and 5 mM for $CaCl_2$. In addition, a pH of 7.4

and a temperature of 37ºC were maintained for the preparation and performance of the experiments.

Actually, previous works focused mainly on microstructure and bulk stiffness analysis, due to their key role in basic cellular events in 2D [128]. Nevertheless, there are accumulating evidences that confinement of cells in 3D migration has a crucial role [34, 41, 45, 46, 77]. Furthermore, the resistance to flow of the ECM biopolymers also controls the transport of the biomolecules in diffusive and convective processes, which regulate the access of nutrients and other factors, as well as the shear stress exerted to the cells. All this together yielded to be a key aspect including not only microstructural and mechanical analysis, but also permeability measurements within the quantitative comparison between hydrogels.

Regarding the tested mechanical response of the hydrogels, it was measured by means of oscillatory strain amplitude sweeps. The network characterization of the repeated straining was done since the ECM *in vivo* is exposed to such deformations due to cellular contractile mechanosensing, cellular motility, beating of blood stream or interstitial flow [108]. Curing reaction was traced for 3 hours by monitoring the elastic and viscous shear modulus. It was visualized the collagen gel to polymerize linearly and the fibrin polymerization evolution to be logarithmic-like, as seen in Fig. 3.7. Although, apparently, fibrin gels cured faster than collagen gels, the network remained to be further cross-linked and stabilized by FXIII for the next hours. The complete cross-linking of a blood clot during coagulation takes longer than the formation of its fibrillar backbone [108], which could explain why confocal scanning micrographs do not show much differences with or without ligation [122].

Besides, FXIII introduced dramatic effects on the viscoelastic properties of fibrin by increasing its stiffness, as it happens in accurate clots to prevent bleeding problems [104]. For fibrin networks, we measured an elastic shear modulus of 300 Pa, which

matched with other published values [105, 108, 116, 141]. However, akin the collagen gels, a 20-fold lower shear modulus than that quantified for fibrin was achieved, being of 15 Pa, which agreed with measurements from other works in which analogous gel preparations were employed [109, 118].

In addition, both gels presented non-linear elasticity. Fibrin showed strain-hardening from 10% of strain on, while in collagen this effect occurred for strains larger than 50%. It was expected, since it is generic to any network composed of semiflexible filamentous proteins, where the main molecular mechanisms are being extendedly studied [27, 108, 109, 122]. Indeed, many soft tissues, such as blood clots, stiffen as they are strained, preventing large deformations that could threaten tissue integrity [109, 117, 145]. Likewise, at cellular level, cells embedded in 3D exert forces that cause deformations ranged within 10-50% in the cell surroundings (20 microns far from the cell margin) and 10% away from the cell [146].

These gel-scaffolds were arranged into branched fibrillar 3D networks, as shown in Fig. 3.3 and 3.4. In the same way that Lai et al. indicated in their works [106, 107], collagen fibers tended to form bundles while the fibers formed in fibrin assembly were straighter, as corresponds to physiological clot structures [104] . As gathered in Table 3.1, the fibrin network was formed tighter than the collagen mesh. It was demonstrated by the measured pore size of fibrin ECM, which was lower than that quantified for collagen structures. Actually, the pore size was quantified approximately 1.7-fold lower for fibrin than for collagen hydrogels. Moreover, it correlated directly with the measured permeabilities, maintaining a similar proportion. In addition, these values are in agreement with other previous measurements [33, 136].

It has been extensively studied the impact that biomechanical and geometrical properties of the ECM exert on cellular behavior. Moreover, it is currently accepted

within the literature that distinct biophysical and biomechanical properties regulate, indeed differently, the migration in 2D and 3D [12]. Although 2D system mechanisms are mostly cleared up, different biomechanical and biophysical properties are being elucidated in order to understand its impact on different 3D migration patterns, such as matrix stiffness [37], microarchitecture [44] or confinement [34]. Thus, all the presented mechanical and biophysical characterization of the fibrin and collagen gels intended to determine these cues, in order to allow for a rational design and interpretation of the cellular 3D *in vitro* studies.

3.5 Summary

Biophysical and biomechanical characterization of physiologically-relevant hydrogels is required in order to rationally use them for *in vitro* models, as well as in tissue engineering applications. In this work, an integral comparative characterization of collagen and fibrin scaffolds has been carried out by analyzing their microstructural architecture, resistance to fluid flow and rheological measurements. On the one hand, the pore size and permeability appear to be proportional features, by presenting approximately 2-fold decrease in fibrin with respect to collagen. Likewise, the stiffness of fibrin gels is 20 times higher, although both gels showed strain-hardening behavior. Indeed, these significant analogies and differences found could induce to cells distinct mechanoregulatory cues while applying them to *in vitro* experiments.

Chapter 4
Application of chemotactic and haptotactic cues

Microfluidic devices allow for the production of physiologically relevant cellular microenvironments by including biomimetic hydrogels and generating controlled chemical gradients. During transport, the biomolecules interact in distinct ways with the fibrillar networks: as purely diffusive factors in the soluble fluid or bound to the matrix proteins. These two main mechanisms may regulate distinct cell responses in order to guide their directional migration: caused by the substrate-bound chemoattractant gradient (haptotaxis) or by the gradient stablished within the soluble fluid (chemotaxis). As shown within this chapter, in this work, 3D diffusion experiments, in combination with ELISAs, are performed using microfluidic platforms in order to quantify the distribution of PDGF-BB and TGF-β_1 across collagen and fibrin gels. Furthermore, to gain a deeper understanding of the

fundamental processes, the experiments are reproduced by computer simulations based on a reaction-diffusion transport model.

4.1 Introduction

Viability of organisms is sustained by the contribution of diverse constituents that compose tissues and organs. Particularly, the extracellular matrix (ECM) performs major functions such as tissue morphogenesis, differentiation and homeostasis, by rendering architectural scaffolding and establishing biomechanical and biochemical cues [25, 147, 148]. Indeed, cells require complex signaling frameworks comprised of specialized molecules, such as growth factors (GFs), for intercellular communication and to carry out physiological processes [25, 147].

During biomolecule transport across the ECM, diverse processes take place leading to a heterogeneous and varied biochemical scenario by means of paracrine and autocrine signaling; actually, the yielding biochemical environment has great effect on major cell responses, such as proliferation, differentiation and migration [21, 149–154]. While diffusion through the matrix pores in form of soluble molecules occurs, the ECM also serves as reservoir by offering binding sites to the GFs and, therefore, leading to a solid-state availability of them [155–158]. In addition, GFs also interact with other molecules resulting in their degradation [159].

Particularly, distinct directional single cell migrations (comprised of chemosensing, polarization and locomotion) are distinguished in function of their specific cause [160]. Migration towards a soluble chemoattractant is usually defined as chemotaxis; otherwise, when the bound GF influence cell motility, by guiding cell adhesion, is denominated haptotaxis [153, 161, 162]. Both mechanisms are crucial to cell migration and, therefore, strongly impact on developmental and regenerative

processes. Thus, a deeper knowledge of the diffusion behavior of GFs within the ECM, and the related adhesion and degradation processes, is critical in order to elucidate and predict the different chemotactic and haptotactic gradients of the biomolecules, which directly affect cellular behavior.

Numerous studies have identified several GFs to play an important role by mediating a wide range of biological processes [163–166]. These studies have been performed using two-dimensional (2D) substrates. However, the *in vivo* microenvironment mostly corresponds to a three-dimensional (3D) structure. Actually, significant differences in the behavior and effect of GFs have been identified by comparing 2D and 3D models, with 3D models mimicking more closely the *in vivo* behavior [167–169].

Furthermore, in the last years, microfluidic approaches have emerged to recreate cellular niches [170–175]. These platforms allow for a controlled 3D microenvironment by including hydrogels (mimicking the ECM of tissues) and the generation of chemical gradients of diverse factors in a systematic way [86, 171, 176–182]. Such microenvironment gives rise to more reliable information about the effect of GFs during *in vitro* assays in order to address biological questions.

Among the many different GFs, Platelet-Derived Growth Factor-BB (PDGF-BB) and Transforming Growth Factor-β_1 (TGF-β_1) have received increasing attention due to their diverse biological effects. PDGF-BB is a pro-migratory factor that plays a key role in the early stage of wound healing by enhancing proliferation and the recruitment of the fibroblasts to the wound site for ECM deposition [29, 68]. On the other hand, TGF-β_1 stimulates fibroblasts differentiation into contractile myofibroblasts, which are mainly responsible for matrix remodeling [29]. Furthermore, it has also been reported the capability of these GFs to bind to different extracellular components exerting their biological activity [147, 155, 157, 181, 183–

185]. This fact points to an important regulatory mechanism in physiological and pathological processes. In fact, their interaction with collagen and fibrin ECM-proteins is of high physiological relevance.

Collagen I is one of the major components of the connective tissue, accounting for up to 30% of the total protein in the human body [25, 50, 52]. Fibrin is an essential constituent of healing or angiogenic processes [102, 104, 186]. Under physiological conditions, both can also be assembled *in vitro* leading to the conformation of hydrogels in which cells are cultured and grown, thereby recreating biomimetic 3D physicochemical environments.

In order to design physiologically-relevant *in vitro* models, gradients of GFs are established across the hydrogels, which are installed into the microfluidic devices. The ability to control cell behavior, by regulating the availability of GFs, provides a powerful tool to study and manipulate a wide array of developmental and regenerative processes that are important in biology, biomedicine and bioengineering [187]. Therefore, knowing the actual character of the distribution and gradients of GFs, becomes essential in order to interpret and quantify cell response of *in vitro* assays. In this work, we present a characterization of the transport of PDGF-BB and TGF-β_1 through two different hydrogels, collagen and fibrin, included in a microfluidic platform. The spatio-temporal distribution of each GF, together with their degradation process, are determined by combining experimental and computational approaches. Moreover, this versatile tool is applied to further quantify the nature of GF-hydrogel interaction allowing for a deep insight into *in vitro* conditions.

4.2 Materials and methods

4.2.1 Microfluidic device fabrication

The geometry of the microfluidic devices is shown in Fig. 4.1: it contained a central channel, in which the hydrogel was located, and two media channels (addition and opposite channels) at both sides of the central channel in direct connection with the gel in order to ensure diffusion and hydration. As shown in Chapter 2 Section 2.1, the microfluidic devices were made of polydimethylsiloxane (PDMS - Dow Corning GmbH Sylgard 184, Dow Chemical, Germany) at a ratio of 10:1 polymer to cross-linker, using SU8-silicon wafers (Stanford University, CA) obtained by soft lithography as previously described [92]. PDMS microdevices were autoclaved and dried at 80 ºC overnight. Finally, they were plasma-bonded and treated with poly-D-lysine (PDL) solution (Sigma-Aldrich, Germany).

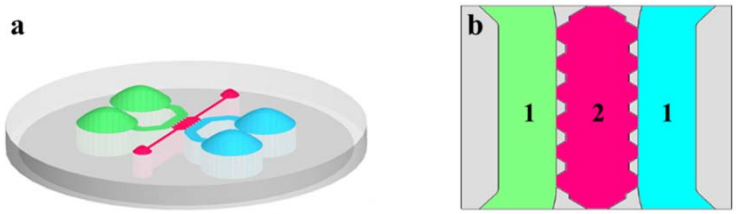

Fig. 4.1. Geometry of the microfluidic device. A general view of the microdevice is shown in picture (a). The central area is demonstrated as a top view in picture (b), in which the geometry and nomenclature of the compartments are detailed: the channel (1) and the hydrogel (2) compartments. The hydrogel is injected into the central cavity (pink), whose dimensions are 2.5 x 1.3 mm; the main channels (green and blue) are filled with culture media or PBS. When a GF or dextran is added in order to establish a chemical gradient, it is included in the addition channel (green) and diffuses through the hydrogel towards the opposite channel (blue).

4.2.2 Hydrogel preparation

Two types of physiologically relevant hydrogels were tested in this study, collagen and fibrin, in order to evaluate two different biomimetic scaffolds with respect to their chemical composition and physical properties. The corresponding procedures are specified in Chapter 2 Section 2.1.

Briefly, collagen I gel solution (BD Biosciences, Spain) was prepared at 2 $mg \cdot ml^{-1}$ and pH 7.4 [92], while for fibrin hydrogel, human fibrinogen (American Diagnostica GmbH, Germany) was diluted in the buffer indicated by the manufacturer (50 mM Tris, 100 mM NaCl and 5 mM EDTA) at pH 7.4, and mixed with human factor XIII (American Diagnostica GmbH, Germany), human α-thrombin (American Diagnostica GmbH, Germany), $CaCl_2$ (Sigma-Aldrich, Germany) and cell culture media FGM-2 BulletKit (Lonza, Belgium).

Hydrogels were then pipetted into the devices followed by gelation for 20 minutes in the incubator and hydrated right afterwards. The gels were kept in the incubator for 24 hours prior to any subsequent experiment. The media channels were then filled with PBS containing 20 kDa-dextran or FGM-2 media with the GFs, PDFG-BB or TGF-β_1, as described in the following sections.

4.2.3 Characterization of dextran diffusion

To characterize the transport of biomolecules in both hydrogels and determine the chemical gradients generated through the device, 20 kDa-fluorescein isothiocyanate-dextran (Sigma-Aldrich, Germany) was prepared in PBS at 15 $\mu g \cdot ml^{-1}$ (Lonza, Belgium) and added in one of the media channels (addition channel), while PBS was added in the opposite media channel (see schematic in Fig. 4.1 and detailed protocol in Chapter 2 Section 2.3). The diffusion phenomenon was imaged by confocal

imaging using a Nikon D-Eclipse C1 Confocal Microscope employing a CFI Plan Apo Lambda 2X objective.

4.2.4 Experimental quantification of GF concentration

The study of degradation and transport processes in microfluidic platforms was performed by the addition of 50 $ng \cdot ml^{-1}$ PDGF-BB (Abcam, UK) or 10 $ng \cdot ml^{-1}$ TGF-β_1 (BD Biosciences, Spain) in the addition channel and the determination of their concentrations by ELISA in both, addition and opposite, channels (see Fig. 4.1). Detailed methodology for chemical gradient generation and sample obtaining for ELISAs are included in Chapter 2 Section 2.3 and Appendix A Protocol A.3, respectively.

The degradation assays were performed without any hydrogel in the central chamber of the device, in order to evaluate the GF concentration reduction without the influence of the gel; hence, avoiding the interference of diffusion and binding mechanisms. Control samples (without GFs) were also assayed. In spite of this, for the experimental quantification of the GFs concentration pattern, the hydrogels were included within the microfluidic platforms.

To determine the PDGF-BB concentration, the PDGF-BB Human ELISA Kit (Abcam, UK) was used according to manufacturer instructions. Standards (0-50 $pg \cdot ml^{-1}$) were prepared from the stock solution. All standards and samples (1:1000) were run in triplicate. After immobilization and antibody binding, and following streptavidin-HRP solution addition, incubation for 30 min with the TMB One-Step Substrate Reagent was performed. Afterwards, the stop solution was added and the absorbance of the reaction was read at 450 nm in a Synergy HT Multi-Mode Microplate Reader (BioTek Instruments, VT).

TGF-β_1 concentration was quantified by the TGF-β_1 ELISA Kit (Invitrogen, UK). First, samples were centrifuged (1000g for 10 minutes). Similarly, standards (0-75 $pg \cdot ml^{-1}$) were obtained from the stock solution added to the microfluidic devices and quantified in triplicate as well as samples (1:100). Then, the immunoassay was carried out by the immobilization of TGF-β_1 and further antibody reaction, followed by the addition of streptavidin-HRP and the stabilized chromogen. After incubation of 20 minutes at room temperature in the dark, the stop solution was added and the absorbance was read at 450 nm in a Synergy HT Multi-Mode Microplate Reader (BioTek Instruments, VT).

4.2.5 Modeling the GF transport within the hydrogels

In order to simulate the transport of factors through the hydrogels, as shown in Fig. 4.1, two compartments of the device were distinguished in the model: the channel compartment (1), where the factor is mixed with the media fluid; and the hydrogel compartment (2), that is the cavity in which the hydrogel is installed into the microdevice. Although the same equation was used for both compartments, the parameters varied depending on them, since different phenomena occurred in these domains.

We proposed a reaction-diffusion transport model, where the transport equation is derived from the law of conservation of mass and a suitable constitutive equation for the flux of the chemical factor (Fick's law):

$$\frac{\partial c(\boldsymbol{x},t)}{\partial t} = D^i \nabla^2 c(\boldsymbol{x},t) + R^i \tag{4.1}$$

where index i refers to the compartment, c is the concentration of the factor, D^i is the effective diffusion coefficient and R^i represents the mass reduction due to both phenomena, the degradation in the channel compartment or the binding to the matrix

in the hydrogel compartment. The reaction term R^i can be written as a function of the specific compartment:

$$R^i = \begin{cases} -k_d c(\boldsymbol{x}, t) & if\ \boldsymbol{x}\ belongs\ to\ the\ compartment\ 1 \\ -k_b c(\boldsymbol{x}, t) & if\ \boldsymbol{x}\ belongs\ to\ the\ compartment\ 2 \end{cases} \quad (4.2)$$

where k_d and k_b are the degradation and binding rates, respectively.

The reaction-diffusion process in the domain, as depicted in Fig. 4.1, is essentially planar. Therefore, we employed a 2D Finite Element simulation based on linear triangle elements and an Euler backward time integration scheme [188]. The mesh contained approximately 3000 elements with characteristic element sizes between 0.1 and 0.4 μm. The total time of 24 hours was subdivided into 864 steps, with a step size of 100 seconds each. On all boundaries of the domain, zero flux boundary conditions were applied.

4.2.6 Diffusion coefficient estimation

The standard diffusion coefficient of an element of radius r within a continuous fluid, can be calculated by the Stokes-Einstein equation as [189]:

$$D_\infty^1 = \frac{k_B T}{6\pi\eta r} \quad (4.3)$$

where k_B is the Boltzmann constant, T the absolute temperature and η the viscosity of the fluid. The values of the standard diffusion coefficient obtained for each chemical factor, together with their radius, are shown in Table 4.1.

Table 4.1. Parameters of the chemical factors.[a]

	Dextran	PDGF-BB	TGF-β_1
r (10^{-9}·m)	3.24	4.50	3.80
D_{∞}^{1} (10^{-11}·m^2·s^{-1})	1.75	1.26	1.49
$D_{collagen}^{2}$ (10^{-11}·m^2·s^{-1})	1.09	0.77	0.92
D_{fibrin}^{2} (10^{-11}·m^2·s^{-1})	1.17	0.83	0.99

[a]The standard and specific diffusion coefficients particularized for each chemical factor, together with the corresponding assumed radius, are shown. For dextran, its radius has been indicated from the provider; the value for PDGF-BB has been estimated from the Protein Data Bank; and the one of TGF-β_1 has been taken from a previous work [190].

However, the diffusivity is altered when these molecules diffuse through a fibrous matrix (for instance, the hydrogel) instead of in a continuous fluid medium. Therefore, an effective diffusion coefficient was defined, which does not depend only on the molecular size but also depends on the void ratio of the porous medium in which the factor is moving. Ogston et al. [191] and Kim and Tarbell [192] defined an effective diffusion coefficient as follows:

$$D^2 = D_{\infty}^{1} \cdot \ exp\left(-\left[\sqrt{\varphi} \ \cdot \left(1 + \frac{r}{r_f}\right)\right]\right) \tag{4.4}$$

where φ is the void ratio of the matrix, r the radius of the molecule and r_f is the fiber radius.

These parameters, which are gathered in Table 4.2, were quantified for both collagen and fibrin gels by means of measurements implemented on Scanning Electron Microscope and Confocal Reflection images. Hence, in function on the matrix through which molecule transport occurred, the assumed effective diffusion coefficients in the hydrogel compartment are shown in Table 4.1.

Table 4.2. Geometrical features of the hydrogels.[b]

	Collagen	Fibrin
r_f (10^{-9}·m)	79.51±33.16	66.53±13.57
φ (%)	80.15±1.82	71.46±1.00

[b]The parameters of the model related to the microstructure of both collagen and fibrin hydrogels: fiber radius and void ratio. The data in this table are reported as mean ± SEM.

4.3 Results

In order to characterize the spatio-temporal distribution of the GFs, experimental assays were performed as well as computational simulations. All the studies were carried out using PDGF-BB and TGF-β_1 as GFs, and establishing chemical gradients across collagen and fibrin hydrogels.

At first, the computational model was validated by characterizing the transport of dextran. Afterwards, in order to elucidate the events occurring during GF transport in the porous-gel media, different aspects were considered: degradation measurements and assessment of the distribution of GF concentration. Next, finite element simulations of GF transport were carried out in order to replicate the *in vitro* experiments, allowing to improve the understanding of the biochemical environmental cues that are induced.

4.3.1 Characterization of dextran transport dynamics

The distribution of the diffusing 20 kDa-fluorescein isothiocyanate-dextran was imaged 4 hours after addition in both collagen and fibrin gels. As demonstrated in Fig. 4.2 (a and b), the diffusive pattern was spread all over the microfluidic device [139].

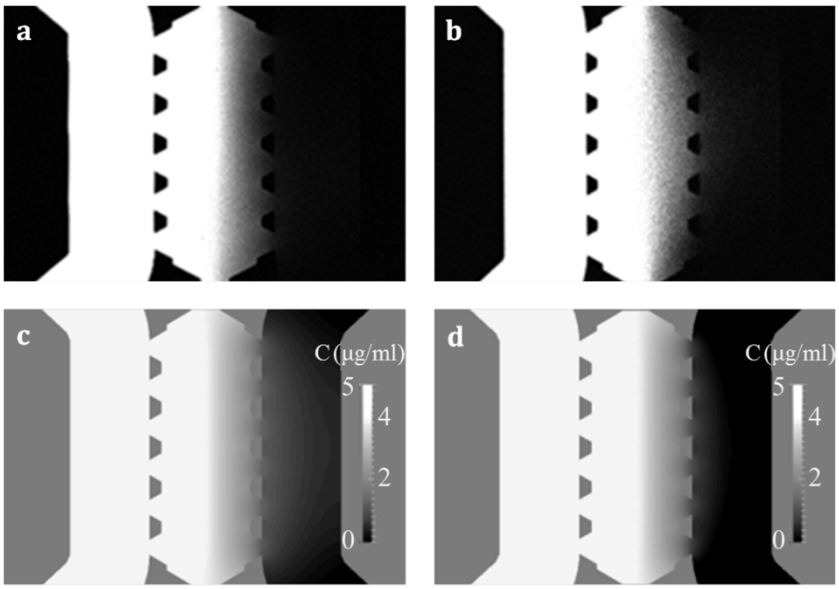

Fig. 4.2. Diffusive gradient of dextran. *In vitro* and in-silico images, respectively, resulting from dextran diffusion in collagen (a,c) and fibrin (b,d) hydrogels 4 hours after addition.

Furthermore, the computational simulation of the experiment for a diffusion coefficient of $1.75 \cdot 10^{-11}$ $m^2 \cdot s^{-1}$, as indicated by the provider, based on the Fick's Law was able to predict the transport of dextran through the scaffold. Hence, as shown in Fig. 4.2, it confirmed the suitability of our model to predict such processes since the dye concentration profile deriving from both methods matched.

4.3.2 Experimental measurements of GF degradation

For the assessment of GF degradation in the devices, the concentration of PDGF-BB and TGF-β_1 were evaluated 24 hours after factor addition. Employing the devices without any hydrogel allowed for an accurate quantification of the decrease in their concentrations by degradation. The samples collected from the media channels were evaluated by Enzyme-Linked ImmunoSorbent Assays (ELISAs) and the concentration

values obtained were plotted with respect to the initial concentrations, 100% being 50 $ng \cdot ml^{-1}$ of PDGF-BB or 10 $ng \cdot ml^{-1}$ of TGF-β_1.

After 24 hours, the concentration values for PDGF-BB and TGF-β_1 were 45% and 70%, respectively, as shown in Fig. 4.3. Hence, the reductions in the concentration of the factors were approximately 55% and 30%, yielding a lower decrease in the concentration of TGF-β_1 than exhibited by PDGF-BB. These results highlighted the differences in the degradation processes of PDGF-BB and TGF-β_1 in the devices, and showed TGF-β_1 to be significantly more stable in our experimental analysis.

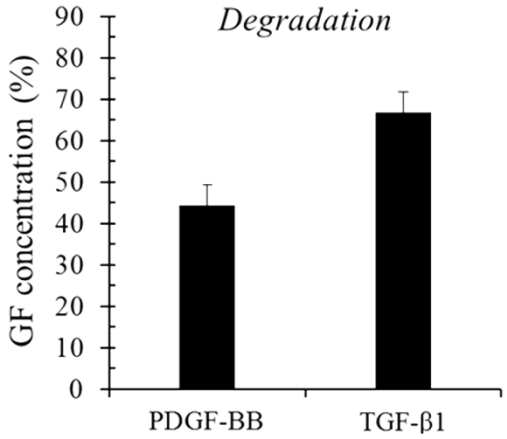

Fig. 4.3. Degradation of the GFs within the microfluidic device. Experimental data as percentage of initial PDGF-BB and TGF-β_1 concentrations (50 $ng \cdot ml^{-1}$ and 10 $ng \cdot ml^{-1}$ are 100%, respectively) obtained from media channels of the device without any hydrogel, 24 hours after addition.

4.3.3 Experimental quantification of GF concentration

ELISAs were performed to quantify the transport of the studied GFs across the hydrogels held in the microfluidic devices. 50 $ng \cdot ml^{-1}$ of PDGF-BB or 10 $ng \cdot ml^{-1}$ of TGF-β_1 were added to one media channel (the addition channel) and the samples were

obtained, after 24 hours, from both media channels (the addition channel and the opposite one).

The GFs, PDGF-BB and TGF-β_1, showed a similar distribution for both hydrogels as displayed in Fig. 4.4 and 4.5. Regarding PDGF-BB, for collagen hydrogels, the GF concentration detected in the addition channel compared to the initial state (50 ng·ml^{-1} = 100%) decreased down to 40%, while the concentration obtained in the opposite channel reached 4%. In fibrin hydrogels, percentages of approximately 45% and 8% were obtained in the addition channel and in the opposite one, respectively, when PDGF-BB was added.

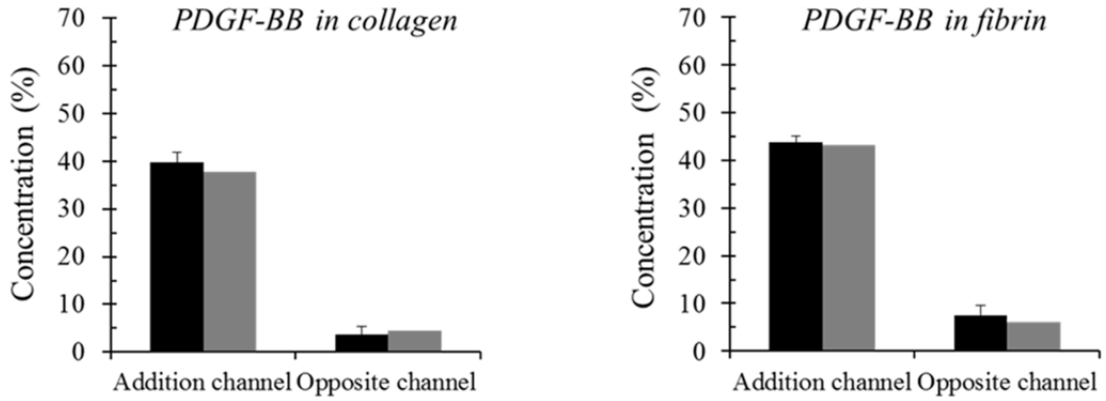

Fig. 4.4. PDGF-BB concentration pattern within collagen and fibrin hydrogels. Experimental and computational data as percentage of the initial PDGF-BB concentration (50 ng·ml^{-1} = 100%) obtained from both media channels, 24 hours after addition.

For the other GF, TGF-β_1, transported through collagen gels, the concentration percentage obtained from the addition channel was 30%, whereas the concentration in the opposite channel was 5%. For fibrin gels, the percentages of TGF-β_1 from the addition and opposite channels were 30% and 4%, respectively. In summary, the results of this subsection precisely show the chemical gradients across the hydrogel in each considered GF-ECM combination.

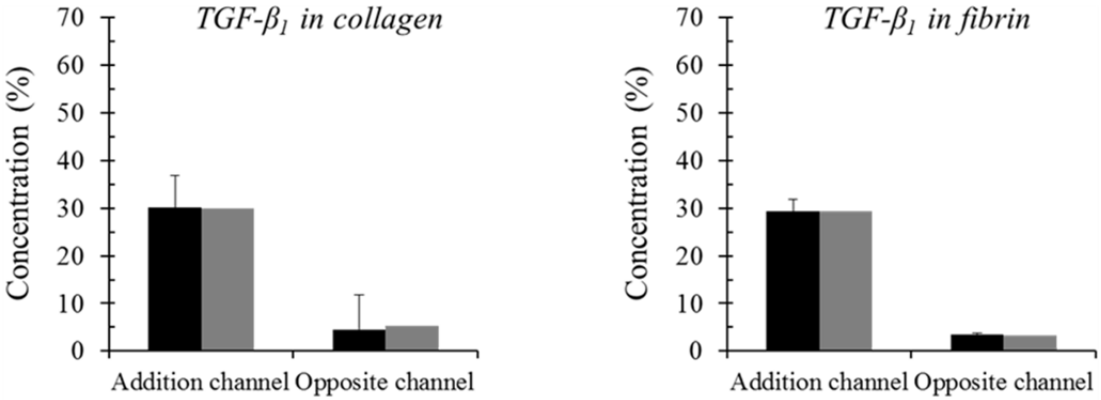

Fig. 4.5. TGF-β_1 concentration pattern within collagen and fibrin hydrogels. Experimental and computational data as percentage of the initial TGF-β_1 concentration (10 ng·ml^{-1} = 100%) obtained from both media channels, 24 hours after addition.

4.3.4 Numerical predictions of GF transport

The model detailed in Subsection 4.2.5 allowed to describe the transport of GFs through hydrogels by means of three main parameters: the effective diffusion coefficient, which strongly depends on the molecular size of the factor and the geometry of the porous scaffold; the degradation rate of each specific element; and the binding factor, which quantifies the ability of the molecule to bind to the matrix.

As a main assumption, we considered that the theoretical estimation of the effective diffusion coefficients in a porous matrix (presented in Subsection 4.2.6) was an accurate approach to model diffusion; indeed, other works also use a similar approach [193, 194]. Here, the degradation and binding rates were obtained by minimizing the difference with respect to the GF concentrations that were observed experimentally. To this end, four distinct cases were studied in order to assess these parameters: (Case 1) the values obtained in the degradation experiments were assumed as degradation rates and binding was omitted; (Case 2) the degradation rates were taken from the degradation experiments and binding rates were fitted to reduce the average difference

in both channels; (Case 3) binding was omitted and the degradation rates were fitted to reduce the average difference in both channels; (Case 4) both degradation and binding rates were fitted to reduce the average difference in both channels.

The parameters estimated for each type of gel and GF are detailed in Table 4.3 and 4.4. The degradation and binding rates, as well as the corresponding differences with respect to the experimental values are shown. These differences are displayed as separated differences for the addition and opposite channels, and also as the average of both differences, which was minimized by the parameter adjustment. Indeed, the average difference was reduced when both binding and degradation rates were adjusted, which corresponded to the denominated Case 4. Fig. 4.4 and 4.5 compare and visualize those optimized differences between the experimental data and the numerical predictions for PDGF-BB and TGF-β_1 in both hydrogels.

Table 4.3. Computational characterization of PDGF-BB transport.[c]

	Collagen				Fibrin			
	Case1	*Case2*	*Case3*	*Case4*	*Case1*	*Case2*	*Case3*	*Case4*
Degradation rate, k_d ($10^{-6}\cdot s^{-1}$)	9.97	9.97	4.00	3.00	9.97	9.97	1.00	3.00
Binding rate, k_b ($10^{-6}\cdot s^{-1}$)	0.00	0.00	0.00	10.00	0.00	0.00	0.00	0.10
Addition channel difference (%)	14.40	14.40	0.61	1.89	17.90	17.90	6.52	0.54
Opposite channel difference (%)	1.49	1.49	2.97	0.95	3.00	3.00	0.92	1.49
Average difference (%)	7.96	7.96	1.79	1.42	10.40	10.40	3.72	1.02

[c]Parameter estimation and difference computation with regard to experimental values considering four different conditions: (Case 1) the values obtained in the degradation experiments are assumed as degradation rates and binding is neglected; (Case 2) the degradation rates are accepted from the degradation experiments and binding ratios are fitted to reduce the average difference in both channels; (Case 3) binding is neglected and the degradation rates are fitted to reduce the average difference in both channels; (Case 4) both degradation and binding rates are fitted to reduce the average difference in both channels.

Table 4.4. Computational characterization of TGF-β_1 transport.[d]

	Collagen				Fibrin			
	Case1	*Case2*	*Case3*	*Case4*	*Case1*	*Case2*	*Case3*	*Case4*
Degradation rate, k_d ($10^{-6}\cdot s^{-1}$)	4.68	4.68	7.00	5.00	4.68	4.68	8.00	4.50
Binding rate, k_b ($10^{-6}\cdot s^{-1}$)	0.00	10.00	0.00	10.00	0.00	20.00	0.00	20.00
Addition channel difference (%)	4.98	0.72	0.38	0.06	6.78	0.42	0.89	0.02
Opposite channel difference (%)	3.59	0.91	2.78	0.83	3.87	0.13	2.87	0.10
Average difference (%)	4.29	0.82	1.58	0.42	5.32	0.28	1.88	0.06

[d]Refer to caption of Table 4.3.

The transport mechanisms predicted by the numerical simulations led to a deeper insight of the chemotactic and haptotactic gradients that are generated across the gels during GF transport. Therefore, the chemotactic and haptotactic gradients, that were established due to matrix binding or fluid diffusion processes for PDGF-BB and TGF-β_1 (corresponding to Case 4), were demonstrated. The distributions of both GFs are plotted and illustrated in Fig. 4.6 and 4.7, which show the concentration pattern established across the collagen and fibrin hydrogels.

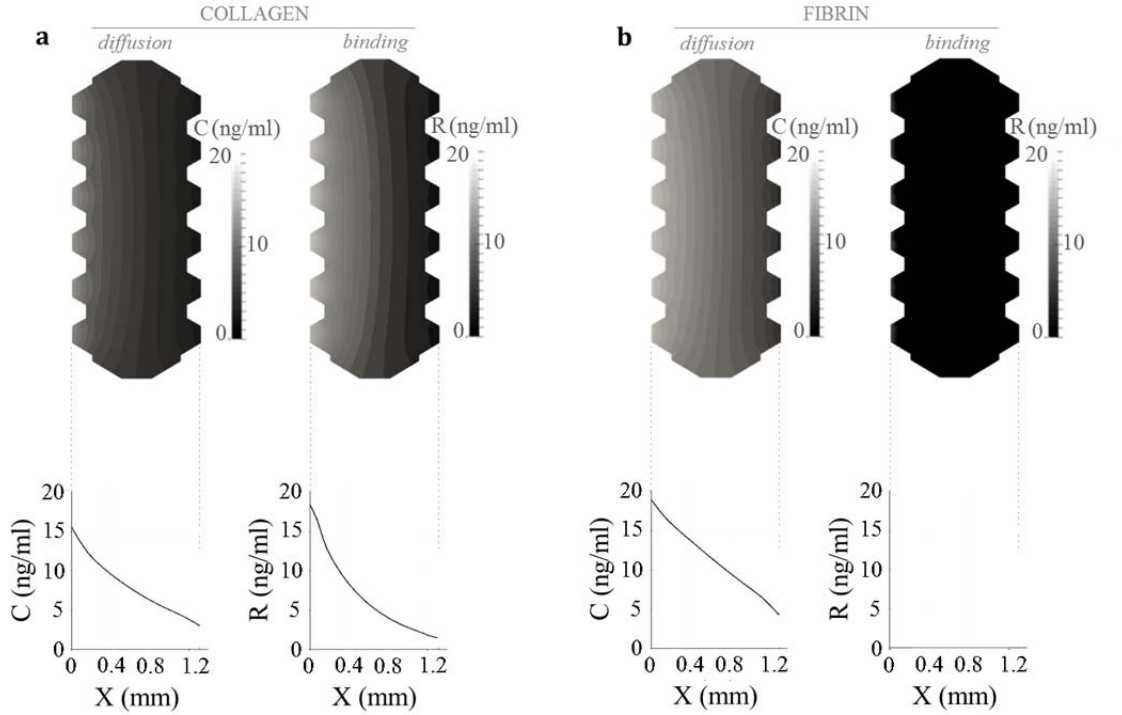

Fig. 4.6. PDGF-BB gradient simulations. The computational model predicts the spatio-temporal distribution of PDGF-BB in collagen (a) and fibrin (b) hydrogels, with respect to Case 4. The simulation figures show diffusion and binding patterns resulting after 24 hours since factor addition, being the added initial concentration of 50 ng•ml^{-1} (source in the left side of the device). The graphs depict the evolution -over the gel width- of diffusion and binding concentration profiles, denoted as C and R, respectively. In collagen gels, both diffusion and binding processes occur simultaneously. Conversely, binding is not relevant in the case of fibrin.

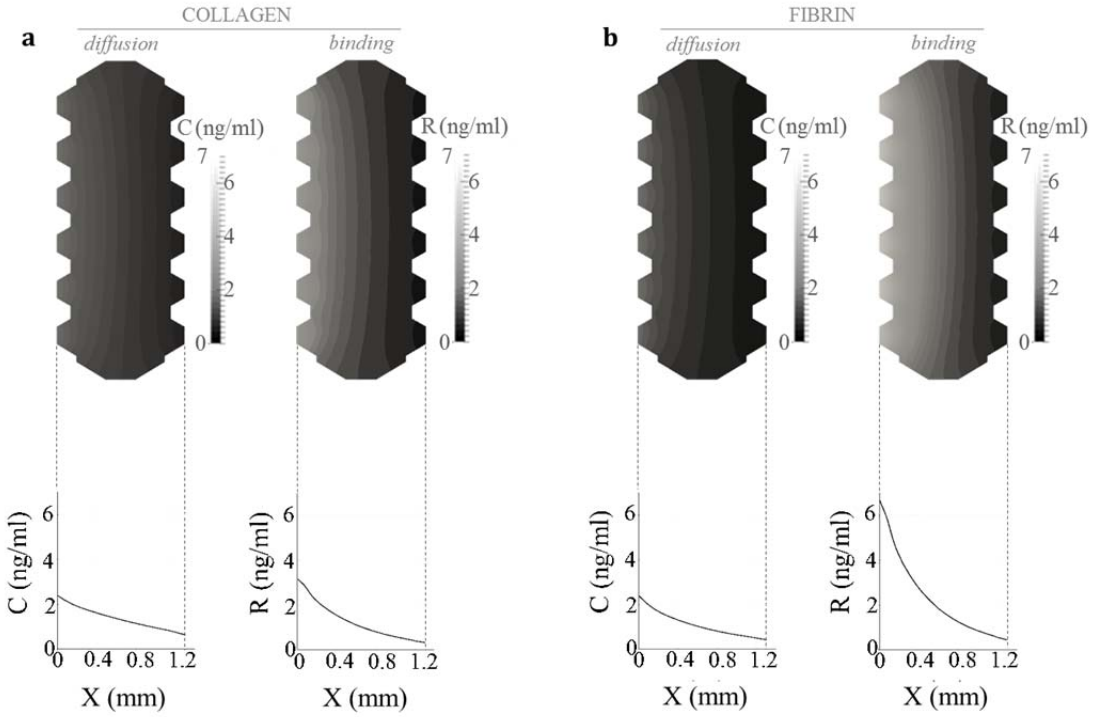

Fig. 4.7. TGF-β_1 gradient simulations. The computational model predicts the spatio-temporal distribution of TGF-β_1 in collagen (a) and fibrin (b) hydrogels, with respect to Case 4. The simulation figures show diffusion and binding patterns resulting after 24 hours since factor addition, being the added initial concentration of 10 ng•ml^{-1} (source in the left side of the device). The graphs depict the evolution -over the gel width- of diffusion and binding concentration profiles, denoted as C and R, respectively. Diffusion in both hydrogels follows a similar fashion. However, the bound factor presents enhanced activity in fibrin comparing to collagen.

4.4 Discussion

Directional cell migration is key to several pathological and physiological processes such as metastasis, morphogenesis and wound healing [195–197]. Particularly, the application of controlled chemical gradients of *in vitro* assays is fundamental to interpret and quantify the cellular response to different biochemical conditions. Microfluidic devices show the unique feature of mimicking real cellular

niches together with well-controlled chemical gradients. For this reason, a huge effort has been dedicated to their development by the scientific community [82, 92, 170, 171, 195, 198].

In 2D, chemical gradients are employed for a wide range of different applications [175, 178, 179, 199, 200]. Nevertheless, 3D systems allow for stable chemical gradients across chips containing hydrogel scaffolds, which better recreate the real ECM, and provide physiologically more relevant models. Indeed, several works are directed to the characterization and application of chemical gradients in 3D microsystems in order to address distinct biological issues [83, 86, 149, 180, 182, 198].

Most of these works consider diffusion and degradation of GFs as the main mechanisms during biomolecule transport. However, there are accumulating data showing the specific binding of GFs to the ECM-proteins *in vivo* as well as *in vitro* [147, 155, 157, 181, 184, 185]. This leads to a heterogeneous spatial distribution of matrix-bound (or solid state) chemical factors that regulates the transport of GFs inside the ECM. Therefore, it is fundamental to distinguish chemotactic (soluble factors regulated by diffusion within the interstitial soluble fluid) from haptotactic (solid state factors determined by binding to the ECM) gradients. Indeed, the high physiological relevance of haptotaxis has been pointed out. For example, Martino et al. [157] have proposed the nature to act as a GF reservoir as the main physiological function of fibrin, highlighting its direct and important role during wound healing.

In addition, several works indicate the distinct impact exerted by both taxis phenomena on the cellular migration patterns, in contrast to those that consider chemotaxis as a process including haptotaxis [152, 162, 201]. Therefore, our work suggests diffusion, binding and degradation mechanisms as main phenomena arising from the 3D transport of biomolecules when chemical gradients are established in

microfluidic platforms that contain hydrogels. To this end, our aim was to combine microfluidic experiments with ELISAs and numerical simulations. This approach was applied to two different GFs, PDGF-BB and TGF-β_1, whose chemical gradients were established in microdevices that hold two different hydrogels, collagen or fibrin. Therefore, the chemical response of the physiologically relevant biomimetic interactions between the studied GF and ECM were elucidated.

The combination of both methodologies allowed for the characterization of the chemical cues (chemotactic and haptotactic) induced within the microfluidic platforms. So, on the one hand, the microfluidic experiments, combined with ELISAs, led to the quantification of the temporal evolution of GF concentration in each compartment. On the other hand, the numerical simulations provided estimations of the spatio-temporal distribution of each GF within the scaffold gel. The quantitative comparison of both experimental and numerical results allowed for calibrating the parameters of the numerical model, as well as to validate the main assumptions in which the mathematical model is based on. Therefore, it was fundamental to set the main simplifications of our model and their implications on our results. The mathematical model here proposed assumed that three phenomena regulate the transport and conservation of GF within the scaffold gel: diffusion within the soluble fluid, temporal degradation and binding to the gel-scaffold.

Firstly, we assumed that the diffusion coefficient of the GF in the interstitial soluble fluid is dominated by the equation of Stokes-Einstein [202], corrected by means of the Ogston approximation [191], that takes into account the complex pore space between the fibers defining the scaffold hydrogel microstructure. Actually, the Ogston approximation is one of the most used techniques to quantify the effective diffusive transport properties of molecules within collagen hydrogels [203]. Then, we supposed the degradation rate of the GFs to be a linear function of the concentration. For each

specific experiment we estimated the degradation rate parameter in order to minimize the differences between *in vitro* and *in silico* experiments. Finally, we accepted that the GF not diffusing within the fluid and not degrading was going to be bound to the matrix. Although we were not able to measure it, this assumption is not new and many different authors have considered a similar hypothesis; for example, Zhang et al. [185] analyzed the role of diffusible binding patterns in modulating the transport and concentration of proteins in cartilage. In addition, there are also other experimental works that report the binding of PDGF-BB and TGF-β_1 to fibrinogen and collagen I as a crucial phenomenon in their transport [157, 158, 184]. Moreover, since GF concentrations are very low, it is considered that enough binding points in the hydrogel are always available and these are never saturated.

Despite these simplifications, this work clearly showed the ability of the model to predict all the results obtained from the *in vitro* experiments by incorporating the effective diffusion, binding and degradation phenomena, as shown in Table 4.3 and 4.4. Among all analyzed conditions the smallest average differences were achieved for Case 4, obtaining a degradation rate very similar to those experimentally measured. Nevertheless, there are significant differences depending on the hydrogel and the GF of interest. Regarding the transport of PDGF-BB in the hydrogels, the binding rate is much more significant for collagen than in the case of fibrin gels, where the effects of degradation and diffusion processes are more relevant. Indeed, Somasundaram and Schuppan [184] confirm the specific binding between PDGF-BB and collagen I: approximately 40% of the added factor was the bound portion in their experiments. In contrast, the promiscuity of PDGF-BB to bind fibrin is published to be of very short term, since Martino et al. [157] measured that in 24 hours 75% of the fibrin-bound PDGF-BB was released to the ECM. This fact explains the insignificant binding activity measured in this case. However, it could not explain whether the factor

continues to be active or inactive once it is released, which could elucidate the possible existence of a shift among the bound and soluble factor proportions.

Concerning the transport behavior of TGF-β_1, although the binding phenomenon is significant for both collagen and fibrin gels, it is 2-fold higher in the case of fibrin. Regarding the binding capability of TGF-β_1, it is known to bind fibronectin and collagen type IV; however, to our knowledge, there is no evidence to bind collagen I. Hence, although our predictions are consistent with the experimental approach, conscious by the existence of bound TGF-β_1 in collagen hydrogels, this event should be further cleared up. In contrast, the data obtained for fibrin hydrogels are compatible with those demonstrated by Martino et al. [157], since 24 hours after addition they still found 55% of the initial amount of bound TGF-β_1.

4.5 Summary

Microfluidic platforms are potential means to create 3D *in vitro* models, since this versatile technology allows for biomimetic microenvironments by including hydrogels and generating chemical gradients that direct cellular processes such as single cell migration. In this work, it is demonstrated that establishing chemical gradients in microdevices with biomimetic hydrogels is not straightforward, but different phenomena have to be considered, such as, effective diffusion, degradation and binding to the matrix. For such *in vitro* assays, therefore, two main regulatory mechanisms determine the cues that cells may sense in these physiological microenvironments: the chemotactic and haptotactic stimuli.

Chapter 5
Quantification of fibroblast 3D migration

Cell migration in 3D is a key process in many physiological and pathological processes. Although valuable knowledge has been accumulated through analysis of various 2D models, some of these insights are not directly applicable to migration in 3D. In this chapter, we have confined two physiologically relevant hydrogels, made of collagen and fibrin, within microfluidic platforms in the presence of a chemoattractant (PDGF-BB). By taking advantage of the biophysical and biochemical characterization shown in Chapter 3 and 4, respectively, we studied the migratory responses of human fibroblasts within these hydrogels, particularly the role of non-muscle myosin II (NMII).

5.1 Introduction

Cellular migration is a central event in physiological and pathological processes [77]. Individual cell migration has been extensively characterized in two-dimensional (2D) models, and these approaches have yielded most of our current knowledge on the molecular regulation of the component processes of cell migration, i.e., polarization, protrusion, adhesion, displacement of the cell body and retraction. However, cell migration *in vivo* is seldom 2D. Hence, cell migration is better addressed in three-dimensional (3D) conditions to resemble the real cellular microenvironment. Several studies have shown that the cellular mechanics and migratory mechanisms of the same cells are quite different in 2D and 3D [9–12].

Cell migration through 3D interstitial tissues is a multi-step process [15]. The ECM constitutes a heterogeneous multi-cue microenvironment [14] that directly affects cell behavior. It provides architectural scaffolding and orchestrates biochemical and biomechanical cues. Therefore, the ECM has a central role in physiological and pathological processes such as metastasis or wound healing [28]. Cells sense the mechanical properties -stiffness as well as external loading- and convert them into biological responses through the cytoskeleton by initiating signaling cascades that, among other responses, exert traction forces [16–20]. In this process, biochemical signals are also able to influence the mechanical sensing capability of the cell [21]. The integration of mechanical sensing and biochemical activation determines the ability of the cell to migrate, its phenotype and its ability to remodel the matrix as it migrates.

The ability of cells to sense and respond to the environmental cues is complex and dynamic [16, 17, 22–27], and alterations in this balance participate in the onset of several pathologies [25, 29]. For instance, in acute wound healing, the contraction

level is regulated by the cells through rigidity-sensing mechanisms, coordinating the healing process [204]. Furthermore, fibroblast differentiation into myofibroblasts -the contractile phenotype-, enables the final closure of the wound and drives locally continuous stiffening, leading to the assembly of fibrotic tissue [29, 51, 205].

Currently, various natural self-assembling ECM proteins are used to construct biomimetic hydrogels to perform *in vitro* studies [30, 31]. However, the combination of mechanical and biochemical properties of these gels drastically determine the migratory ability of the embedded cells [32–34], making it essential to thoroughly characterize these properties if we are going to decouple their individual contributions to the cellular migratory response.

3D cell migration depends on the physicochemical balance between cell deformability and physical tissue constraints [35]. These depend on ligand density, cross-linking level and architecture [28]. Ligand density correlates with binding sites for integrin receptors. Cross-linking concentration determines the susceptibility of the network to degradation by proteolytic enzymes and the fibrillar 3D arrangement -porosity, pore size and fiber diameter- [36], thus critically controlling the stiffness of the gel [30, 37]. The microstructure determines the permeability of the matrix, which directs the transport of biomolecules and local hydraulic asymmetries in the cell surrounding [23]. Together, all these parameters critically control cell migration: the ligand density [38, 39], stiffness [32, 40, 80], microstructure [12, 34, 41–44], local permeability gradients [45, 46] and external loading [18, 47].

In 3D, some of the biochemical cues that enable cell migration are immobilized in the matrix, whereas others diffuse through the meshwork. For example, growth factors (GFs), chemokines and other biomolecules diffuse through the pores of the network forming chemical gradients. The matrix may act not only as a diffusion controller through pore size and connectivity, but also as a factor-reservoir, by providing

available binding sites to the biomolecules. Therefore, they may get bound or remain as soluble factors. Based on this, chemical gradients at the microscopic level are heterogeneous in a context-dependent manner [23].

Microfluidics enables precise control of this microenvironmental complexity. It also offers versatility for a rational design of the experiments -by defining biochemical and biomechanical cues- and real-time visualization -allowing *in vivo* quantification-. Due to all these advantages, the use of microfluidic platforms is on the rise for studying 3D migration [81, 82], including angiogenesis [83, 84], metastasis [85, 86] and neuronal migration [87, 88].

Another key example of relevant migratory phenomenon is wound healing. Different aspects have been analyzed, including fibroblast mechanics, growth factor signaling and matrix remodeling [22, 47, 51, 60–62, 64, 66, 68, 70–73, 206]. These approaches have also addressed the role of multiple spatial cues, requirement for integrin-dependent adhesion and the assembly of actin-based structures [26, 74, 78, 79]. Responses have turned out to be context-dependent, by adapting dynamically the migration mode to local architecture, proteolytic and mechanical properties [44, 75–77].

To the best of our knowledge, 3D fibroblast migration has not been studied by using microfluidic devices. In this work, two physiologically relevant matrices have been characterized, and their ability to support fibroblast migration analyzed in a highly quantitative manner. We have used collagen I and fibrin matrices due to their crucial role in different phases of wound healing. Fibrin is the main constituent of the matrix during clotting, whereas collagen I is synthesized and remodeled by migrating fibroblasts to form the scar. The hydrogels were injected and confined into the microdevices to mimic confined processes such as granulation [16] and connective tissue remodeling [29].

Initially, we have characterized the biophysical properties of each matrix, followed by quantification of fibroblast migration in the two matrices in response to chemotactic stimulation with Platelet-Derived Growth Factor-BB (PDGF-BB). Finally, we have addressed the role of non-muscle myosin II (NMII) in fibroblast migration under these conditions. Our results indicate that fibroblast migration is critically controlled by the biophysical properties of the matrix in a NMII-dependent manner. Our results also indicate that, although chemotactic and haptotactic signals enhance directional migration, they are not sufficient by themselves, to overcome the restrictions imposed by the microarchitecture of the microenvironment or the lack of functional myosin II in live cells.

5.2 Materials and methods

5.2.1 Microfluidic platform

As mentioned in Chapter 2 Section 2.1, microdevices were carried out following the methodology proposed by Shin et al. [92]. Hence, soft lithography was employed to achieve positive SU8 300 μm-relief patterns of the desired geometry onto a silicon wafer (Stanford University). Polydimethylsiloxane (PDMS, Sylgard 184, Dow Corning GmbH), mixed at a 10:1 ratio of base to curing agent, was then poured and cured onto the SU8 master. The replica-molded layer was trimmed, perforated and autoclaved. Finally, the PDMS devices and 35 mm glass-bottom petri dishes (Ibidi) were plasma bonded and treated with poly-D-lysine (PDL) solution at 1 $mg \cdot ml^{-1}$ (Sigma-Aldrich) for an enhanced surface-matrix attachment (see Fig. 5.1a).

The geometry of the device was based on that used by Farahat et al. [83], as shown in Fig. 5.1b. It comprised a central cage which contained the hydrogel with the embedded cells. In direct contact to the gel, it also had two media channels in order to

ensure hydration and transport of nutrients and other chemical factors throughout the hydrogel.

Fig. 5.1. Microfluidic platform for migration experiments. It fits within a 35 mm glass-bottom petri dish, as shown in detail in picture (a). It comprises a central channel (pink) -in which the hydrogel is injected- and two media channels (green and blue) in direct contact to the gel.

5.2.2 Hydrogel preparation and cell seeding

Cell culture. Normal Human Dermal Fibroblasts (NHDF, Lonza) were cultured up to passage 10 using Fibroblast Growth Medium-2 (FGM-2, Lonza) (see detailed procedure in Appendix A Protocol A.2). The cells were passaged or used for experiments when they reached 80% of confluence. Hydrogels were loaded with cells harvested by sequential trypsinization and centrifugation, and mixed with the gel solutions at a final concentration of $0.5 \cdot 10^6$ cells·ml^{-1}, approximately.

Collagen solution. As indicated in Chapter 2 Section 2.1, we followed the procedure described in Shin et al. [92]. Briefly, collagen type I (BD Biosciences) was buffered to a final concentration of 2 mg·ml^{-1} with 10x DPBS -calcium, magnesium- (Gibco), cell culture grade water (Lonza) and the cell solution. The dilution was brought to pH 7.4 with NaOH.

Fibrin solution. Summarizing the method detailed in Chapter 2 Section 2.1, Human Fibrinogen -plasminogen, fibronectin, factor XIII depleted- (American Diagnostica GmbH) was diluted in buffer (50 mM Tris, 100 mM NaCl and 5 mM EDTA at a pH 7.4) as indicated by the provider. After mixing it with Human Factor XIII (American Diagnostica GmbH), the mixture was allowed to polymerize in presence of Human Alpha-Thrombin (American Diagnostica GmbH) along with $CaCl_2$ (Sigma) and the cell solution, at a final pH of 7.4.

Hydrogel polymerization. Throughout the manipulation, the reagents and mixture were maintained on ice for both preparations. As soon as the gel solution was ready, it was pipetted into the gel cavity using the auxiliary channels (see Fig. 5.1). Upon insertion, the samples were allowed to polymerize inside humid chambers. The gels were then hydrated with FGM-2 and stored in the incubator for 24 hours before initiating the experiments, to ensure stabilization of the matrix and cell adhesion and conditioning.

5.2.3 Microstructural and rheology studies

An integral biophysical and biomechanical characterization of the hydrogels was performed in order to elucidate the microenvironmental cues. The methodology is detailed in Chapter 3 Section 3.2. In brief, microstructural analysis was carried out using Scanning Electron Microscopy and Confocal Reflection Imaging analysis. The resistance to flow of the gels was also assessed quantifying their permeability or hydraulic conductivity. Finally, oscillatory strain amplitude sweeps were performed using a rheometer and the elastic and viscous shear moduli were measured.

5.2.4 Chemical conditioning

After 24 hours of incubation since polymerization, the 3D systems were ready to use. As controls, culture media was renewed in both media channels. In inhibition experiments, medium in both channels contained 30 μM (+/-) blebbistatin (EMD Millipore) or vehicle control (DMSO, Amresco), respectively. Detailed procedure for media replacement is shown in Chatper 2 Section 2.3.

The establishment of PDGF-BB (Abcam) gradient across the gel was achieved by adding the growth factor (GF) containing culture media (5 $ng \cdot ml^{-1}$) to only one channel -green-, while new medium alone was added to the other channel -blue- (refer to Fig. 5.1b). For more specified procedure information see Chapter 2 Section 2.3.

The spatial distribution of PDGF-BB chemical gradient in both collagen and fibrin hydrogels was predicted by numerical simulations. As detailed in Chapter 4 Section 4.2, a computer framework was developed based on a reaction-diffusion transport model, which was validated with experimental results. This mathematical approach is able to estimate diffusion and binding mechanism patterns yielded from an established chemical gradient through fibrous matrices.

5.2.5 Immunofluorescence staining and imaging

The samples were stained for both vinculin and phalloidin and imaged using a Nikon D-Eclipse C1 Confocal Microscope -equipped with a Plan Apo VC 60XH objective- and an Olympus Fluoview FV10i Confocal Microscope -with an UPLSAPO 60XW objective-. As specified in Chapter 2 Section 2.4, once the cells were fixed in 4% paraformaldehyde (Affymetrix) in PBS for 20 min at room temperature, samples were washed in PBS three times and permeabilized with 0.1% Triton X-100 (Calbiochem) in PBS at room temperature. Cells were washed another

three times and blocked with 3% goat serum (Sigma) in 5% BSA/PBS solution for 4 hours at room temperature. Afterwards, the devices were incubated overnight at 4ºC with mouse anti-human hVin-1 antibody (ab11194, Abcam) at 1:100 in 0.5% BSA/PBS. Then, after washing the samples five times with 0.5% BSA/PBS, incubation with Alexa Fluor® 488 goat anti-mouse antibody (A11029, Molecular Probes) at 1:100 and the conjugated Alexa Fluor® 594 phalloidin (A12381, Molecular Probes) at 1:200 was done for 3 hours at room temperature in the dark. Finally, cells were washed three times with 0.5% BSA/PBS, two more times with PBS, and subsequently imaged.

5.2.6 Cell tracking

Once the chemical arrangement for each device was done, all the samples were allowed to warm up for 30 min. Then, time-lapse imaging was carried out by acquiring phase contrast images every 20 minutes for 24 hours. The focal plane was chosen to be in the middle along the z-axis of the device. It intended to minimize the edge effects resulting from the glass and PDMS surfaces by ensuring that the tracked cells were fully embedded within the 3D network. During the whole experiment, the incubation conditions were controlled and held at 37ºC, 5% of CO_2 and 95% of humidity.

Approximately 150 cells were tracked out of each set of experimental samples. Cell trajectory acquisition was performed using a hand coded semi-automatic Matlab script. By comparison of pixel intensities and using matrix convolution techniques, the software was able to find and track cell centroids, requesting the user for visual correction, and finally post-processing the migration results. As to the measurements, the whole trajectories of each individual cell were outlined in red, green and blue for zone 1, 2 and 3, respectively. In addition, the polar histograms were employed to

display the directionality of the migratory cell, with respect to the final point. Likewise, the mean -referring to the instantaneous- and effective -as to the euclidean- cell speed were quantified. By demonstrating different boxplots, these values were gathered averaged or discerning the zone to which cells corresponded.

5.3 Results

5.3.1 Biophysical and biomechanical cues

We initially characterized the biophysical features of collagen I and fibrin gels (refer to Chapter 3 for details). As summarized in Table 5.1, our results showed that, on average, pore size and permeability are 2-fold higher in collagen than in fibrin gels. Stiffness of the collagen scaffolds is approximately 20-fold higher than those made of fibrin; elastic shear moduli of 15 and 300 Pa were measured, respectively. We have used these experimental parameters to interpret the migration of human dermal fibroblasts (next sections).

Table 5.1. Biophysical and biomechanical properties of collagen and fibrin hydrogels.[a]

	Collagen	Fibrin
Pore size (μm)	2.84±0.94	1.69±0.33
Darcy's permeability (m^2)	$1.00 \cdot 10^{-12}$	$5.73 \cdot 10^{-13}$
Elastic shear modulus (Pa)	15	300

[a]The data for pore size are presented as mean ± SEM. Detailed characterization is shown in Chapter 3.

5.3.2 Cell morphology

Fibroblasts seeded in collagen I and fibrin matrices exhibited important differences in terms of cell shape and morphology. As shown in Fig. 5.2, fibroblasts in collagen gels were stretched out and displayed multiple, branched, long, protruding structures with actin. Conversely, cells in fibrin hydrogels presented frayed spindle-like protrusions and fewer actin patches in the projections.

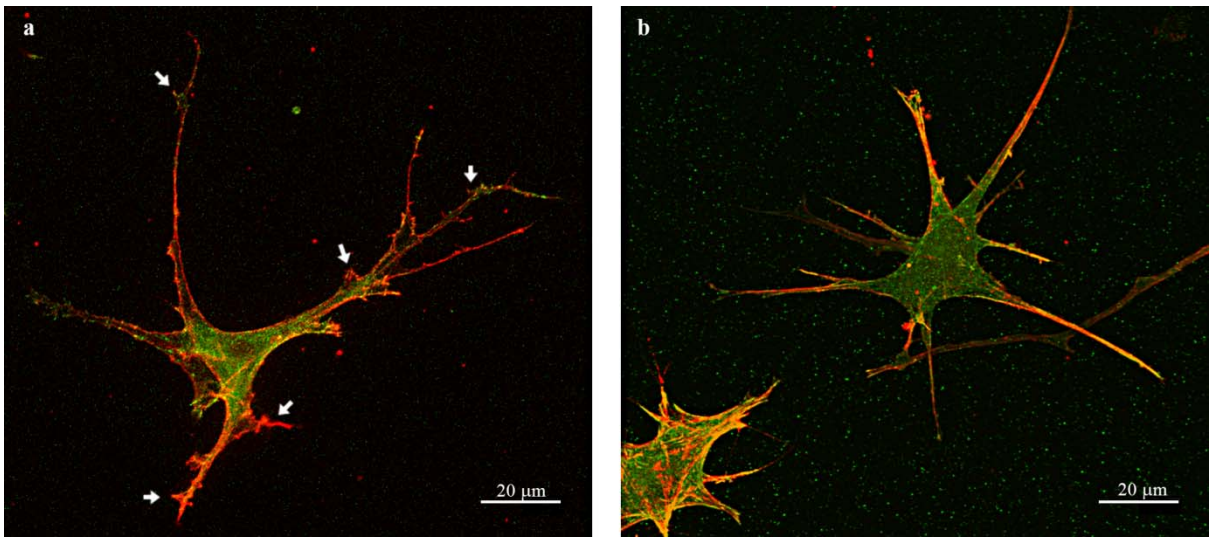

Fig. 5.2. Fibroblasts morphology in 3D. It is shown by distribution of actin (red) and vinculin (green). The image in collagen was taken by the Nikon D-Eclipse C1 Confocal Microscope (a) and the one in fibrin employing the Olympus Fluoview FV10i Confocal Microscope (b). The white arrows point to some of the varicosities.

5.3.3 Quantitative comparison of migration in collagen and fibrin

When we compared the migratory behavior of dermal fibroblasts in both control gels, we observed important differences. Cells were less motile in fibrin. In the absence of a chemoattractant, cells were not persistently migratory in either matrix (Fig. 5.3a-b, e-f) and migratory speed was low in collagen (Fig. 5.3c-d), but even

lower in fibrin (Fig. 5.3g-h). This was not due to an intrinsic inability of the cells to polarize or extend projections (Fig. 5.4). Interestingly, fibroblasts in collagen displayed robust "contractile shaking", which was not observed in cells in fibrin gels.

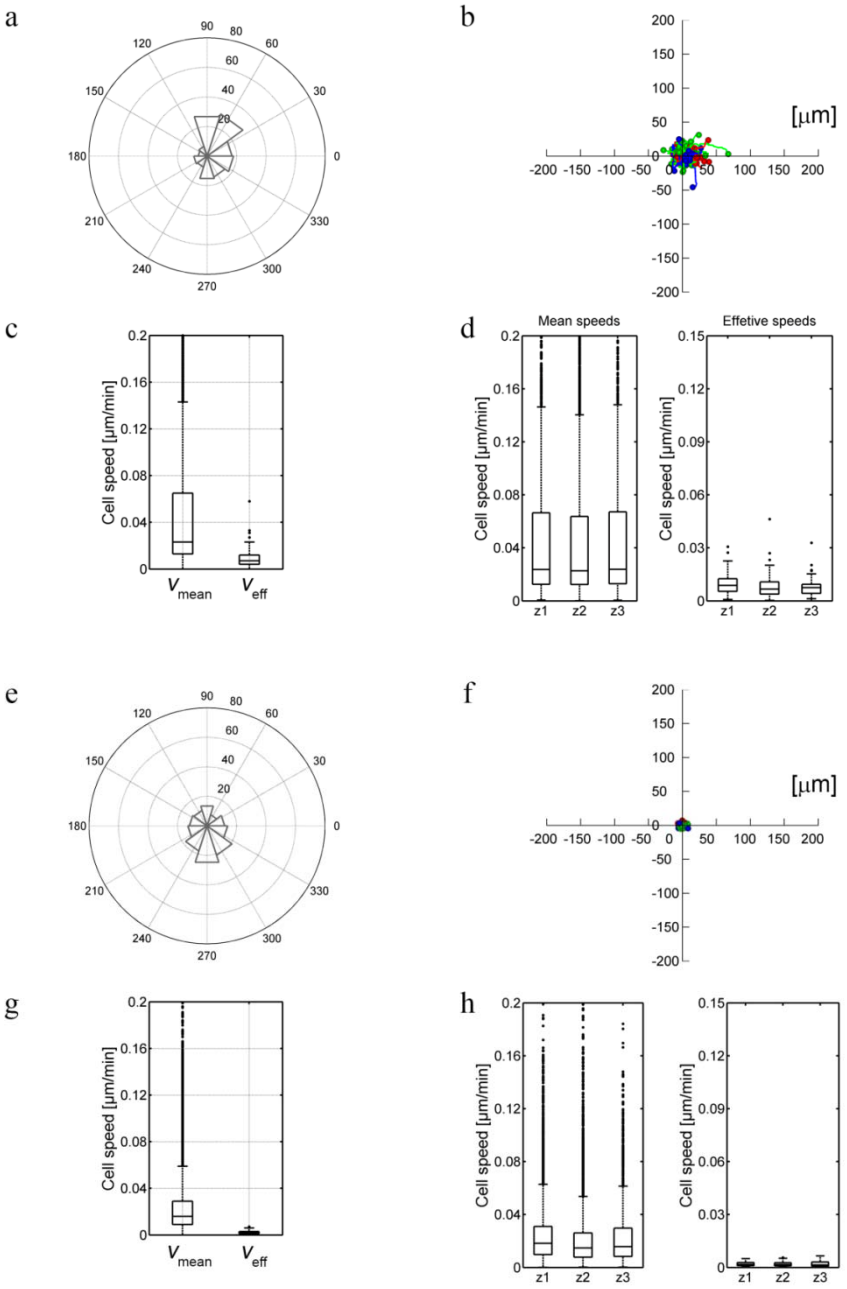

Fig. 5.3. Migration quantification in control collagen (a-d) and fibrin (e-h) gels. The polar histograms (a,e) show the directionality of the migratory cell. The trajectories of individual cells are outlined in (b,f). The boxplots show the mean and effective speed of cells considering the whole device (c,g) or distinguishing the zone they belong to. The median values are gathered in Table 5.2.

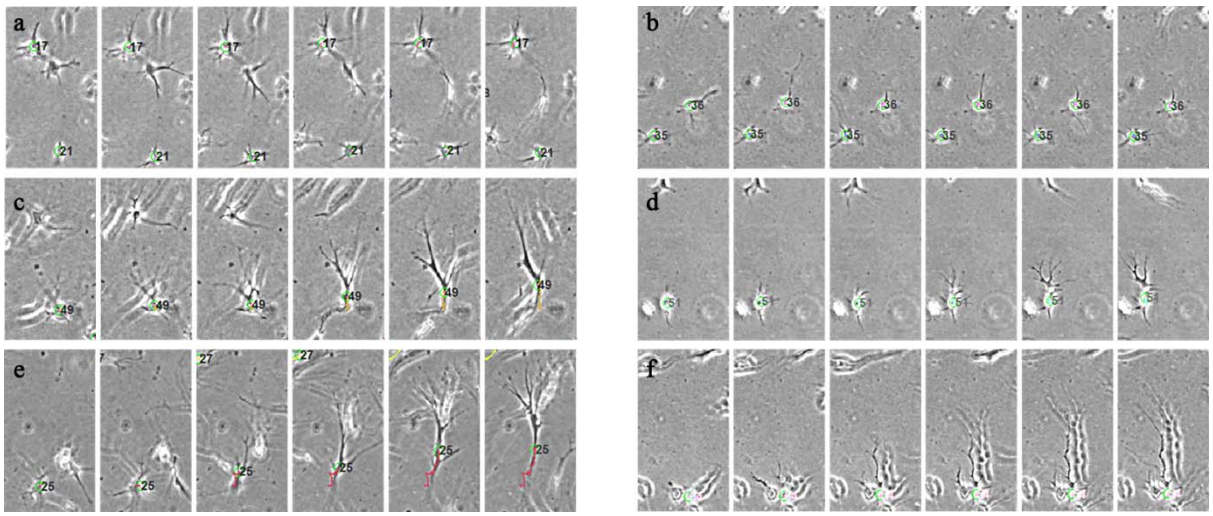

Fig. 5.4. Sample time-lapse images of cells migrating in control samples (a, b), under PDGF-BB gradient (c,d) and under PDGF-BB gradient including blebbistatin (e,f). Samples correspond to fibroblasts 3D migration in collagen (a, d, e) and fibrin (b, d, f) gels.

5.3.4 Characterization of PDGF-BB gradients in microfluidic hydrogels

PDGF-BB is secreted by platelets during clotting and acts as a natural chemoattractant for dermal fibroblasts during wound healing. We took advantage of the intrinsic polarity of the microfluidic device to generate gradients of PDGF-BB and quantify the migratory properties of dermal fibroblasts as they navigate the hydrogels in its presence.

As shown in Chapter 4, we have validated a computational tool to assess transport and distribution of soluble growth factors in 3D hydrogels. This tool determines diffusion and binding processes that regulate the distribution and transport of chemical gradients. This is quite relevant to estimate cell migration as it accounts for possible binding events that trigger haptotaxis (migration in response to immobilized factors) in addition to chemotaxis.

The predicted spatio-temporal distribution of the GF inside the both collagen and fibrin hydrogels is shown in Fig. 5.5a. In collagen gels, diffusion and binding events dominated the distribution of PDGF-BB inside the hydrogel. On the contrary, fibrin matrices display non-significant binding; hence diffusion is the leading factor during its distribution in the hydrogel.

Based on this information, we defined three zones in the hydrogels, depicted in Fig. 5.5b. In zone 1, effects are characterized by the strong effect of bound PDGF-BB, which decreases in zone 2 and 3. Soluble PDGF-BB would follow a linear-like distribution from the PDGF-BB-loaded channel. Conversely, binding is negligible in fibrin gels, hence the distribution of PDGF-BB is solely determined by a linear gradient stemming from the PDGF-BB-containing channel.

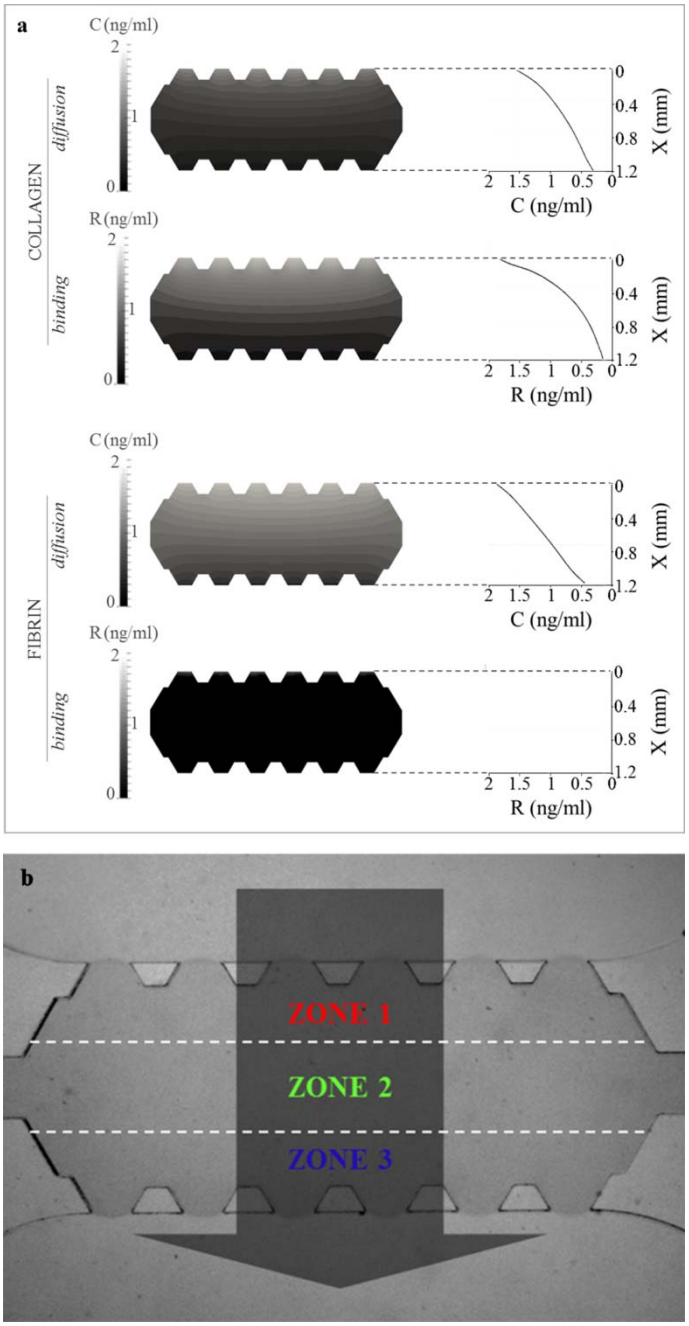

Fig. 5.5. Spatial distribution of PDGF-BB in collagen and fibrin hydrogels (a). Three zones are traced by the white dashed-lines within the devices for migration quantification (b). The dark arrow indicates the direction in which the chemical gradient is set; its origin would denote the maximum concentration. Trajectories corresponding to zone 1, 2 and 3 will be drawn in red, green and blue, respectively.

5.3.5 Differential effect of PDGF-BB on migration in collagen and fibrin

We then sought to determine the effect of PDGF-BB on fibroblast migration in collagen and fibrin hydrogels. Embedded fibroblasts were exposed to PDGF-BB gradients and observed in collagen and fibrin gels (Fig. 5.4c and 5.4d, respectively). In both cases, cells exhibited an increased number of dendritic protrusions towards the source of PDGF-BB, as previously reported [62, 66, 207]. However, protrusions were longer and more stable in cells within collagen. Increased protrusiveness correlated with increased motility (Fig. 5.6). The effect was much more significant in cells in collagen (compare Fig. 5.4b and 5.4f). Furthermore, cells within zone 1 displayed much higher speed than those in zone 2 (Fig. 5.6d). Comparatively, cells in zone 3 had no significant response to the gradient. Conversely, cells on fibrin displayed increased protrusiveness that resulted into a modest increase in cellular "wandering" (non-directional migration), but that effect did not translate into increased effective speed in any of the zones (Fig. 5.6h).

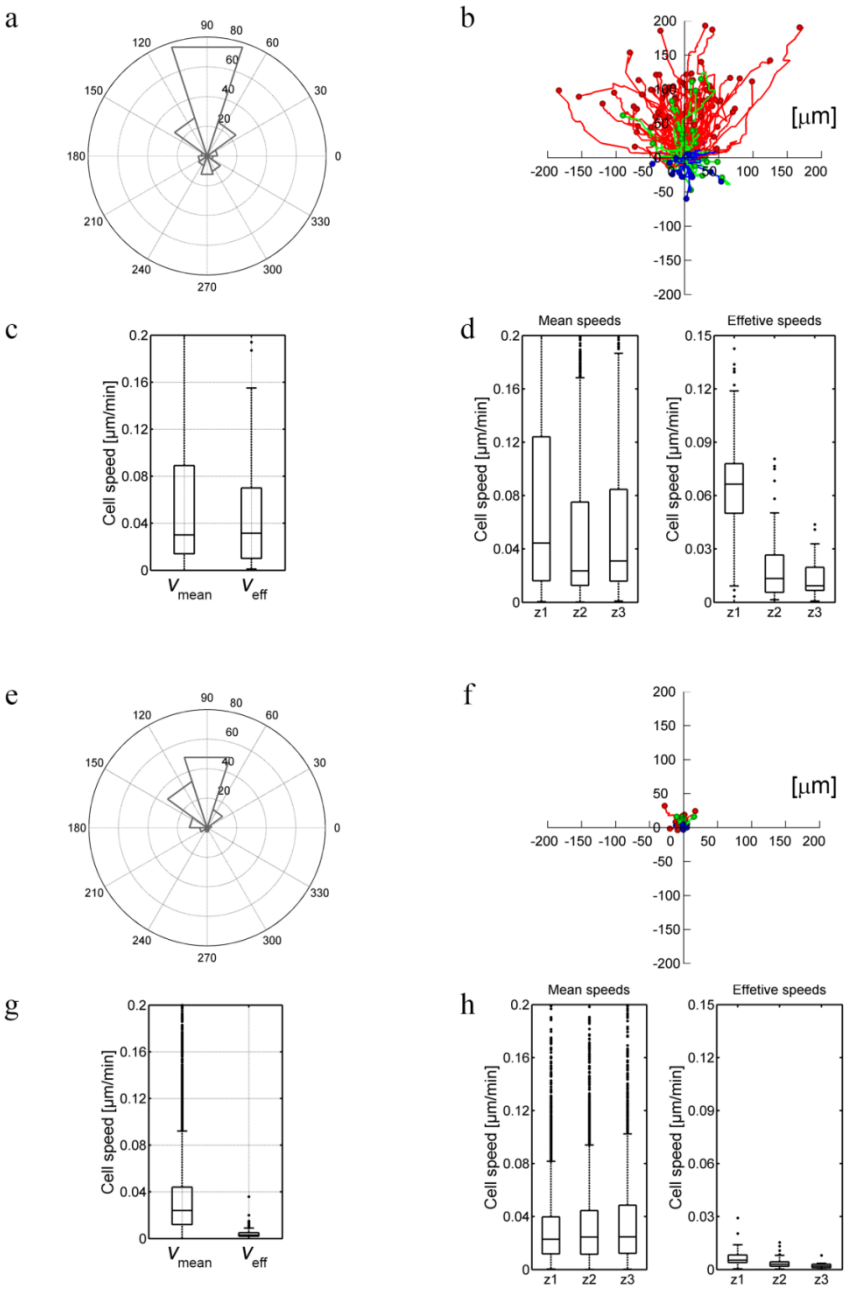

Fig. 5.6. Migration quantification in PDGF-BB gradient-generated collagen (a-d) and fibrin (e-h) gels. The polar histograms (a,e) show the directionality of the migratory cell. The trajectories of individual cells are outlined in (b,f). The boxplots show the mean and effective speed of cells considering the whole device (c,g) or distinguishing the zone they belong to. The median values are gathered in Table 5.2.

5.3.6 Non-muscle myosin II controls migratory speed in collagen

Non-muscle myosin II (NMII) modulates spontaneous fibroblast migration in 3D [44]. To assess its role in directional 3D migration we infused the hydrogels with blebbistatin, which is a highly specific inhibitor of the ATPase activity of NMII, hence, blocking contractility [208]. We found that, in fibrin, blebbistatin increases protrusiveness, consistent with its effect in 2D [209], but this effect does not translate into increased migration (Fig. 7e-h). In collagen, blebbistatin did not affect the orientation of the cells towards the gradient (Fig. 7a), or the emission of protrusions in the direction of the higher concentration of PDGF-BB (Fig. 4e). However, it attenuated migration towards PDGF-BB, particularly that of cells in zone 1 (Fig. 7b-d). Together, these results suggest that NMII does not control the orientation of fibroblasts towards a chemotactic gradient in collagen hydrogels, but it does control the ability of cells to migrate efficiently.

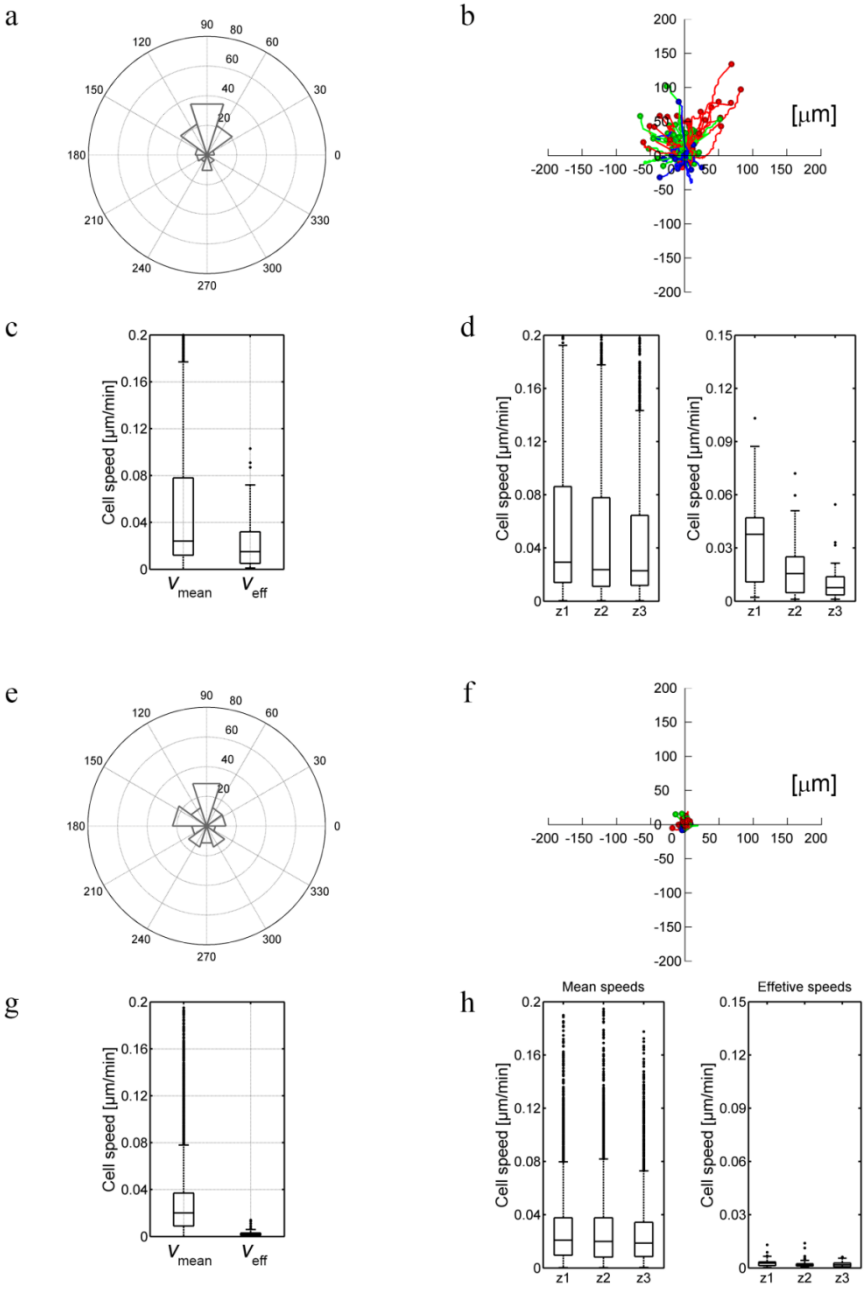

Fig. 5.7. Migration quantification in PDGF-BB gradient-generated collagen (a-d) and fibrin (e-h) gels, including 30 μM blebbistatin. The polar histograms (a,e) show the directionality of the migratory cell. The trajectories of individual cells are outlined in (b,f). The boxplots show the mean and effective speed of cells considering the whole device (c,g) or distinguishing the zone they belong to. The median values are gathered in Table 5.2.

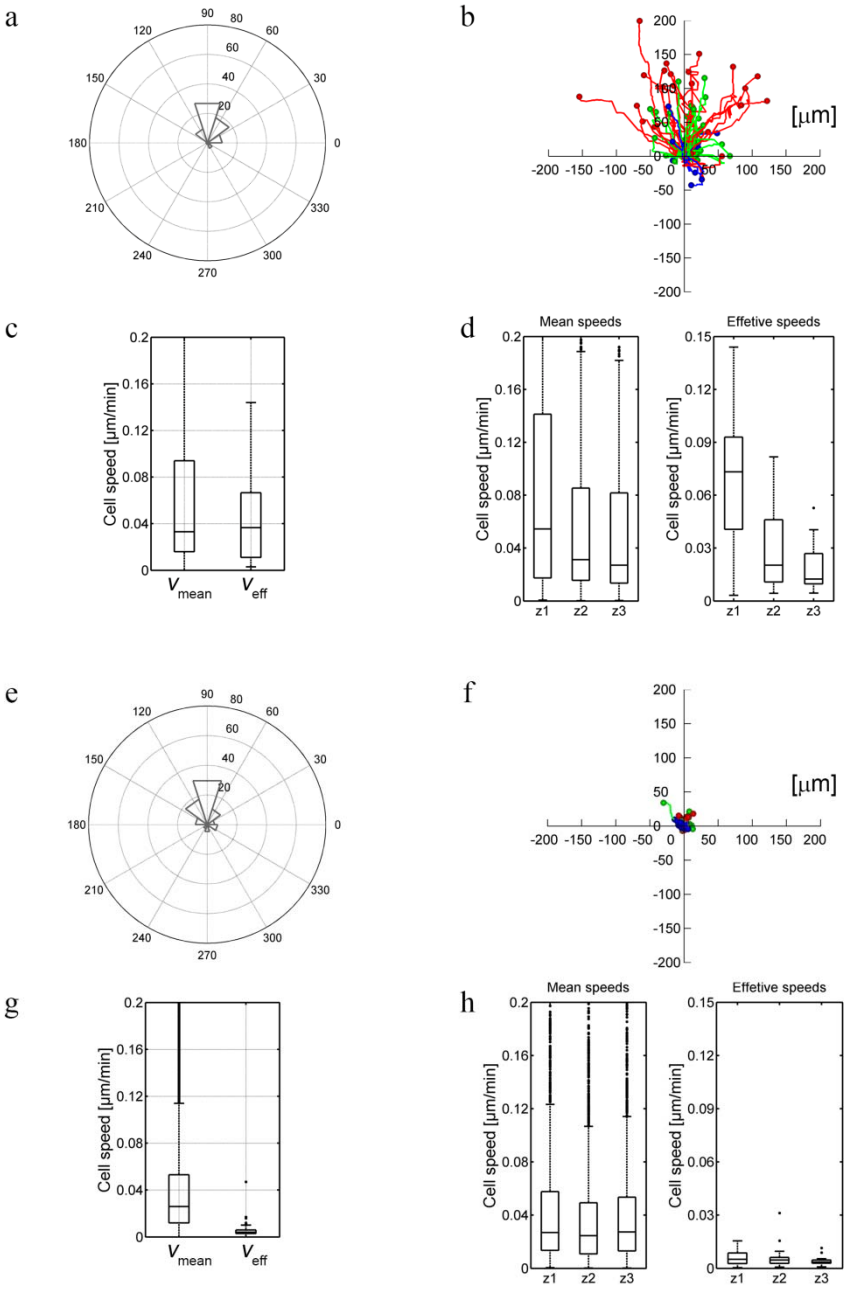

Fig. 5.8. Migration quantification in PDGF-BB gradient-generated collagen (a-d) and fibrin (e-h) gels, including vehicle-control. The polar histograms (a,e) show the directionality of the migratory cell. The trajectories of individual cells are outlined in (b,f). The boxplots show the mean and effective speed of cells considering the whole device (c,g) or distinguishing the zone they belong to. The median values are gathered in Table 5.2.

Table 5.2. Median values obtained from the migration quantification[b].

		Collagen			
		Control	PDGF-BB	Vehicle-control	Blebbistatin
All speeds	Mean	0.023	0.030	0.033	0.024
	Effective	0.007	0.031	0.036	0.015
Mean speed per zone	Zone 1	0.024	0.044	0.054	0.029
	Zone 2	0.023	0.024	0.031	0.024
	Zone 3	0.024	0.030	0.027	0.023
Effective speed per zone	Zone 1	0.008	0.066	0.073	0.038
	Zone 2	0.007	0.013	0.020	0.015
	Zone 3	0.007	0.009	0.012	0.008

		Fibrin			
		Control	PDGF-BB	Vehicle-control	Blebbistatin
All speeds	Mean	0.016	0.024	0.026	0.020
	Effective	0.002	0.005	0.006	0.003
Mean speed per zone	Zone 1	0.018	0.023	0.026	0.021
	Zone 2	0.015	0.024	0.025	0.020
	Zone 3	0.016	0.025	0.026	0.019
Effective speed per zone	Zone 1	0.005	0.005	0.005	0.003
	Zone 2	0.003	0.004	0.005	0.002
	Zone 3	0.001	0.003	0.005	0.002

[b]This values refer to Fig. 5.3, 5.6, 5.7 and 5.8 and are expressed in $\mu m \cdot min^{-1}$.

5.4 Discussion

In this work, we have combined microfluidics with hydrogels and gradients of soluble growth factors in order to gain a better insight into fibroblast sensing and migratory mechanisms. We have used two biomimetic hydrogels, collagen and fibrin,

characterized them and applied growth factors to form a gradient and study fibroblast migration.

In general, our observations indicate that collagen gels promote fibroblast migration more efficiently. In collagen, fibroblasts showed “contractile shaking”, likely due to cycles of protrusion extension and retraction. This is accompanied by net translation of the cell body, particularly in response to a directional chemical cue, e.g. PDGF-BB in a gradient. In this interpretation, extension and retraction forces are coordinately transmitted to the cell body to support its forward motion. In fibrin, the cells display comparable extension and retraction of protrusions. However, the cell body does not move. This could be interpreted as lack of traction on fibrin, which would prevent transmission of the traction to the cell body for movement. This is a major difference that likely underlies the different biochemical response observed when cells are confronted with a gradient of PDGF-BB in collagen or fibrin. Additional reasons may relate to biophysical issues such as pore size, permeability, the degree of polymer cross-linking and stiffness. Stiffness in collagen is 20-fold lower than in fibrin. However, it has been demonstrated that fibroblast migration is independent of matrix stiffness [80]. Fibrin is more cross-linked than collagen, which decreases its susceptibility to degradation. Additionally, pore size and permeability in fibrin are approximately half the size of collagen gels. On the one hand, migration through small gaps has been shown to require proteolytic degradation of the matrix [12, 37]. In this context, the nucleus becomes a spatial hindrance for migration in the absence of degradation [32]. On the other hand, confined migration has been shown to prefer environments with lower hydraulic resistance, even in chemotaxis-competing contexts [46]. Actually, fibroblast migration has been pointed to be porosity-dependent [80], which could be underlying permeability capabilities. As to this interpretation, the narrower pore, reduced degradation and increased hydraulic resistance of the fibrin gels would impede productive migration in 3D.

In general, cells are faster in collagen gels in response to PDGF-BB gradients, which is not surprising. However, segmentation of the migratory behavior of the cells with respect to the origin of the gradient revealed a non-linear response in terms of speed. Closer to the origin of the gradient (zone 1), cells displayed an 8-fold increase in effective speed, whereas it was only 2-fold in zone 2, i.e., more removed from the origin of the gradient. Cells in zone 3 (far from the origin) displayed no significant increase in speed. The most obvious interpretation relies on the difference of diffusion-based PDGF-BB concentration between zones 1 and 2 (zone 1 is closer to the source). However, this would likely imply an almost linear difference between zones, which is not the case. Hence, some factor contributes to amplify the difference between zones 1 and 2. We have noted that in collagen I zone 1, two populations of PDGF-BB appear: one follows the rules of diffusion, but the other appears immobile. We hypothesize that this second population is adsorbed or otherwise immobilized on collagen fibers, constituting a potent haptotactic signal. Several studies using EGF have demonstrated that immobilized growth factors modify their properties towards inducing cell migration [210]. This is likely due to increased signaling due to clustering of the receptor. An additional possibility is that PDGF-BB enhances integrin-mediated adhesion through a cross-talk mechanism [211].

The decrease in cell migration due to non-muscle myosin II (NMII) inhibition may owe to a number of reasons: one is that NMII controls nuclear repositioning in migrating cells [212]. In 3D, emerging evidence indicates that the nucleus is the main steric hindrance towards productive migration. It is feasible that NMII-inhibited cells get their nuclei “stuck” in the pores and are unable to migrate forward. In this interpretation, exaggerated protrusion results from inefficient attempts to compensate increased nuclear drag. Additional possibilities include deficient adhesion assembly. A recent study has shown that NMII inhibition prevents adhesion enlargement in 3D [44]. Even if adhesions assemble, they do not reach a threshold size to transmit

traction to the cell body, resulting in the same phenotype caused by nuclear drag. This possibility is further supported by the more dramatic effect of blebbistatin in zone 1 cells compared to zone 2, which suggests that the inhibition mechanism is related to the haptotactic response to PDGF-BB in this region by a more active participation of NMII in the cellular response to immobilized than soluble growth factors in 3D, since immobilized PDGF-BB requires more of NMII participation in order to transactivate the integrins or/and produce traction.

5.5 Summary

Multiple 3D migration-modes have been proposed in several previous works. The context-dependent phenomenon is established by a dynamic and interrelated physicochemical balance, which makes complex elucidating the underlying mechanisms. In this work, employing collagen and fibrin -based microfluidic models, we quantified and compared migration in 3D. By analyzing the chemotactic and haptotactic response to PDGF-BB cues, as well as to NMII inhibition, it has been determined that local microarchitecture of the 3D networks, along with haptotactic cues, regulates migration in a NMII-dependent manner by controlling the physicochemical medium-nucleus deformability balance.

Chapter 6
Conclusions and future work

This chapter serves as the closure of the Thesis dissertation. It comprises the main conclusions yielded from the work, suggests some potentially interesting future research lines, and also cites the main outcome contributions.

6.1 Conclusions

Throughout the dissertation, three main keystones have pointed out to be the bases of this Thesis: the biophysical arrangement of the fibrillar networks, the biochemistry of the microenvironment and the cell mechanics as the epicenter. Indeed, in this work the interplay among the three bases has been studied. In this regard, we recreate the basic principles that regulate the wound healing progression, by elucidating the complex interaction between fibroblasts and the three-dimensional matrices and

growth factors. Hence, the main conclusions of the Thesis are summarized organized in a thematic manner below:

1. With respect to the biophysical properties, an integral and physiologically-relevant characterization has been performed in order to overcome the diversification of the existing data. The most relevant features of the biophysical definition are cited below:

- Physiological composition of the fibrin hydrogels has been settled.
- Although fibers within both lattices are similar in diameter (70-80 nm), fibers within collagen networks tend to form bundles, whereas those in fibrin are formed mainly individually.
- The collagen mesh has been determined to be looser than fibrin: the pore size and permeability are 2-fold higher in collagen than in fibrin gels.
- Stiffness of the collagen scaffolds is approximately 20-fold higher than those made of fibrin, being the elastic shear moduli of 15 and 300 Pa, respectively.
- Both gels have presented non-linear elasticity by means of strain-hardening. However, in fibrin it occurs at 10 % of strain, whereas for collagen starts at 50% of strain.

2. Akin established chemical gradients, the spatio-temporal distribution yielded from growth factor (GF) transport has been determined for TGF-β_1 and PDGF-BB. The GF-matrix interaction has been studied in collagen and fibrin hydrogels and has been determined to induce chemotactic as well as haptotactic cues, as follows:

- The computational model here proposed is able to predict degradation, diffusion and binding phenomena of the biomolecules.
- TGF-β_1 is more stable than PDGF-BB when diluted in culture media.

- Both diffusion and binding processes regulate the transport of PDGF-BB in 3D collagen scaffolds. Hence, the GF is distributed in a heterogeneous non-linear manner.
- During PDGF-BB transport through fibrin, diffusion prevails. Since the binding mechanism is negligible, the chemical compound is finally distributed linearly alongside, only inducing chemotactic cues.
- TGF-β_1 transport across collagen gels leads to a similar behavior of both diffusion and binding phenomena. Hence, the overall distribution responds to a parallel distribution of the biomolecules, although both distinct availability natures coexist.
- Diffusion pattern of TGF-β_1 in fibrin networks is similar to that in collagen. However, it binds significantly more in fibrin, which yields in a dissimilar overall distribution.

3. In order to analyze the three-dimensional (3D) fibroblast migration, several tests have been performed by confining collagen and fibrin hydrogels within the microdevices. The major conclusions are listed below:

- The cells display important differences in terms of cell shape and morphology: fibroblasts in collagen appear stretched out with multiple dendritic protruding structures with actin, whereas in fibrin gels present frayed spindle-like protrusions with a lower number of actin patches in the projections.
- Collagen promotes fibroblast migration in 3D more effectively than fibrin.

- Biophysical factors such as degradability, pore size and the resistance to fluid flow have been pointed out to be main factors for limiting productive migration in fibrin.
- Non-muscle myosin II is required for an efficient migratory response of the fibroblasts.
- Haptotaxis mechanism has been proven to regulate fibroblast migration in 3D, when exposed to PDGF-BB gradients in collagen hydrogels.

6.2 Future lines

Although the obtained conclusions add further insight into fibroblast mechanics within the early phase of wound healing, the obtained conclusions have opened other questions in that respect. Actually, suggestions of potentially interesting future research lines are mentioned within this section.

Study of focal adhesion and stress fiber structures. In this Thesis, context-dependent cues have been studied to understand how they affect to the 3D migration process. However, the formation of focal adhesions (FAs) and stress fibers (SFs) is essential to elucidate the structures that cells generate to effectively migrate. Hence, unraveling the linkage of these structures to the standpoints studied within this work could be of high relevance. To do so, the development of analytical tools that allow for both systematic and quantitative analysis of FAs and SFs is essential. In this regard, framed within this formation period, we have anticipated and collaborated in the development of an image-based analytical tool that allow extracting quantitative information departing from immunofluorescence images stained for phalloidin and actin (published work) [213]. An example of FA and SF

quantification is shown in Fig. 6.1. Hence, as future work, it would be interesting applying such tool to our experiments in order to complete our knowledge with regard to fibroblast mechanics in 3D.

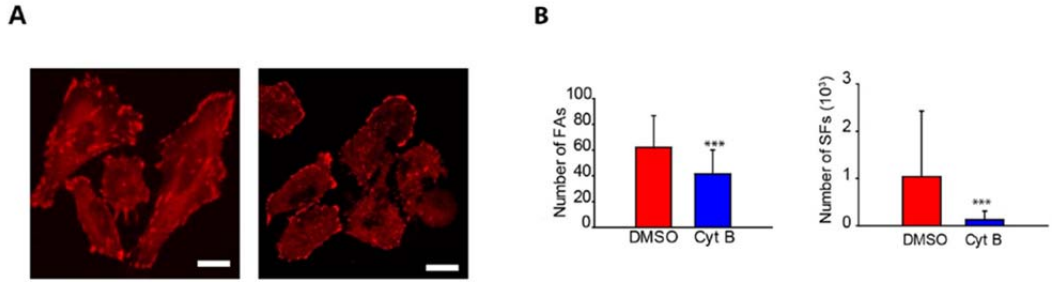

Fig. 6.1. FA and SF quantification. The tool discerns that the effect of cytochalasin B (Cyt B) is more pronounced on SFs than on FAs. (A) Image samples of vinculin in DMSO control cells and Cyt B-treated cells. (B) Quantification of the number of FAs and SFs per cell (number of cells: DMSO, n = 33; Cy B, n = 29). Scale bars are 20 μm. ***:p<0.001. [213]

Microstructural modifications. Since pore size *in vivo* undergoes a wide range of variety, it could add valuable information varying biophysical factors of both matrices in order to evaluate the impact on cell migration and transmigration. To do so, several techniques have been pointed in the literature. For example, as to the collagen, by modifying the polymerization temperature or pH, different ranges of pore and fiber sizes can be achieved [214]. It also can be cross-linked by glutaraldehyde or lysyl-oxidase [108, 215]. With regard to fibrin, varying the constituents within the physiological range would also lead to distinct fibrillar layout [216]. It also would be interesting to assess the effect of the cross-linking within the clot, since it has been noted that its lack brings bleeding problems in patients [104].

Decoupling permeability from pore-size and degradability. We have interpreted the permeability differences as a potential factor to impact on the productive completion of 3D migration. Moreover, myofibroblast rigidity-sensing mechanism has

been proposed to be through the interstitial fluid-pressure that accompanies inflammation and tissue regeneration [66]. Hence, decoupling permeability, pore size and degradability of the networks would be meaningful. In this regard, although natural matrices bring valuable knowledge, it hardly would be possible to decouple effects such as permeability and pore size in order to assess their individual contribution to cell migration. Therefore, synthetic scaffolds that resemble *in vivo*-like environments could help in this interpretation.

Interstitial fluid flow. Since interstitial fluid-pressure may play an important role regulating the fibroblast mechanics, it would be interesting to apply interstitial flow (IF) to the microsystems in order to assess its effect. As mentioned, IF determines the GF distribution through convective transport, which leads to a heterogeneous biochemical environment in the pericellular vicinity composed of both autocrine and paracrine signaling. In this interpretation, other works have pointed to the IF as a key modulator of migration processes through competing mechanisms with chemotaxis [33] and as a key regulator of mechanotransduction in 3D [18].

Matrix biosynthesis and remodeling. Although the main goal of the Thesis has focused on cell migration quantification, it would also be pertinent to correlate these data with the matrix remodeling and degradation processes. By taking advantage of the matrix visualization techniques presented hereby, along with immunofluorescence of matrix-protein staining, the rate of collagen remodeling (for collagen gels) or deposition (in fibrin) could be assessed.

Co-culture of fibroblasts. It has been proven that biophysical properties regulate fibroblast migration in 3D. However, *in vivo* not only the environmental physicochemical arrangement impact on the 3D migratory response, but other cells also contribute to the biochemical signaling by actively segregating paracrine factors. In this regard, co-culturing the fibroblasts with other cell types would yield in a closer

representation of *in vivo*-like conditions and could allow gaining added knowledge of the healing-concerning processes.

Collagen to fibrin transmigration studies. As to the experimental set-up, since microfluidic platforms allow for versatility, not only migration but also transmigration assays could be of high relevance. We have seen that collagen promotes more efficiently migration than fibrin hydrogels. However, in physiology, transmigration from collagen to fibrin matrices occurs. Experiments mimicking such boundary would permit to study the phenomena. A hypothesis could be that cells in the wound-surrounding connective tissue require migration in order to reach the clot, but once within, they require carrying out remodeling work rather that migration. Nevertheless, varying the set-up from the biophysical as well as biochemical standpoints, as suggested in the previous research lines, would add relevant information to this interpretation too.

6.3 Publications in peer-reviewed journals

1. Elosegui-Artola, A., Jorge-Peñas, A., **Moreno-Arotzena, O.**, Oregi, A., Lasa, M., García-Aznar, J.M., de Juan-Pardo E.M., & Aldabe, R., Image analysis for the quantitative comparison of stress fibers and focal adhesions. *PLoS One* **9,** e107393 (2014).

2. **Moreno-Arotzena, O.,** Borau, C., Vicente-Manzanares, M., Movilla N. & García-Aznar, J.M. Local microarchitecture and haptotaxis determine fibroblast 3D migration in a non-muscle myosin II-dependent manner. *Under review.*

3. **Moreno-Arotzena, O.,** Mendoza, G., Cóndor, M., Rüberg, T. & García-Aznar, J. M. Inducing chemotactic and haptotatic cues in microfluidic devices for three-dimensional in vitro assays. *Under review.*

4. **Moreno-arotzena, O.,** Meier, J. G., del Amo, C. & García-aznar, J. M. Fibrin and collagen 3D networks : a comparative biophysical and biomechanical characterization. *Under review.*

Chapter 7
Conclusiones y trabajo futuro

Este capítulo reúne las conclusiones principales extraídas de la presente Tesis. A su vez, también señala algunas futuras líneas de investigación, así como las publicaciones derivadas del trabajo.

7.1 Conclusiones

A lo largo de la Tesis se han destacado tres pilares fundamentales: la disposición biofísica de los andamiajes fibrilares, la bioquímica del microambiente y la mecánica celular como el epicentro del análisis que aquí se presenta. Concretamente, el trabajo se ha centrado en el estudio de la interacción entre estos tres pilares fundamentales. Para ello, se han recreado los principios básicos que regulan la cicatrización de

heridas, estudiando la compleja interacción entre los fibroblastos con la matriz extracelular y los factores de crecimiento. En este sentido, a continuación se resumen de forma agrupada las principales conclusiones de la tesis:

1. Con respecto a las propiedades biofísicas, se ha llevado a cabo una caracterización integral con objeto de unificar la diversificación existente entre los datos actuales. Los aspectos biofísicos más relevantes se citan a continuación:

- Se ha determinado una composición fisiológica para los hidrogeles de fibrina.
- Aunque las fibras de ambas redes son similares en diámetro (70-80 nm), las fibras de colágeno tienden a presentar una disposición empaquetada, mientras que las de fibrina se forman mayormente de manera individual.
- La malla de colágeno ha resultado ser más holgada que la de la fibrina: las medidas de tamaño de poro y permeabilidad son el doble para el colágeno en comparación con la fibrina.
- La rigidez del gel de colágeno es aproximadamente veinte veces mayor que el de la fibrina, siendo el modulo elástico de 15 y 300 Pa, respectivamente.
- Ambos hidrogeles muestran elasticidad no-lineal, presentando endurecimiento por deformación. No obstante, en el caso de la fibrina este fenómeno ocurre a partir del 10 % de deformación, mientras que para el colágeno sucede a partir de deformaciones del 50%.

4. En cuanto a los gradientes químicos de factores de crecimiento generados, se ha determinado la distribución espacio-temporal resultante del transporte de TGF-β_1 y PDGF-BB. Tras analizar la interacción del factor de crecimiento con la matriz de colágeno y fibrina, se ha visto que, dependiendo de la naturaleza de la interacción,

surgen diversos patrones de señalización incluyendo gradientes quimiotácticos y haptotácticos:

- El modelo computacional propuesto es capaz de predecir los fenómenos de degradación, difusión y pegado de las biomoléculas.
- Una vez disueltos en medio de cultivo, el TGF-β_1 es más estable que el PDGF-BB.
- Los procesos de difusión y adhesión regulan el transporte de PDGF-BB en matrices de colágeno tridimensionales. Por tanto, el factor de crecimiento queda distribuido heterogéneamente con una disposición no-lineal.
- Durante el transporte de PDGF-BB a través de la fibrina, prevalece la difusión. Puesto que el pegado es despreciable, el compuesto químico queda distribuido linealmente a lo largo del hidrogel, induciendo sólo señalización quimiotáctica.
- El transporte de TGF-β_1 a través de los geles de colágeno, presenta comportamientos similares de difusión y adhesión. Por tanto, la disposición final de las biomoléculas responde a una distribución paralela de las mimas.
- El patrón de difusión de TGF-β_1 en redes de fibrina es similar al del colágeno. De todas formas, el fenómeno de adhesión se acentúa notablemente en el caso de la fibrina, lo cual resulta en distribuciones netas dispares.

5. A fin de analizar la migración de fibroblastos tridimensional, se han realizado diversos ensayos confinando los hidrogeles colágeno y fibrina dentro de los microdispositivos. Las conclusiones principales son las siguientes:

- Las células muestran diferencias importantes en términos de morfología celular: en colágeno, los fibroblastos se presentan estirados con múltiples protrusiones dendríticas de actina, mientras que en fibrina muestran protuberancias en forma de huso y con un menor número de cúmulos localizados de actina en las proyecciones.
- Los geles de colágeno promueven la migración de fibroblastos en 3D de manera más efectiva que los de fibrina.
- Los factores biofísicos así como la degradabilidad, el tamaño de poro y la resistencia al paso de fluido han sido destacados como principales factores en limitar la migración efectiva en la fibrina.
- La miosina II es necesaria para una eficiente respuesta migratoria de los fibroblastos.
- Se ha demostrado que, ante un gradiente de PDGF-BB en colágeno, la haptotaxis regula la migración en 3D de fibroblastos.

7.2 Líneas futuras

Las conclusiones obtenidas agregan mayor conocimiento en la mecánica de la migración de los fibroblastos implicada en la fase temprana de la cicatrización de heridas. Dichos resultados han abierto, a su vez, nuevas preguntas que pueden potencialmente mejorar el conocimiento del fenómeno de curación de heridas. Por consiguiente, en esta sección se mencionan brevemente diversas propuestas como futuras líneas de investigación.

Estudio de adhesiones focales y fibras de estrés. En la presente Tesis se ha estudiado la señalización del microentorno para entender cómo afecta al proceso de migración en 3D. Sin embargo, la formación de adhesiones focales y fibras de estrés es esencial para interpretar las estructuras que generan las células para migrar con eficacia. Por lo tanto, incluir al trabajo realizado el estudio de la vinculación de estas estructuras podría ser de gran importancia. Para ello, es esencial el desarrollo de herramientas analíticas que permitan el análisis tanto sistemático como cuantitativo de adhesiones focales y fibras de estrés. Ante dicha previsión, y enmarcado dentro de este período de formación, hemos colaborado en el desarrollo de una herramienta analítica que permite extraer información cuantitativa partiendo de imágenes de inmunofluorescencia teñidas para faloidina y vinculina (trabajo publicado) [213]. En la Fig. 7.1 se muestra un ejemplo de la cuantificación de adhesiones focales y fibras de estrés. Por lo tanto, como trabajo futuro, sería interesante aplicar dicha herramienta a nuestros experimentos para complementar las conclusiones obtenidas en cuanto a la mecánica migratoria del fibroblasto en 3D.

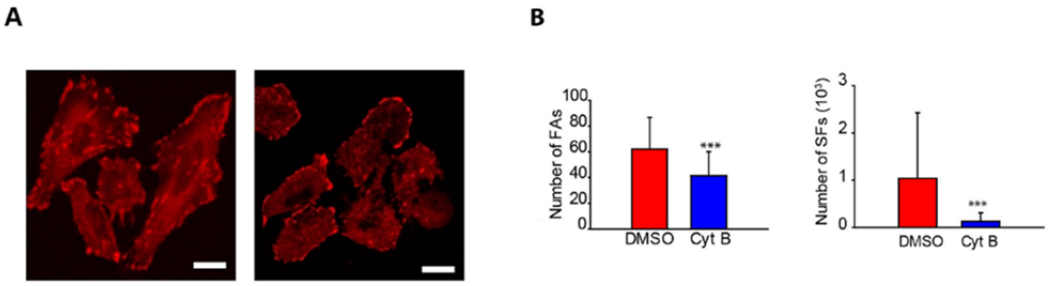

Fig. 7.1. Cuantificación de adhesiones focales y fibras de estrés. Este estudio muestra que el efecto de Citocalasina B (Cit B) es más notable en fibras de estrés que en las adhesiones focales. (A) Ejemplos de imágenes de vinculina en células de control con DMSO y tratadas con Cit B. (B) Cuantificación del número de adhesiones focales y fibras de estrés por célula (número de células: DMSO, n = 33; Cit B, n = 29). Las escalas corresponden a 20 µm. ***:p<0.001. [213]

Modificaciones microestructurales. Puesto que el tamaño de poro *in vivo* está sometido a un amplio rango, variar la conformación biofísica de ambas matrices podría agregar información relevante acerca de la migración celular y transmigración. Con dicho fin, en la literatura se han señalado varias técnicas. En el caso del colágeno, se ha demostrado que pueden obtenerse diferentes rangos de tamaño de poro y diámetro de fibra modificando la temperatura de polimerización o pH [214]. El grado de *cross-linking* también ha sido variado añadiendo glutaraldehído o *lisil-oxidase* [108, 215]. Con respecto a la fibrina, variar la concentración de los componentes dentro de la gama fisiológica conlleva a distintas configuraciones fibrilares [216]. Además, también sería de gran interés evaluar el efecto del *cross-linking* del coágulo, puesto que se ha observado que su carencia produce problemas de hemorragia en pacientes [104].

Desacoplar la permeabilidad del tamaño de poro y la degradabilidad de la matriz extracellular. En las conclusiones obtenidas, la diferencia en permeabilidad de los hidrogeles se ha interpretado como un posible factor que influye en la migración celular en 3D. Además, en la bibliografía se ha propuesto que el mecanismo sensor de la rigidez de los miofibroblastos podría producirse a través de la presión del fluido intersticial que acompaña a la inflamación y la regeneración de tejidos [66]. Por lo tanto, desacoplar la permeabilidad, del tamaño de poro y la degradabilidad de las redes posibilitaría un mayor entendimiento del rol específico que ejerce la permeabilidad. En este sentido, aunque las matrices de proteína natural son esenciales para los estudios de esta índole, no es posible separar dichos efectos con el fin de evaluar su contribución individual a la migración celular. Por lo tanto, andamiajes sintéticos que representan las condiciones *in vivo* podrían aportar un valor añadido en este tipo de estudios.

Flujo de fluido intersticial. Puesto que la presión del fluido intersticial puede desempeñar un papel importante regulando la mecánica migratoria del fibroblasto, podría resultar de interés aplicar flujo intersticial a los microdispositivos para evaluar su efecto. Tal y como se ha señalado anteriormente, la distribución de la señalización autocrina y paracrina produce un ambiente bioquímico heterogéneo en la proximidad pericelular, debido al transporte convectivo producido por el flujo intersticial. En este sentido, otros trabajos han señalado que el flujo intersticial es un factor clave de los procesos de migración -que compite, a su vez, con mecanismos como la quimiotaxis- [33]. A su vez, a este artículo se le ha atribuido también la coordinación de la mecanotransducción en 3D [18].

Biosíntesis y remodelación de la matriz. Aunque el principal objetivo de la Tesis se ha centrado en la cuantificación de la migración celular, también sería pertinente correlacionar los datos obtenidos con procesos de remodelación y degradación de la matriz. Haciendo uso de las técnicas de visualización presentadas y de inmunofluorescencia de las matrices, podría estudiarse el proceso de remodelación del colágeno (en hidrogeles de colágeno) y deposición del mismo en los geles de fibrina.

Co-cultivo de fibroblastos. Las propiedades biofísicas regulan la migración de fibroblastos en 3D. Sin embargo, *in vivo* no sólo contribuyen los parámetros fisicoquímicos en la respuesta migratoria en 3D, sino que otras células también están implicadas en la señalización secretando activamente factores paracrinos. En este sentido, el co-cultivo de fibroblastos con otros tipos celulares representaría más estrechamente las condiciones *in vivo* y permitiría avanzar más en el conocimiento de los procesos de curación.

Transmigración colágeno-fibrina. Puesto que las plataformas microfluídicas ofrecen gran flexibilidad en el diseño experimental, además de los ensayos de migración, podrían realizarse estudios de transmigración. En las conclusiones

obtenidas se ha demostrado que el colágeno promueve más eficientemente la migración que los hidrogeles de fibrina. Sin embargo, fisiológicamente, se produce la transmigración de colágeno a fibrina. Por ello, experimentos que pudieran mimetizar dicha intercara permitirían estudiar este fenómeno. Una hipótesis podría ser que las células en el tejido conectivo circundante de la herida requieren de la migración con el fin de alcanzar el coágulo, pero una vez dentro, precisan de la remodelación de la matriz más que de la migración. Por tanto, también podría añadir información relevante a este respecto variar la configuración biofísico-química, como se sugiere en las líneas de investigación anteriores.

7.3 Publicaciones

1. Elosegui-Artola, A., Jorge-Peñas, A., **Moreno-Arotzena, O.**, Oregi, A., Lasa, M., García-Aznar, J.M., de Juan-Pardo, E.M. & Aldabe, R., Image analysis for the quantitative comparison of stress fibers and focal adhesions. *PLoS One* 9, e107393 (2014).

2. **Moreno-Arotzena, O.,** Borau, C., Vicente-Manzanares, M., Movilla N. & García-Aznar, J.M. Local microarchitecture and haptotaxis determine fibroblast 3D migration in a non-muscle myosin II-dependent manner. *En revisión.*

3. **Moreno-Arotzena, O.,** Mendoza, G., Cóndor, M., Rüberg, T. & García-Aznar, J. M. Inducing chemotactic and haptotatic cues in microfluidic devices for three-dimensional in vitro assays. *En revisión.*

4. **Moreno-arotzena, O.,** Meier, J. G., del Amo, C. & García-aznar, J. M. Fibrin and collagen 3D networks : a comparative biophysical and biomechanical characterization. *En revisión.*

Appendix A
Protocols

A.1 SU8 photolithography

Reagents and materials:

- Polished silicon wafer
- Transparency photomask printed at 20,000 dpi
- SU8 photoresist and appropriate developer

Procedure:

- It is a key point to ensure thorough wash of the silicon wafer.
- Then, it is dehydrated at 200 ºC for 20 mins. Afterwards, the wafer should be allowed to relax at room temperature for 5 mins.
- The corresponding SU8 photoresist is poured (1 ml per inch), avoiding bubbles.
- It is spined onto the wafer conveniently.
- Next, the wafer is placed in a hot plate raising its temperature progressively. Once it has reached 95 ºC, the photoresist is prebaked for 30 mins. Then, it should be allowed to relax at room temperature for 10 mins.
- Afterwards, expose the wafer to an appropriate dose of UV light employing the photomask. Then, it should be allowed to relax at room temperature for 10 mins.
- Next, the wafer is ramped to 95ºC again and baked for 30 mins. Then, it should be allowed to relax at room temperature for 10 mins.
- Develop the photoresist in the proper developer for 16 mins approximately*.
- Neutralize the developer in IPA and rinse it with deionized water. Finally, dry it with pressurized nitrogen gas (see result in Fig. A.1).

Note1: keeping the level throughout the process is a key point.

Note2: note that all these parameters should be adjusted in function of photoresist, desired depth and clean-room conditions.

*****The developer gets saturated easily. Hence, two different sets of 8 mins could be required.

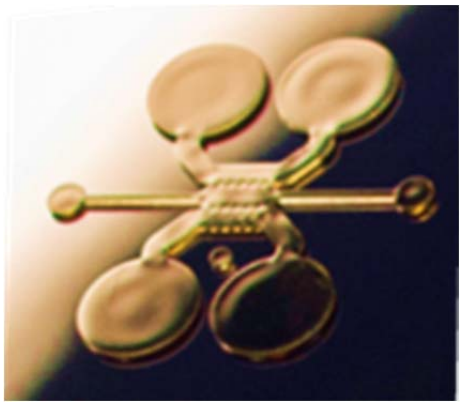

Fig. A.1. Individual SU8 geometry-pattern. The SU8 positive-relief is adhered to silicon.

A.2 Cell culture of NHDF

Reagents:

- Normal Human Dermal Fibroblasts (NHDF) from Lonza
- Fibroblast Growth Medium-2 (FGM-2) from Lonza
- PBS from Lonza
- Trypsin from Biochrom
- DMSO (Amresco)

Procedure:

- Trypsinization:
  - Aspirate de culture media.
  - Wash the cells with PBS.
  - Add 0.5 ml of trypsin and incubate the cells in the incubator for 1.5 mins.
  - Once the cells are detached, add 1.5 ml of FGM-2.
  - Harvest the cells by centrifugation at 1200 rpm for 5 minutes at room temperature.
  - Dilute the pellet to the desired cellular concentration and the cells are ready to be seeded elsewhere or be frozen.

  Note: the cells were passaged once they were at 80% of confluence up to the tenth passage.

- Freezing:
  - Pipet 50 ul of DMSO in each cryotube.
  - Add 450 ul of the cell suspension to the cryotubes.

- Bring the cryotubes to the -80ºC ultrafreezer within the froster and keep them for 24 hours.
- Then, they should be kept in the nitrogen tank until they are required.

- Thawing:
  - Place the cryotubes in the waterbath at 37ºC for roughly two minutes.
  - Mix the defrost cell solution (500 ul) with 4.5 ml of cell media.
  - Harvest the cells by centrifugation at 1200 rpm for 5 minutes at room temperature.
  - Dilute the pellet to the desired cellular concentration and seed them in corresponding flasks.
  - After 24 hours, the culture media should be changed in order to discard the dead cells.
  - In order to let them to get conditioned, thawed cells should be passaged at least once -at 80% of confluence- before using them for subsequent experiments.

A.3 Experimental quantification of GF concentration

Reagents:

- Corresponding ELISA kit:
    - PDGF-BB Human ELISA Kit from Abcam (ab100624)
    - TGF-β1 ELISA Kit from Invitrogen (KAC1688)

Reagent preparation:

- As indicated from the provider

Procedure:

- Sample obtaining:
    - After 24 hours since factor addition, the media from the reservoirs should be aspirated and discarded.
    - The medium from the channels is taken and used as our samples (5 ul).
    - As the volume obtained is very low, it is recommended to spin and dilute the samples before use.
- Sample processing:
    - As indicated from the provider

A.4 Cell tracker

Reagents:

- CellTracker™ Green CMFDA from Molecular Probes: store at -20ºC
- Uncomplemented and complemented media

Reagent preparation:

- CellTracker™ Green CMFDA:
    - Dissolve the dye as indicated by the supplier up to 10 mM in DMSO
    - Re-dissolve it in HBSS (or uncomplemented media) up to 1 mM
    - Aliquot and freeze at -20ºC
    - Thaw an aliquot before its use and then refreeze it

Procedure:

- Harvest the trypsinized cells by centrifugation and aspirate the supernatant.
- Resuspend the pellet in 1 ml of uncomplemented prewarmed dye-containing media at 0.5 uM.
- Incubate the tube for 15 mins.
- Harvest the cells by centrifugation and aspirate the supernatant.
- Resuspend the pellet in 1 ml of uncomplemented prewarmed media.
- Incubate the tube for 30 mins.
- Harvest the cells by centrifugation and aspirate the supernatant.
- Resuspend the cells in prewarmed complemented media up to the desired concentration.
- The stained cells are ready to be seeded in either 2D or 3D.

Note: the dye and the stained cells should be protected from light.

A.5 Viability test

Reagents:

- Kit live/dead viability/cytotoxicity from Invitrogen (L3224): store at 4ºC:
  - calcein-AM (green).
  - ethidium homodimer-1 (red).

Reagent preparation:

- Add ethidium at 4 uM to DPBS and vortex it.
- Next, add calcein at 2 uM and vortex it again.
- Solution preparation should be done in the dark and fresh solution should be prepared prior to each test.

Procedure:

- Change the media from the devices by the just prepared solution.
- Incubate the samples in the incubator for 30 min and image them.

Note: *negative control samples could be checked incubating them with 70% ethanol for 30 mins prior to test performance.*

References

1. Vicente-Manzanares M, Webb DJ, Horwitz a R: **Cell migration at a glance.** *J Cell Sci* 2005, **118**(Pt 21):4917–9.

2. Alberts B, Johnson A, Lewis J, Raff M, Roberts K, Walter P: *The Cell*. Garland Science; 2002.

3. DuFort CC, Paszek MJ, Weaver VM: **Balancing forces: architectural control of mechanotransduction.** *Nat Rev Mol Cell Biol* 2011, **12**:308–19.

4. Vicente-Manzanares M, Horwitz AR: **Adhesion dynamics at a glance.** *J Cell Sci* 2011, **124**(Pt 23):3923–7.

5. Stricker J, Falzone T, Gardel ML: **Mechanics of the F-actin cytoskeleton.** *J Biomech* 2010, **43**:9–14.

6. Kanchanawong P, Shtengel G, Pasapera AM, Ramko EB, Davidson MW, Hess HF, Waterman CM: **Nanoscale architecture of integrin-based cell adhesions.** *Nature* 2010, **468**:580–4.

7. Ananthanarayanan B, Kim Y, Kumar S: **Elucidating the mechanobiology of malignant brain tumors using a brain matrix-mimetic hyaluronic acid hydrogel platform.** *Biomaterials* 2011, **32**:7913–23.

8. Ananthakrishnan R, Ehrlicher A: **The Forces Behind Cell Movement**. *Int J Biol Sci* 2007, **3**:303–317.

9. Kraning-Rush CM, Carey SP, Califano JP, Smith BN, Reinhart-King CA: **The role of the cytoskeleton in cellular force generation in 2D and 3D environments.** *Phys Biol* 2011, **8**:015009.

10. Harunaga JS, Yamada KM: **Cell-matrix adhesions in 3D**. *Matrix Biol* 2011, **30**:363–368.

11. Vu LT, Jain G, Veres BD, Rajagopalan P: **Cell Migration on Planar and Three-Dimensional Matrices: A Hydrogel-Based Perspective.** *Tissue Eng Part B Rev* 2014.

12. Doyle AD, Petrie RJ, Kutys ML, Yamada KM: **Dimensions in cell migration.** *Curr Opin Cell Biol* 2013, **25**:642–9.

13. Hynes RO, Naba A: **Overview of the matrisome--an inventory of extracellular matrix constituents and functions.** *Cold Spring Harb Perspect Biol* 2012, **4**:a004903.

14. Lara Rodriguez L, Schneider IC: **Directed cell migration in multi-cue environments.** *Integr Biol (Camb)* 2013, **5**:1306–23.

15. Starke J, Maaser K, Wehrle-Haller B, Friedl P: **Mechanotransduction of mesenchymal melanoma cell invasion into 3D collagen lattices: filopod-mediated extension-relaxation cycles and force anisotropy.** *Exp Cell Res* 2013, **319**:2424–33.

16. Kural MH, Billiar KL: **Regulating tension in three-dimensional culture environments.** *Exp Cell Res* 2013, **319**:2447–59.

17. Bao G, Suresh S: **Cell and molecular mechanics of biological materials.** *Nat Mater* 2003, **2**:715–25.

18. Polacheck WJ, German AE, Mammoto A, Ingber DE, Kamm RD: **Mechanotransduction of fluid stresses governs 3D cell migration.** *Proc Natl Acad Sci U S A* 2014, **111**:2447–52.

19. Minton K: **Mechanotransduction: A stiff response**. *Nat Rev Mol Cell Biol* 2014, **15**:500–500.

20. Kumar S: **Cellular mechanotransduction: Stiffness does matter.** *Nat Mater* 2014, **13**:918–20.

21. Roca-Cusachs P, Sunyer R, Trepat X: **Mechanical guidance of cell migration: lessons from chemotaxis.** *Curr Opin Cell Biol* 2013, **25**:543–9.

22. Grinnell F, Petroll WM: **Cell motility and mechanics in three-dimensional collagen matrices.** *Annu Rev Cell Dev Biol* 2010, **26**:335–61.

23. Griffith LG, Swartz M a: **Capturing complex 3D tissue physiology in vitro.** *Nat Rev Mol Cell Biol* 2006, **7**:211–24.

24. Hynes RO: **The extracellular matrix: not just pretty fibrils.** *Science* 2009, **326**:1216–9.

25. Frantz C, Stewart KM, Weaver VM: **The extracellular matrix at a glance.** *J Cell Sci* 2010, **123**(Pt 24):4195–200.

26. Friedl P, Sahai E, Weiss S, Yamada KM: **New dimensions in cell migration.** *Nat Rev Mol Cell Biol* 2012, **13**:743–7.

27. Pritchard RH, Huang YYS, Terentjev EM: **Mechanics of biological networks: from the cell cytoskeleton to connective tissue.** *Soft Matter* 2014, **10**:1864–84.

28. Ladoux B, Nicolas A: **Physically based principles of cell adhesion mechanosensitivity in tissues.** *Rep Prog Phys* 2012, **75**:116601.

29. Tomasek JJ, Gabbiani G, Hinz B, Chaponnier C, Brown RA: **Myofibroblasts and mechano-regulation of connective tissue remodelling.** *Nat Rev Mol Cell Biol* 2002, **3**:349–63.

30. Wolf K, Alexander S, Schacht V, Coussens LM, von Andrian UH, van Rheenen J, Deryugina E, Friedl P: **Collagen-based cell migration models in vitro and in vivo.** *Semin Cell Dev Biol* 2009, **20**:931–41.

31. Achterberg VF, Buscemi L, Diekmann H, Smith-Clerc J, Schwengler H, Meister J-J, Wenck H, Gallinat S, Hinz B: **The nano-scale mechanical properties of the extracellular matrix regulate dermal fibroblast function.** *J Invest Dermatol* 2014, **134**:1862–72.

32. Zaman MH, Trapani LM, Sieminski AL, Siemeski A, Mackellar D, Gong H, Kamm RD, Wells A, Lauffenburger D a, Matsudaira P: **Migration of tumor cells in 3D matrices is governed by matrix stiffness along with cell-matrix adhesion and proteolysis.** *Proc Natl Acad Sci U S A* 2006, **103**:10889–94.

33. Polacheck WJ, Charest JL, Kamm RD: **Interstitial flow influences direction of tumor cell migration through competing mechanisms.** *Proc Natl Acad Sci U S A* 2011, **108**:11115–20.

34. Pathak A, Kumar S: **Independent regulation of tumor cell migration by matrix stiffness and confinement.** *Proc Natl Acad Sci U S A* 2012, **109**:10334–9.

35. Wolf K, Te Lindert M, Krause M, Alexander S, Te Riet J, Willis AL, Hoffman RM, Figdor CG, Weiss SJ, Friedl P: **Physical limits of cell migration: control by ECM space and nuclear deformation and tuning by proteolysis and traction force.** *J Cell Biol* 2013, **201**:1069–84.

36. Harley B a C, Kim H-D, Zaman MH, Yannas I V, Lauffenburger D a, Gibson LJ: **Microarchitecture of three-dimensional scaffolds influences cell migration behavior via junction interactions.** *Biophys J* 2008, **95**:4013–24.

37. Ehrbar M, Sala a, Lienemann P, Ranga a, Mosiewicz K, Bittermann a, Rizzi SC, Weber FE, Lutolf MP: **Elucidating the role of matrix stiffness in 3D cell migration and remodeling.** *Biophys J* 2011, **100**:284–93.

38. Wen JH, Vincent LG, Fuhrmann A, Choi YS, Hribar KC, Taylor-Weiner H, Chen S, Engler AJ: **Interplay of matrix stiffness and protein tethering in stem cell differentiation**. *Nat Mater* 2014, **13**:979–987.

39. Trappmann B, Gautrot JE, Connelly JT, Strange DGT, Li Y, Oyen ML, Cohen Stuart MA, Boehm H, Li B, Vogel V, Spatz JP, Watt FM, Huck WTS: **Extracellular-matrix tethering regulates stem-cell fate.** *Nat Mater* 2012, **11**:642–9.

40. Pathak A, Kumar S: **Biophysical regulation of tumor cell invasion: moving beyond matrix stiffness.** *Integr Biol (Camb)* 2011, **3**:267–78.

41. Balzer EM, Tong Z, Paul CD, Hung W-C, Stroka KM, Boggs AE, Martin SS, Konstantopoulos K: **Physical confinement alters tumor cell adhesion and migration phenotypes.** *FASEB J* 2012, **26**:4045–56.

42. Hung W-C, Chen S-H, Paul CD, Stroka KM, Lo Y-C, Yang JT, Konstantopoulos K: **Distinct signaling mechanisms regulate migration in unconfined versus confined spaces**. *J Cell Biol* 2013, **202**:807–824.

43. Haeger A, Krause M, Wolf K, Friedl P: **Cell jamming: collective invasion of mesenchymal tumor cells imposed by tissue confinement.** *Biochim Biophys Acta* 2014, **1840**:2386–95.

44. Kubow KE, Conrad SK, Horwitz AR: **Matrix Microarchitecture and Myosin II Determine Adhesion in 3D Matrices**. *Curr Biol* 2013, **23**:1607–1619.

45. Stroka KM, Gu Z, Sun SX, Konstantopoulos K: **Bioengineering paradigms for cell migration in confined microenvironments.** *Curr Opin Cell Biol* 2014, **30C**:41–50.

46. Prentice-Mott H V, Chang C-H, Mahadevan L, Mitchison TJ, Irimia D, Shah J V: **Biased migration of confined neutrophil-like cells in asymmetric hydraulic environments.** *Proc Natl Acad Sci U S A* 2013, **110**:21006–11.

47. Shreiber DI, Enever P a, Tranquillo RT: **Effects of pdgf-bb on rat dermal fibroblast behavior in mechanically stressed and unstressed collagen and fibrin gels.** *Exp Cell Res* 2001, **266**:155–166.

48. **Skin cross section**
[http://www.ucdmc.ucdavis.edu/publish/news/newsroom/6853]

49. Singer AJ, Clark RAF: **Cutaneous Wound Healing**. *N Engl J Med* 1999:738–746.

50. Timmons J: **Skin function and wound healing physiology**. *Wound Essentials* 2006, **1**:8–17.

51. Hinz B: **Formation and function of the myofibroblast during tissue repair.** *J Invest Dermatol* 2007, **127**:526–537.

52. Diegelmann RF, Evans MC: **Wound healing: an overview of acute, fibrotic and delayed healing**. *Front Biosci* 2004, **9**:283–289.

53. Guo S, Dipietro L a: **Factors affecting wound healing.** *J Dent Res* 2010, **89**:219–29.

54. Valero C, Javierre E, Garc JM: **Challenges in the modeling of wound healing**. *Ann Biomed Eng (in Rev* 2014.

55. Mori M, Almeida P V., Cola M, Anselmi G, Mäkilä E, Correia A, Salonen J, Hirvonen J, Caramella C, Santos HA: **In vitro assessment of biopolymer-modified porous silicon microparticles for wound healing applications**. *Eur J Pharm Biopharm* 2014.

56. Magalhães MSF, Fechine FV, Macedo RN de, Monteiro DLS, Oliveira CC, Brito GA de C, Moraes MEA de, Moraes MO de: **Effect of a combination of medium**

chain triglycerides, linoleic acid, soy lecithin and vitamins A and E on wound healing in rats. *Acta Cir Bras* , **23**:262–9.

57. Liu Z, Ho C-H, Grinnell F: **The different roles of myosin IIA and myosin IIB in contraction of 3D collagen matrices by human fibroblasts.** *Exp Cell Res* 2014.

58. Cook H, Davies KJ, Harding KG, Thomas DW: **Defective extracellular matrix reorganization by chronic wound fibroblasts is associated with alterations in TIMP-1, TIMP-2, and MMP-2 activity.** *J Invest Dermatol* 2000, **115**:225–33.

59. Barron L, Wynn T a: **Fibrosis is regulated by Th2 and Th17 responses and by dynamic interactions between fibroblasts and macrophages.** *Am J Physiol Gastrointest Liver Physiol* 2011, **300**:G723–8.

60. Rhee S: **Fibroblasts in three dimensional matrices: cell migration and matrix remodeling.** *Exp Mol Med* 2009, **41**:858–865.

61. Jiang H, Grinnell F: **Cell-matrix entanglement and mechanical anchorage of fibroblasts in three-dimensional collagen matrices.** *Mol Biol Cell* 2005, **16**:5070–5076.

62. Rhee S, Grinnell F: **Fibroblast mechanics in 3D collagen matrices.** *Adv Drug Deliv Rev* 2007, **59**:1299–1305.

63. Carlson MA, Longaker MT: **The fibroblast-populated collagen matrix as a model of wound healing: a review of the evidence.** *Wound Repair Regen* , **12**:134–47.

64. Miron-Mendoza M, Seemann J, Grinnell F: **Collagen fibril flow and tissue translocation coupled to fibroblast migration in 3D collagen matrices.** *Mol Biol Cell* 2008, **19**:2051–2058.

65. Thievessen I, Thompson PM, Berlemont S, Plevock KM, Plotnikov S V, Zemljic-Harpf A, Ross RS, Davidson MW, Danuser G, Campbell SL, Waterman CM: **Vinculin-actin interaction couples actin retrograde flow to focal adhesions, but is dispensable for focal adhesion growth.** *J Cell Biol* 2013, **202**:163–77.

66. Grinnell F: **Fibroblast biology in three-dimensional collagen matrices.** *Trends Cell Biol* 2003, **13**:264–269.

67. Kessler D, Dethlefsen S, Haase I, Plomann M, Hirche F, Krieg T, Eckes B: **Fibroblasts in mechanically stressed collagen lattices assume a "synthetic" phenotype.** *J Biol Chem* 2001, **276**:36575–36585.

68. Grinnell F: **Fibroblast-collagen-matrix contraction : growth-factor signalling and mechanical loading**. *Trends Cell Biol* 2000, **10**:377–380.

69. Grinnell F, Ho C-H, Lin Y-C, Skuta G: **Differences in the Regulation of Fibroblast Contraction of Floating Versus Stressed Collagen Matrices**. *J Biol Chem* 1999, **274**:918–923.

70. Hakkinen KM, Harunaga JS, Doyle AD, Yamada KM: **Direct comparisons of the morphology, migration, cell adhesions, and actin cytoskeleton of fibroblasts in four different three-dimensional extracellular matrices.** *Tissue Eng Part A* 2011, **17**:713–724.

71. Grinnell F, Rocha LB, Iucu C, Rhee S, Jiang H: **Nested collagen matrices: a new model to study migration of human fibroblast populations in three dimensions.** *Exp Cell Res* 2006, **312**:86–94.

72. Greiling D, Clark R a: **Fibronectin provides a conduit for fibroblast transmigration from collagenous stroma into fibrin clot provisional matrix.** *J Cell Sci* 1997, **110**:861–870.

73. Rouillard AD, Holmes JW: **Mechanical boundary conditions bias fibroblast invasion in a collagen-fibrin wound model.** *Biophys J* 2014, **106**:932–43.

74. Sixt M: **Cell migration: fibroblasts find a new way to get ahead.** *J Cell Biol* 2012, **197**:347–9.

75. Petrie RJ, Gavara N, Chadwick RS, Yamada KM: **Nonpolarized signaling reveals two distinct modes of 3D cell migration.** *J Cell Biol* 2012, **197**:439–55.

76. Lämmermann T, Sixt M: **Mechanical modes of "amoeboid" cell migration.** *Curr Opin Cell Biol* 2009, **21**:636–44.

77. Wolf K, Friedl P: **Extracellular matrix determinants of proteolytic and non-proteolytic cell migration.** *Trends Cell Biol* 2011, **21**:736–44.

78. Bear JE, Haugh JM: **Directed migration of mesenchymal cells: where signaling and the cytoskeleton meet.** *Curr Opin Cell Biol* 2014, **30C**:74–82.

79. Friedl P, Wolf K: **Plasticity of cell migration: a multiscale tuning model.** *J Cell Biol* 2010, **188**:11–9.

80. Miron-Mendoza M, Seemann J, Grinnell F: **The differential regulation of cell motile activity through matrix stiffness and porosity in three dimensional collagen matrices.** *Biomaterials* 2010, **31**:6425–35.

81. Ni M, Tong WH, Choudhury D, Rahim NAA, Iliescu C, Yu H: **Cell culture on MEMS platforms: a review.** *Int J Mol Sci* 2009, **10**:5411–41.

82. Polacheck WJ, Li R, Uzel SGM, Kamm RD: **Microfluidic platforms for mechanobiology.** *Lab Chip* 2013, **13**:2252–67.

83. Farahat WA, Wood LB, Zervantonakis IK, Schor A, Ong S, Neal D, Kamm RD, Asada HH: **Ensemble analysis of angiogenic growth in three-dimensional microfluidic cell cultures.** *PLoS One* 2012, **7**:e37333.

84. Kim C, Chung S, Yuchun L, Kim M-C, Chan JKY, Asada HH, Kamm RD: **In vitro angiogenesis assay for the study of cell-encapsulation therapy.** *Lab Chip* 2012, **12**:2942–50.

85. Jeon JS, Zervantonakis IK, Chung S, Kamm RD, Charest JL: **In vitro model of tumor cell extravasation.** *PLoS One* 2013, **8**:e56910.

86. Zervantonakis IK, Hughes-Alford SK, Charest JL, Condeelis JS, Gertler FB, Kamm RD: **Three-dimensional microfluidic model for tumor cell intravasation and endothelial barrier function.** *Proc Natl Acad Sci U S A* 2012, **109**:13515–20.

87. Park JW, Kim HJ, Kang MW, Jeon NL: **Advances in microfluidics-based experimental methods for neuroscience research.** *Lab Chip* 2013, **13**:509–21.

88. Tharin S, Kothapalli CR, Ozdinler PH, Pasquina L, Chung S, Varner J, DeValence S, Kamm R, Macklis JD: **A microfluidic device to investigate axon targeting by limited numbers of purified cortical projection neuron subtypes.** *Integr Biol (Camb)* 2012, **4**:1398–405.

89. Murrell M, Kamm R, Matsudaira P: **Tension , Free Space , and Cell Damage in a Microfluidic Wound Healing Assay**. 2011, **6**.

90. Felder M, Sallin P, Barbe L, Haenni B, Gazdhar A, Geiser T, Guenat O: **Microfluidic wound-healing assay to assess the regenerative effect of HGF on wounded alveolar epithelium.** *Lab Chip* 2012, **12**:640–6.

91. Moreno-Arotzena O, de Juan-Pardo E, Arana S: **PDMS vs. COC in microfluidic systems for controlled in-vitro studies of 3D cell migration**. *Proc 2nd Int Conf Tissue Eng* 2011:pp 175–80.

92. Shin Y, Han S, Jeon JS, Yamamoto K, Zervantonakis IK, Sudo R, Kamm RD, Chung S: **Microfluidic assay for simultaneous culture of multiple cell types on surfaces or within hydrogels.** *Nat Protoc* 2012, **7**:1247–59.

93. Ahmed TAE, Dare E V., Hincke M: **Fibrin: a versatile scaffold for tissue engineering applications.** *Tissue Eng Part B Rev* 2008, **14**:199–215.

94. Wong VW, Akaishi S, Longaker MT, Gurtner GC: **Pushing back: wound mechanotransduction in repair and regeneration.** *J Invest Dermatol* 2011, **131**:2186–96.

95. Castells-Sala C, Semino CE: **Biomaterials for stem cell culture and seeding for the generation and delivery of cardiac myocytes**. *Curr Opin Organ Transplant* 2012, **17**:681–687.

96. Demol J, Eyckmans J, Roberts SJ, Luyten FP, Van Oosterwyck H: **Does tranexamic acid stabilised fibrin support the osteogenic differentiation of human periosteum derived cells?** *Eur Cell Mater* 2011, **21**:272–85.

97. Ortinau S, Schmich J, Block S, Liedmann A, Jonas L, Weiss DG, Helm CA, Rolfs A, Frech MJ: **Effect of 3D-scaffold formation on differentiation and survival in human neural progenitor cells.** *Biomed Eng Online* 2010, **9**:70.

98. Buehler MJ: **Nature designs tough collagen: explaining the nanostructure of collagen fibrils.** *Proc Natl Acad Sci U S A* 2006, **103**:12285–90.

99. Janmey P a, Winer JP, Weisel JW: **Fibrin gels and their clinical and bioengineering applications.** *J R Soc Interface* 2009, **6**:1–10.

100. Lorand L: **Factor XIII: structure, activation, and interactions with fibrinogen and fibrin.** *Ann N Y Acad Sci* 2001, **936**:291–311.

101. Chernysh IN, Nagaswami C, Purohit PK, Weisel JW: **Fibrin clots are equilibrium polymers that can be remodeled without proteolytic digestion.** *Sci Rep* 2012, **2**:879.

102. Sidelmann JJ, Gram J, Jespersen J, Kluft C: **Fibrin clot formation and lysis: basic mechanisms.** *Semin Thromb Hemost* 2000, **26**:605–618.

103. Standeven KF, Ariëns R a S, Grant PJ: **The molecular physiology and pathology of fibrin structure/function.** *Blood Rev* 2005, **19**:275–288.

104. Weisel JW: **The mechanical properties of fibrin for basic scientists and clinicians.** *Biophys Chem* 2004, **112**:267–76.

105. Rowe SL, Stegemann JP: **Interpenetrating collagen-fibrin composite matrices with varying protein contents and ratios.** *Biomacromolecules* 2006, **7**:2942–8.

106. Lai VK, Frey CR, Kerandi AM, Lake SP, Tranquillo RT, Barocas VH: **Microstructural and mechanical differences between digested collagen–fibrin co-gels and pure collagen and fibrin gels**. *Acta Biomater* 2012, **8**:4031–4042.

107. Lai VK, Lake SP, Frey CR, Tranquillo RT, Barocas VH: **Mechanical behavior of collagen-fibrin co-gels reflects transition from series to parallel interactions with increasing collagen content**. *J Biomech Eng* 2012, **134**:011004.

108. Münster S, Jawerth LM, Leslie BA, Weitz JI, Fabry B, Weitz DA: **Strain history dependence of the nonlinear stress response of fibrin and collagen networks.** *Proc Natl Acad Sci U S A* 2013, **110**:12197–202.

109. Storm C, Pastore JJ, MacKintosh FC, Lubensky TC, & Janmey PA: **Nonlinear elasticity in biological gels**. *Lett to Nat* 2005, **435**(May):191–194.

110. Haugh MG, Thorpe SD, Vinardell T, Buckley CT, Kelly DJ: **The application of plastic compression to modulate fibrin hydrogel mechanical properties.** *J Mech Behav Biomed Mater* 2012, **16**:66–72.

111. You C, Wang X, Zheng Y, Han C: **Three types of dermal grafts in rats: the importance of mechanical property and structural design.** *Biomed Eng Online* 2013, **12**:125.

112. Gersh KC, Edmondson KE, Weisel JW: **Flow rate and fibrin fiber alignment.** *J Thromb Haemost* 2010, **8**:2826–8.

113. Collet JP, Park D, Lesty C, Soria J, Soria C, Montalescot G, Weisel JW: **Influence of fibrin network conformation and fibrin fiber diameter on fibrinolysis speed: dynamic and structural approaches by confocal microscopy.** *Arterioscler Thromb Vasc Biol* 2000, **20**:1354–1361.

114. Hartmann A, Boukamp P, Friedl P: **Confocal reflection imaging of 3D fibrin polymers.** *Blood Cells Mol Dis* 2006, **36**:191–3.

115. Mickel W, Münster S, Jawerth LM, Vader DA, Weitz DA, Sheppard AP, Mecke K, Fabry B, Schröder-Turk GE: **Robust pore size analysis of filamentous networks from three-dimensional confocal microscopy.** *Biophys J* 2008, **95**:6072–80.

116. Ryan E a, Mockros LF, Weisel JW, Lorand L: **Structural origins of fibrin clot rheology.** *Biophys J* 1999, **77**:2813–2826.

117. Shah J V., Janmey PA: **Strain hardening of fibrin gels and plasma clots**. *Rheol Acta* 1997, **36**:262–268.

118. Ulrich T a, Jain A, Tanner K, MacKay JL, Kumar S: **Probing cellular mechanobiology in three-dimensional culture with collagen-agarose matrices.** *Biomaterials* 2010, **31**:1875–84.

119. Malagón-Romero D, Hernández N, Cardozo C, Godoy-Silva RD: **Rheological characterization of a gel produced using human blood plasma and alginate mixtures.** *J Mech Behav Biomed Mater* 2014, **34**:171–80.

120. Yang Y-L, Leone LM, Kaufman LJ: **Elastic moduli of collagen gels can be predicted from two-dimensional confocal microscopy.** *Biophys J* 2009, **97**:2051–60.

121. Lim BBC, Lee EH, Sotomayor M, Schulten K: **Molecular basis of fibrin clot elasticity.** *Structure* 2008, **16**:449–459.

122. Collet J-P, Shuman H, Ledger RE, Lee S, Weisel JW: **The elasticity of an individual fibrin fiber in a clot.** *Proc Natl Acad Sci U S A* 2005, **102**:9133–9137.

123. Helms CC, Ariëns RAS, Uitte de Willige S, Standeven KF, Guthold M: **α−α cross-links increase fibrin fiber elasticity and stiffness**. *Biophys J* 2012, **102**:168–175.

124. Liu W, Jawerth LM, Sparks E a, Falvo MR, Hantgan RR, Superfine R, Lord ST, Guthold M: **Fibrin fibers have extraordinary extensibility and elasticity.** *Science* 2006, **313**:634.

125. Shen ZL, Dodge MR, Kahn H, Ballarini R, Eppell SJ: **Stress-strain experiments on individual collagen fibrils.** *Biophys J* 2008, **95**:3956–63.

126. Julias M, Edgar LT, Buettner HM, Shreiber DI: **An in vitro assay of collagen fiber alignment by acupuncture needle rotation.** *Biomed Eng Online* 2008, **7**:19.

127. Lo CM, Wang HB, Dembo M, Wang YL: **Cell movement is guided by the rigidity of the substrate.** *Biophys J* 2000, **79**:144–52.

128. Engler AJ, Sen S, Sweeney HL, Discher DE: **Matrix elasticity directs stem cell lineage specification.** *Cell* 2006, **126**:677–89.

129. Ulrich TA, de Juan Pardo EM, Kumar S: **The mechanical rigidity of the extracellular matrix regulates the structure, motility, and proliferation of glioma cells.** *Cancer Res* 2009, **69**:4167–74.

130. Tilghman RW, Cowan CR, Mih JD, Koryakina Y, Gioeli D, Slack-Davis JK, Blackman BR, Tschumperlin DJ, Parsons JT: **Matrix rigidity regulates cancer cell growth and cellular phenotype.** *PLoS One* 2010, **5**:e12905.

131. Swartz M a, Fleury ME: **Interstitial flow and its effects in soft tissues.** *Annu Rev Biomed Eng* 2007, **9**:229–56.

132. Haessler U, Teo JCM, Foretay D, Renaud P, Swartz M a: **Migration dynamics of breast cancer cells in a tunable 3D interstitial flow chamber.** *Integr Biol* 2012, **4**:401–9.

133. Ng CP, Swartz M a: **Fibroblast alignment under interstitial fluid flow using a novel 3-D tissue culture model.** *Am J Physiol Heart Circ Physiol* 2003, **284**:H1771–7.

134. Shieh AC, Swartz M a: **Regulation of tumor invasion by interstitial fluid flow.** *Phys Biol* 2011, **8**:015012.

135. Karande TS, Ong JL, Agrawal CM: **Diffusion in musculoskeletal tissue engineering scaffolds: design issues related to porosity, permeability, architecture, and nutrient mixing.** *Ann Biomed Eng* 2004, **32**:1728–43.

136. Wufsus a R, Macera NE, Neeves KB: **The hydraulic permeability of blood clots as a function of fibrin and platelet density.** *Biophys J* 2013, **104**:1812–23.

137. Lim BCB, Ariëns RAS, Carter AM, Weisel JW, Grant PJ: **Genetic regulation of fibrin structure and function: complex gene-environment interactions may modulate vascular risk.** *Lancet* 2003, **361**:1424–31.

138. Antoine EE, Vlachos PP, Rylander MN: **Review of Collagen I Hydrogels for Bioengineered Tissue Microenvironments: Characterization of Mechanics, Structure, and Transport.** *Tissue Eng Part B Rev* 2014.

139. Sudo R, Chung S, Zervantonakis IK, Vickerman V, Toshimitsu Y, Griffith LG, Kamm RD: **Transport-mediated angiogenesis in 3D epithelial coculture.** *FASEB J* 2009, **23**:2155–64.

140. Ramanujan S, Pluen A, McKee TD, Brown EB, Boucher Y, Jain RK: **Diffusion and convection in collagen gels: implications for transport in the tumor interstitium.** *Biophys J* 2002, **83**:1650–60.

141. Stabenfeldt SE, Gourley M, Krishnan L, Hoying JB, Barker TH: **Engineering fibrin polymers through engagement of alternative polymerization mechanisms**. *Biomaterials* 2012, **33**:535–544.

142. Mann KG, Butenas S, Brummel K: **The dynamics of thrombin formation.** *Arterioscler Thromb Vasc Biol* 2003, **23**:17–25.

143. Lansdown ABG, Path FRC: **Calcium : a potential central regulator in wound healing in the skin**. 2002, **10**:271–285.

144. Collet J-P, Lesty C, Montalescot G, Weisel JW: **Dynamic changes of fibrin architecture during fibrin formation and intrinsic fibrinolysis of fibrin-rich clots.** *J Biol Chem* 2003, **278**:21331–21335.

145. Mitsak AG, Dunn AM, Hollister SJ: **Mechanical characterization and non-linear elastic modeling of poly(glycerol sebacate) for soft tissue engineering.** *J Mech Behav Biomed Mater* 2012, **11**:3–15.

146. Legant WR, Miller JS, Blakely BL, Cohen DM, Genin GM, Chen CS: **Measurement of mechanical tractions exerted by cells in three-dimensional matrices**. 2010, **7**.

147. Taipale J, Keski-Oja J: **Growth factors in the extracellular matrix.** *FASEB J* 1997, **11**:51–9.

148. Plant AL, Bhadriraju K, Spurlin T a, Elliott JT: **Cell response to matrix mechanics: focus on collagen.** *Biochim Biophys Acta* 2009, **1793**:893–902.

149. Pujic Z, Goodhill GJ: **A dual compartment diffusion chamber for studying axonal chemotaxis in 3D collagen.** *J Neurosci Methods* 2013, **215**:53–9.

150. Perrimon N, Pitsouli C, Shilo B-Z: **Signaling mechanisms controlling cell fate and embryonic patterning.** *Cold Spring Harb Perspect Biol* 2012, **4**:a005975.

151. Lázár-Molnár E, Hegyesi H, Tóth S, Falus A: **Autocrine and paracrine regulation by cytokines and growth factors in melanoma.** *Cytokine* 2000, **12**:547–54.

152. Daub JT, Merks RMH: **A cell-based model of extracellular-matrix-guided endothelial cell migration during angiogenesis.** *Bull Math Biol* 2013, **75**:1377–99.

153. Petrie RJ, Doyle AD, Yamada KM: **Random versus directionally persistent cell migration.** *Nat Rev Mol Cell Biol* 2009, **10**:538–49.

154. Polacheck WJ, Zervantonakis IK, Kamm RD: **Tumor cell migration in complex microenvironments.** *Cell Mol Life Sci* 2013, **70**:1335–56.

155. Brizzi MF, Tarone G, Defilippi P: **Extracellular matrix, integrins, and growth factors as tailors of the stem cell niche.** *Curr Opin Cell Biol* 2012, **24**:645–51.

156. Ferrara N: **Binding to the extracellular matrix and proteolytic processing: two key mechanisms regulating vascular endothelial growth factor action.** *Mol Biol Cell* 2010, **21**:687–90.

157. Martino MM, Briquez PS, Ranga A, Lutolf MP, Hubbell JA: **Heparin-binding domain of fibrin(ogen) binds growth factors and promotes tissue repair when incorporated within a synthetic matrix.** *Proc Natl Acad Sci U S A* 2013, **110**:4563–8.

158. Martino MM, Briquez PS, Güç E, Tortelli F, Kilarski WW, Metzger S, Rice JJ, Kuhn GA, Müller R, Swartz MA, Hubbell JA: **Growth factors engineered for super-affinity to the extracellular matrix enhance tissue healing.** *Science* 2014, **343**:885–8.

159. Kihara T, Ito J, Miyake J: **Measurement of biomolecular diffusion in extracellular matrix condensed by fibroblasts using fluorescence correlation spectroscopy.** *PLoS One* 2013, **8**:e82382.

160. Roussos ET, Condeelis JS, Patsialou A: **Chemotaxis in cancer.** *Nat Rev Cancer* 2011, **11**:573–87.

161. Aznavoorian S, Stracke ML, Krutzsch H, Schiffmann E, Liotta LA: **Signal transduction for chemotaxis and haptotaxis by matrix molecules in tumor cells.** *J Cell Biol* 1990, **110**:1427–38.

162. Li S, Huang NF, Hsu S: **Mechanotransduction in endothelial cell migration.** *J Cell Biochem* 2005, **96**:1110–26.

163. Garrett Q, Khaw PT, Blalock TD, Schultz GS, Grotendorst GR, Daniels JT: **Involvement of CTGF in TGF-beta1-stimulation of myofibroblast differentiation and collagen matrix contraction in the presence of mechanical stress.** *Invest Ophthalmol Vis Sci* 2004, **45**:1109–16.

164. Jester J V., Ho-Chang J: **Modulation of cultured corneal keratocyte phenotype by growth factors/cytokines control in vitro contractility and extracellular matrix contraction**. *Exp Eye Res* 2003, **77**:581–592.

165. Long CJ, Roth MR, Tasheva ES, Funderburgh M, Smit R, Conrad GW, Funderburgh JL: **Fibroblast growth factor-2 promotes keratan sulfate proteoglycan expression by keratocytes in vitro.** *J Biol Chem* 2000, **275**:13918–23.

166. Tuli SS, Liu R, Chen C, Blalock TD, Goldstein M, Schultz GS: **Immunohistochemical localization of EGF, TGF-alpha, TGF-beta, and their receptors in rat corneas during healing of excimer laser ablation.** *Curr Eye Res* 2006, **31**:709–19.

167. Kraning-Rush CM, Carey SP, Califano JP, Smith BN, Reinhart-King CA: **The role of the cytoskeleton in cellular force generation in 2D and 3D environments.** *Phys Biol* 2011, **8**:015009.

168. Chen X, Thibeault SL: **Response of fibroblasts to transforming growth factor-β1 on two-dimensional and in three-dimensional hyaluronan hydrogels.** *Tissue Eng Part A* 2012, **18**:2528–38.

169. Sun T, Jackson S, Haycock JW, MacNeil S: **Culture of skin cells in 3D rather than 2D improves their ability to survive exposure to cytotoxic agents.** *J Biotechnol* 2006, **122**:372–381.

170. Yeo LY, Chang H-C, Chan PPY, Friend JR: **Microfluidic devices for bioapplications.** *Small* 2011, **7**:12–48.

171. Wu J, Wu X, Lin F: **Recent developments in microfluidics-based chemotaxis studies.** *Lab Chip* 2013, **13**:2484–99.

172. Bb-homodimer PGF, Hollinger JO, Ph D: **Regenerative Tendon and Ligament Healing : Opportunities with Recombinant Human**. 2012, **18**:225–234.

173. Li X, Ballerini DR, Shen W: **A perspective on paper-based microfluidics: Current status and future trends.** *Biomicrofluidics* 2012, **6**:11301–1130113.

174. Lee J-H, Gu Y, Wang H, Lee WY: **Microfluidic 3D bone tissue model for high-throughput evaluation of wound-healing and infection-preventing biomaterials.** *Biomaterials* 2012, **33**:999–1006.

175. Li J, Zhu L, Zhang M, Lin F: **Microfluidic device for studying cell migration in single or co-existing chemical gradients and electric fields.** *Biomicrofluidics* 2012, **6**:24121–2412113.

176. Kothapalli CR, van Veen E, de Valence S, Chung S, Zervantonakis IK, Gertler FB, Kamm RD: **A high-throughput microfluidic assay to study neurite response to growth factor gradients.** *Lab Chip* 2011, **11**:497–507.

177. Chung S, Sudo R, Vickerman V, Zervantonakis IK, Kamm RD: **Microfluidic Platforms for Studies of Angiogenesis, Cell Migration, and Cell–Cell Interactions**. *Ann Biomed Eng* 2010, **38**:1164–1177.

178. Xu H, Heilshorn SC: **Microfluidic investigation of BDNF-enhanced neural stem cell chemotaxis in CXCL12 gradients.** *Small* 2013, **9**:585–95.

179. Atencia J, Morrow J, Locascio LE: **The microfluidic palette: a diffusive gradient generator with spatio-temporal control.** *Lab Chip* 2009, **9**:2707–14.

180. Jeong GS, Han S, Shin Y, Kwon GH, Kamm RD, Lee S-H, Chung S: **Sprouting angiogenesis under a chemical gradient regulated by interactions with an endothelial monolayer in a microfluidic platform.** *Anal Chem* 2011, **83**:8454–9.

181. Helm C-LE, Fleury ME, Zisch AH, Boschetti F, Swartz MA: **Synergy between interstitial flow and VEGF directs capillary morphogenesis in vitro through a gradient amplification mechanism.** *Proc Natl Acad Sci U S A* 2005, **102**:15779–84.

182. Pagano G, Ventre M, Iannone M, Greco F, Maffettone PL, Netti P a.: **Optimizing design and fabrication of microfluidic devices for cell cultures: An effective approach to control cell microenvironment in three dimensions**. *Biomicrofluidics* 2014, **8**:046503.

183. Paralkar VM, Vukicevic S, Reddi AH: **Transforming growth factor β type 1 binds to collagen IV of basement membrane matrix: Implications for development**. *Dev Biol* 1991, **143**:303–308.

184. Somasundaram R, Schuppan D: **Type I, II, III, IV, V, and VI Collagens Serve as Extracellular Ligands for the Isoforms of Platelet-derived Growth Factor (AA, BB, and AB)**. *J Biol Chem* 1996, **271**:26884–26891.

185. Zhang L, Gardiner BS, Smith DW, Pivonka P, Grodzinsky AJ: **On the role of diffusible binding partners in modulating the transport and concentration of proteins in tissues.** *J Theor Biol* 2010, **263**:20–9.

186. Van Hinsbergh VW, Collen A, Koolwijk P: **Role of fibrin matrix in angiogenesis.** *Ann N Y Acad Sci* 2001, **936**:426–37.

187. Richardson TP, Peters MC, Ennett AB, Mooney DJ: **Polymeric system for dual growth factor delivery.** *Nat Biotechnol* 2001, **19**:1029–34.

188. Ern A, Guermond JL: **Theory and Practice of Finite Elements**. Edited by Antman SS, Marsden JE, Sirovich L. New York; 2004.

189. Einstein A: **On the Electrodynamics of Moving Bodies**. *Ann Phys (N Y)* 1905, **17**:891.

190. Sáez P: **PhD dissertation**. University of Zaragoza; 2103.

191. Ogston AG, Preston BN, Wells JD: **On the Transport of Compact Particles Through Solutions of Chain-Polymers**. *Proc R Soc A Math Phys Eng Sci* 1973, **333**:297–316.

192. Kim WS, Tarbell JM: **Macromolecular Transport Through the Deformable Porous Media of an Artery Wall**. *J Biomech Eng* 1994, **116**:156.

193. Flury M, Gimmi TF: **Solute diffusion**. In *Methods Soil Anal Part 4, Phys Methods*. Soil Scien. Edited by Dane JH, Topp GC. Madison; 2002.

194. Jiao Y, Torquato S: **Quantitative characterization of the microstructure and transport properties of biopolymer networks.** *Phys Biol* 2012, **9**:036009.

195. Li J, Lin F: **Microfluidic devices for studying chemotaxis and electrotaxis**. *Trends Cell Biol* 2011, **21**:489–497.

196. Knapp DM, Helou EF, Tranquillo RT: **A fibrin or collagen gel assay for tissue cell chemotaxis: assessment of fibroblast chemotaxis to GRGDSP.** *Exp Cell Res* 1999, **247**:543–553.

197. Schneider L, Cammer M, Lehman J, Sonja K, Guerra CF, Veland IR, Stock C, Hoffmann K, Yoder BK, Schwab A, Satir P, Christensen ST: **Directional Cell Migration and Chemotaxis in Wound Healing Response to PDGF-AA are Coordinated by the Primary Cilium in Fibroblasts**. *Cell Physiol Biochem* 2010, **25**:279.

198. Kim S, Kim HJ, Jeon NL: **Biological applications of microfluidic gradient devices.** *Integr Biol* 2010, **2**:584–603.

199. Wang SJ, Saadi W, Lin F, Minh-Canh Nguyen C, Li Jeon N: **Differential effects of EGF gradient profiles on MDA-MB-231 breast cancer cell chemotaxis.** *Exp Cell Res* 2004, **300**:180–9.

200. Van der Meer AD, Vermeul K, Poot A a, Feijen J, Vermes I: **A microfluidic wound-healing assay for quantifying endothelial cell migration.** *Am J Physiol Heart Circ Physiol* 2010, **298**:H719–25.

201. Lu J, Zhou S, Siech M, Habisch H, Seufferlein T, Bachem MG: **Pancreatic stellate cells promote hapto-migration of cancer cells through collagen I-mediated signalling pathway.** *Br J Cancer* 2014, **110**:409–20.

202. Jost W: **Diffusion in solids, liquids, gases**. *Angew Chemie* 1952, **65**:496.

203. Jiao Y, Torquato S: **Quantitative Characterization of the Microstructure and Transport Properties of Biopolymer Networks**. *Phys Biol* 2012, **9**:036009.

204. Valero C, Javierre E, García-Aznar JM, Gómez-Benito MJ: **A cell-regulatory mechanism involving feedback between contraction and tissue formation guides wound healing progression**. *PLoS One* 2014, **9**:e92774.

205. Li B, Wang JH-C: **Fibroblasts and myofibroblasts in wound healing: force generation and measurement.** *J Tissue Viability* 2011, **20**:108–20.

206. Vavken P, Joshi SM, Murray MM: **Fibrin concentration affects ACL fibroblast proliferation and collagen synthesis.** *Knee* 2011, **18**:42–46.

207. Ridley AJ, Paterson HF, Johnston CL, Diekmann D, Hall A: **The small GTP-binding protein rac regulates growth factor-induced membrane ruffling**. *Cell* 1992, **70**:401–410.

208. Kovács M, Tóth J, Hetényi C, Málnási-Csizmadia A, Sellers JR: **Mechanism of blebbistatin inhibition of myosin II.** *J Biol Chem* 2004, **279**:35557–63.

209. Vicente-Manzanares M, Zareno J, Whitmore L, Choi CK, Horwitz AF: **Regulation of protrusion, adhesion dynamics, and polarity by myosins IIA and IIB in migrating cells.** *J Cell Biol* 2007, **176**:573–80.

210. Iyer AK V, Tran KT, Griffith L, Wells A: **Cell surface restriction of EGFR by a tenascin cytotactin-encoded EGF-like repeat is preferential for motility-related signaling.** *J Cell Physiol* 2008, **214**:504–12.

211. Schwartz MA, Ginsberg MH: **Networks and crosstalk: integrin signalling spreads.** *Nat Cell Biol* 2002, **4**:E65–8.

212. Gomes ER, Jani S, Gundersen GG: **Nuclear movement regulated by Cdc42, MRCK, myosin, and actin flow establishes MTOC polarization in migrating cells.** *Cell* 2005, **121**:451–63.

213. Elosegui-Artola A, Jorge-Peñas A, Moreno-Arotzena O, Oregi A, Lasa M, García-Aznar JM, De Juan-Pardo EM, Aldabe R: **Image analysis for the quantitative comparison of stress fibers and focal adhesions.** *PLoS One* 2014, **9**:e107393.

214. Sung KE, Su G, Pehlke C, Trier SM, Eliceiri KW, Keely PJ, Friedl A, Beebe DJ: **Control of 3-dimensional collagen matrix polymerization for reproducible human mammary fibroblast cell culture in microfluidic devices.** *Biomaterials* 2009, **30**:4833–41.

215. Elbjeirami WM, Yonter EO, Starcher BC, West JL: **Enhancing mechanical properties of tissue-engineered constructs via lysyl oxidase crosslinking activity.** *J Biomed Mater Res A* 2003, **66**:513–21.

216. Duong H, Wu B, Tawil B: **Modulation of 3D fibrin matrix stiffness by intrinsic fibrinogen-thrombin compositions and by extrinsic cellular activity.** *Tissue Eng Part A* 2009, **15**:1865–1876.